# Theoretical and Experimental Determination of Matrix Diffusion and Related Solute Transport Properties of Fractured Tuffs From the Nevada Test Site

G. R. Walter*

*Department of Hydrology and Water Resources, University of Arizona, Tucson, AZ 85721.

# Los Alamos
Los Alamos National Laboratory
Los Alamos, New Mexico 87545

CONTENTS

FIGURES (Cont)

## TABLES

# THEORETICAL AND EXPERIMENTAL DETERMINATION

## OF MATRIX DIFFUSION AND RELATED SOLUTE TRANSPORT

## PROPERTIES OF FRACTURED TUFFS FROM THE NEVADA TEST SITE

by

G. R. Walter

---

## ABSTRACT

Theoretical and experimental studies of the chemical and physical factors which affect molecular diffusion of dissolved substances from fractures into a tuffaceous rock matrix have been made on rocks from G-Tunnel and Yucca Mountain at the Nevada Test Site (NTS). A variety of groundwater tracers, which may be useful in field tests at the NTS, have also been developed and tested.

Although a number of physical/chemical processes may cause nonconvective transport of dissolved species from fractures into the tuff matrix, molecular diffusion seems to be the most important process. Molecular diffusion in these rocks is controlled by the composition of the groundwater through multicomponent effects and several rock properties.

The effective molecular-diffusion coefficient in the tuff of a particular specie can be related to its free aqueous-diffusion coefficient by

$$D_e = \phi_m (\alpha/\tau^2) D_o$$

where

$\phi_m$ is porosity,

$\alpha$ is a constrictivity factor, and

$\tau$ is a tortuosity factor.

The porosities of the samples studied ranged from about 0.1 to 0.4. The parameter $(\alpha/\tau^2)$ ranged from 0.1 and 0.3 and effective matrix-diffusion coefficients were measured to be between 2 to 17. x $10^{-7}$ $cm^2/s$ for sodium halides and sodium pentafluorobenzoate.

Total porosity was found to be the principle factor accounting for the variation in effective-diffusion coefficients. The constrictivity-tortuosity factor was found to have a fair correlation (r = 0.75) with the median pore diameters measured by mercury intrusion. Measurements of bulk-rock electrical impedance changes with frequency indicate that the constrictivity factor, $\alpha$, has a maximum value of 0.8 to 1, but may be smaller. If the larger values are correct, then the diffusion paths in tuff are more tortuous than in granular media.

Computation of the full diffusion-coefficient matrix for various tracers in J-13 well water from the NTS indicates coupling of the diffusion fluxes of all ionic species. These effects are being incorporated into a numerical model of multi-component-matrix diffusion.

# I. INTRODUCTION

The importance of molecular diffusion as a mechanism for transporting dissolved substances from pores and fractures, where convective transport dominates, into a rock or soil matrix of much lower permeability has been discussed for some time in the fields of ore geochemistry, marine geochemistry, and soil chemistry (Garrels and others, 1949; Lerman, 1975; Norton and Knapp, 1977, van Genuchten and Wierenga, 1976). Molecular diffusion may also be the rate-controlling step in various sorption and ion-exchange processes (van Genuchten and Wierenga, 1976). Interest in molecular diffusion as a solute-dispersing mechanism in groundwater flow through fractured rocks has been aroused recently by the theoretical and laboratory studies of Grisak and Pickens (1980a, 1980b) and Grisak and others (1980).

These studies, in particular Grisak and Pickens (1980a), indicate that matrix diffusion (diffusion from a fracture into blocks of porous rock) may be a very important process in retarding movement of solutes and attenuating their concentrations. Given the high porosities of tuff and its low permeability, matrix diffusion may be the dominant transport phenomema in tuffaceous rocks.

At the outset of this project, no definite field or laboratory study had been made to determine the true importance of matrix diffusion in solute transport through fractured rocks. Although the laboratory-column study reported by Grisak and others (1980) suggests that matrix diffusion may have been observed in fractured till, the complex chemistry of the solutions used, the unknown fracture pattern and aperture distribution in the test

3

material, and the simple form of their diffusion model leave these results open to interpretation.

The purpose of the research described here was three-fold: first, to identify and measure the most important physical and chemical parameters controlling matrix diffusion in fractured tuff; second, to identify and apply ground-water tracers suitable for use in both field and bench-scale tests of matrix diffusion in tuff; and third, to develop a detailed numerical model of local convective-diffusion from fractures to a rock matrix. Task one is near completion. Task two is in progress. The theoretical aspects of task three have been completed, but development of the numerical model is still in progress.

II. PHYSICAL AND CHEMICAL FACTORS AFFECTING MATRIX DIFFUSION

The purpose of this section is to present the theoretical groundwork for identifying and measuring those transport processes which may affect the movement of dissolved substances between a fracture and the porous-tuff matrix. To accomplish this goal we begin with a very general description of all transport processes based on the laws of irreversible thermodynamics in continuous systems.

## A. Transport Processes

Consider the conceptual model of a fracture shown in Fig. II.A.1. In general, we are interested in the case where a solvent (water) containing N components flows through the fracture. The matrix (unfractured tuff) is assumed to possess some solution-saturated porosity, through which aqueous transport takes place. The interface between the fracture may be the unaltered surface of the tuff matrix or an altered surface with physical properties different from the rest of the matrix.

If we assume that the transport through the fracture in the x-direction is only by convection and hydrodynamic dispersion, then we can apply the principles of irreversible thermodynamics to completely describe the mass fluxes from the fracture into the matrix and through the matrix. Based on the linear-law postulate of irreversible thermodynamics (Haase, 1969), the mass and heat fluxes in the system with N components are described by the phenomenological equations

$$\underline{J}_i = \sum_{k=1}^{N} L^*_{ik} \underline{X}_k \qquad \text{(II.A.1)}$$

5

POROUS
ROCK
MATRIX

POROUS
ROCK
MATRIX

FRACTURE

$\mathbb{C}$

$C_1$

$J_d$

$J_c$

$C_1$

$b$

$\mathbb{C}$
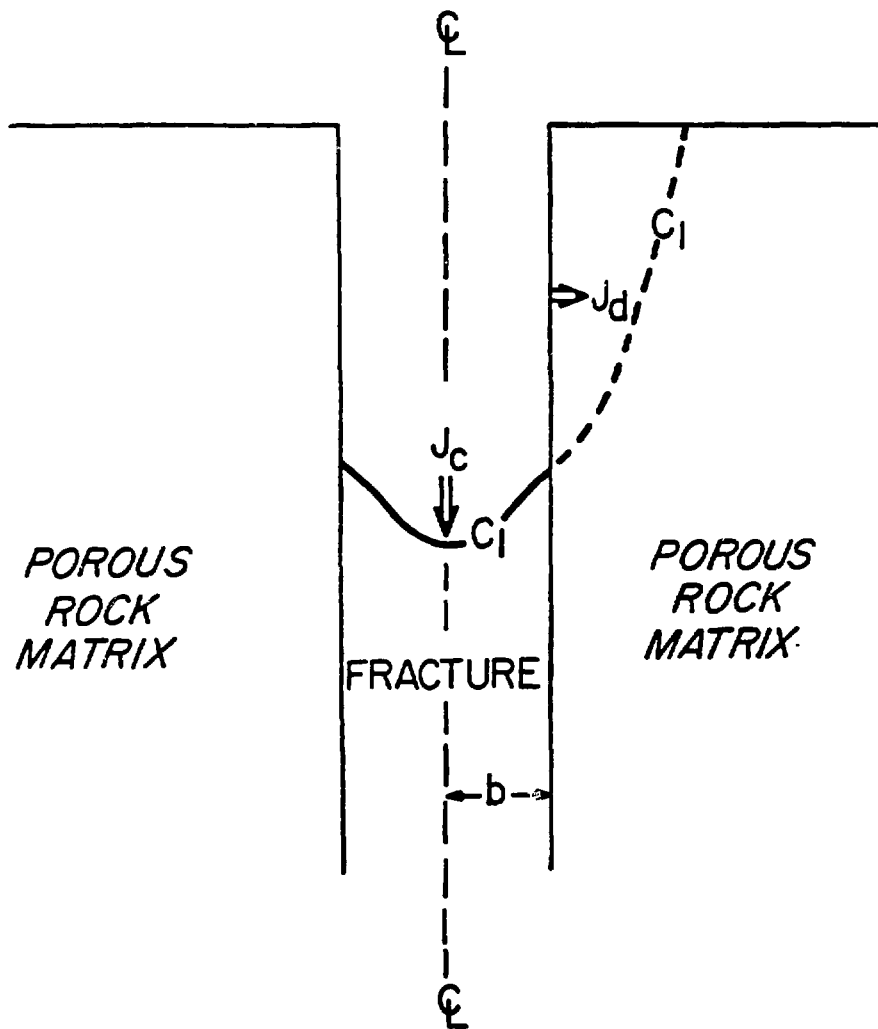
Fig. II.A.1.   Conceptual model of single fracture convective transport with
matrix diffusion.

6

$$\underline{J}_Q = \sum_{k=1}^{N} L^*_{Qk} \underline{X}_k + L^*_{QQ} \underline{X}_Q \qquad\qquad (II.A.2)$$

where

> $\underline{J}_i$ is the molar flux of the ith component (i = 1 for solvent)
>
> $L^*_{ik}$ is the phenomenological coefficient relating the
>
> > ith flux to the kth force,
>
> $\underline{X}_k$ is the kth generalized force per mole,
>
> $\underline{J}_Q$ is the heat flux,
>
> $\underline{X}_Q$ is the thermal force,

and the underlining indicates a vectorial quantity.

The assumption is made that the phenomenological coefficients do not depend on the fluxes and forces, but can be arbitrary functions of the state variables temperature, pressure and concentration.

Following the development of Haase (1969), the generalized molar forces, $X_k$, for creeping motions are given by

$$\underline{X}_k = M_k \underline{g} - \dot{V}_k \nabla P - \nabla \mu_k + z_k F \nabla E \qquad\qquad (II.A.3)$$

where

> $M_k$ is the molecular weight of component k,
>
> $\dot{V}_k$ is the partial molar volume of k,
>
> $\underline{g}$ is the gravitational acceleration,
>
> $P$ is the thermodynamic pressure,
>
> $\mu_k$ is the chemical potential of the kth component at constant T and P,
>
> $\nabla$ is the gradient operator,
>
> $z_k$ is the charge on k,

7

F is the Faraday Constant, and

E is the electrical potential.

The thermal force is given by

$$\underline{X}_Q = -\ 1/T\ \nabla T \qquad\qquad\qquad\qquad \text{(II.A.4)}$$

where

T is absolute temperature.

In the remainder of this report, we restrict ourselves to isothermal conditions so that the heat flux and its effect on other fluxes will be ignored. This is not to say, however, that it may not be important in some parts of the transport field in a repository.

Combining Eq. (II.A.1) and Eq. (II.A.3) and multiplying each force by the molar concentration of k, $m_k$, we obtain flux equations in terms of the force per unit volume:

$$\underline{J}_i = L_{ii}^{*}\ (m_i M_i \underline{g} - m_i \dot{V}_i \nabla P) - L_{ii}^{*} m_i \nabla \mu_i$$

$$+ \sum_{k=2}^{N} L_{ik}^{*}(m_k M_k \underline{g} - m_k \dot{V}_k \nabla P\ )$$

$$+ \sum_{k=2}^{N} L_{ik}^{*}(-m_k \nabla \mu_k + m_k z_k F \nabla E\ ) \qquad\qquad \text{(II.A.5)}$$

Noting that

$$m_i M_i = c_i \qquad\qquad\qquad\qquad\qquad \text{(II.A.6)}$$

and

$$m_i \dot{V}_i = \dot{n}_i \qquad\qquad\qquad\qquad\qquad \text{(II.A.7)}$$

8

where

$c_i$ is the mass concentration of $i$, and

$n_i$ is the volume fraction of $i$,

Eq. (II.A.5) can be rewritten as

$$\underline{J}_i = \overset{*}{L}_{ii}(c_i\underline{g} - \dot{n}_i\nabla P) - \overset{*}{L}_{ii}m_i\nabla\mu_i$$

$$+ \sum_{k=2}^{N} \overset{*}{L}_{ik}(c_k\underline{g} - \dot{n}_k\nabla P)$$

$$+ \sum_{k=2}^{N} \overset{*}{L}_{ik}(-m_k\nabla\mu_k + m_k z_k F\nabla E) \qquad\qquad \text{(II.A.8)}$$

As shown by Groenvelt and Bolt (1969), in order to obtain a set of flux equations whose terms are amenable to experimental measurement, we need to rewrite Eq. (II.A.8) in terms of a volume flux, a set of mass or molar fluxes, and a current or charge flux. Substituting the identities

$$\underline{J}_v = \sum_{i=1}^{N} \bar{V}_i\underline{J}_i \qquad\qquad\qquad\qquad \text{(II.A.9)}$$

$$J_{mi} = M_i\underline{J}_i \qquad\qquad\qquad\qquad \text{(II.A.10)}$$

$$\underline{J}_z = \sum_{i=1}^{N} z_i\underline{J}_i \qquad\qquad\qquad\qquad \text{(II.A.11)}$$

into Eq. (II.A.8) gives

$$\underline{J}_v = \sum_{i=1}^{N} \bar{V}_i \sum_{k=1}^{N} \overset{*}{L}_{ik}(c_k\underline{g} - \dot{n}_k\nabla P)$$

$$- \sum_{i=1}^{N} \bar{V}_i \sum_{k=1}^{N} \overset{*}{L}_{ik}m_k\nabla\mu_k$$

$$+ \sum_{i=1}^{N} \bar{V}_i \sum_{k=1}^{N} \overset{*}{L}_{ik}m_k z_k F\nabla E \qquad\qquad (II.A.12)$$

$$\underline{J}_{mi} = M_i \sum_{k=1}^{N} \overset{*}{L}_{ik}(c_k\underline{g} - \dot{n}_k\nabla P)$$

$$- M_i \sum_{k=1}^{N} \overset{*}{L}_{ik}m_k\nabla\mu_k$$

$$+ M_i \sum_{k=1}^{N} \overset{*}{L}_{ik}m_k z_k F\nabla E \qquad\qquad (II.A.13)$$

and

$$\underline{J}_z = \sum_{i=1}^{N} z_i \sum_{k=1}^{N} \overset{*}{L}_{ik}(c_k\underline{g} - \dot{n}_k\nabla P)$$

$$- \sum_{i=1}^{N} z_i \sum_{k=1}^{N} \overset{*}{L}_{ik}m_k\nabla\mu_k$$

$$+ \sum_{i=1}^{N} z_i \sum_{k=1}^{N} \overset{*}{L}_{ik}m_k z_k F\nabla E \qquad\qquad (II.A.14)$$

10

After some lengthy algebraic manipulations (Appendix I), the rather complicated flux equations represented by Eq. (II.A.12, 13 and 14) can be simplified and formulated in terms of familiar forces and phenomenological coefficients

$$\underline{J}_v = L_{vv} \nabla \phi_v + \ldots + L_{vi}\nabla\mu_i + \ldots L_{vz}\nabla E$$

.

.

$$\underline{J}_{mi} = L_{iv}\nabla\phi_v + \ldots + L_{ii}\nabla\mu_i + \ldots L_{iz}\nabla E \qquad (II.A.15)$$

.

.

$$\underline{J}_z = L_{zv}\nabla\phi_v + \ldots + L_{zi}\nabla\mu_i + \ldots L_{zz}\nabla E$$

where

$\phi_v$ is $(\rho_s \underline{g} - \nabla P)$, and

$\rho_s$ is the solution density.

A similar set of phenomenological equations was developed by Groenvelt and Bolt (1969) and have been shown to be valid for transport through porous media. Groenvelt and Bolt also point out the correspondence between the phenomenological coefficients in Eq. (II.A.15) and more familiar transport coefficients. To see this correspondence, we note that the first subscript of each coefficient denotes the quantity transported, and the second subscript denotes the potential gradient responsible for that flux. The physical significance of each term in Eq. (II.A.15) is given in Table II.A.1.

TABLE II.A.1. CORRESPONDENCE BETWEEN PHENOMENOLOGICAL COEFFICIENTS
AND COMMON TRANSPORT COEFFICIENTS

| Phenomenological Coefficient | Process |
| --- | --- |
| $L_{vv}$ | Darcian flow |
| $L_{vi}$ | Osmosis |
| $L_{vz}$ | Electrosmosis |
| $L_{iv}$ | Convection and ion filtration |
| $L_{ii}$ | Diffusion |
| $L_{ij}$ | Multicomponent diffusion |
| $L_{iz}$ | Electrophoresis |
| $L_{zv}$ | Streaming current |
| $L_{zi}$ | Diffusion current |
| $L_{zz}$ | Electrical conduction |

The significance of the phenomenological equations for studies of solute transport through fractured tuff is that they summarize all of the processes by which solutes can move from a fracture into the matrix under isothermal conditions. Although they are applicable to both saturated and unsaturated rocks, this report deals only with transport under fully saturated conditions.

Under such conditions, the conceptual models of matrix diffusion presented by most previous investigators (e.g., Grisak and Pickens, 1980; Neretniks, 1981; and Tang, 1981) have assumed that convective transport from the fracture into the matrix can be ignored. That this assumption, with some qualification, can be applied to the tuffs is seen by a simple calculation.

Permeability measurements of tuff samples indicate that their intrinsic permeability is on the order of $10^{-14}$ cm$^2$. Applying Darcy's Law, the convective-solute flux from a fracture into the matrix under a unit hydraulic gradient is

$$\underline{J}_{iv} = c_i \underline{J}_{vv} = 10^{-9} \text{ cm/s} \cdot c_i \qquad (II.A.16)$$

As will be discussed later, the interstitial molecular-diffusion coefficients for most simple ions will be of the order of $10^{-6}$ cm/s. Assuming a unit concentration gradient and a solute concentration of $c_i$ within the fracture, the diffusion flux will be

$$J_{ii} = 10^{-6} \text{ cm/s} \ c_i \qquad (II.A.17)$$

13

Thus, concentration gradients are about three orders of magnitude more effective in transporting solute to the matrix than are hydraulic gradients. For this reason, the assumption of no convective transport through the tuff matrix is justified for the range of hydraulic gradients likely to develop under saturated conditions.

The qualification to this statement is that if the tuffs possess membrane or ion-selective properties, osmotic pressure gradients may exist or be created which will cause a volume flux into the matrix. Preliminary experimental evidence for each flux will be presented later in this report.

Even if the convective flux terms are ignored, there remain other non-convective flux terms which have not been considered in previous matrix-diffusion models. First, previous models have considered only diffusion of a single component. Eq. (II.A.15), however, indicates that to some extent the diffusion fluxes of all the dissolved components are coupled. For ionic species, Lasaga (1979) and Anderson and Graf (1978) have shown that in natural waters the off-diagonal phenomenological coefficients and related diffusion coefficients which couple the flux of one species to the concentration gradients of other species are not zero and cannot be ignored. Simple single-component diffusion rigorously applies only in the case of true tracer diffusion where a concentration gradient exists only for an isotope of the specie of interest. It may be closely approximated by neutral species. The theoretical importance of multicomponent diffusion in transport in the tuffs will be discussed in a later section and related to the results of laboratory-diffusion experiments.

14

Lastly, the importance of the electrical-current or charge-flux equation must be considered. Throughout this project, we have made the assumption that no macroscopic electrical potentials exist and that the current flux is zero. The possibility exists, however, that corrosion reactions involving metallic cannisters might give rise to electrical potentials or currents, in which case the current flux and coupled electrophoretic fluxes would need to be considered. Such consideration is outside the scope of this study.

In summary, this report deals primarily with experimental and theoretical studies of diffusional transport through the tuff. Preliminary experiments have been conducted to evaluate the membrane properties of the tuffs and to evaluate the importance of osmotic-transport processes.

## B. Rock Properties

The extent to which matrix diffusion is effective in dispersing a given solute depends on a number of rock properties. The numerical study by Grisak and Pickens (1980b) indicates that the diffusion porosity (interconnected pores) in the matrix, the fracture aperture, and the convective velocity through the fracture are the principal physical factors influencing the effect of matrix diffusion on the solute-breakthrough curve.

The roles of these parameters can readily be seen by examining the analytical solution for transport through a single fracture with matrix diffusion given by Grisak and Pickens (1980a)

$$c_f/c_0 = 1 - erf\left[\frac{[D_e/vb] \, x}{2[(t-x/v)D_e/\phi_m]^{1/2}}\right] \qquad (II.B.1)$$

15

where

   $c_0$ is the initial concentration,

   $c_f$ is the local concentration in the fracture,

   $\phi_m$ is the diffusion porosity of the matrix,

   $D_e$ is the effective molecular-diffusion coefficient within the matrix,

   b is the fracture aperture,

   t is the time since injection, and

   v is the flow velocity in the fracture.

From Eq. (II.B.1) the attenuating effect of matrix diffusion is seen to be directly proportional to the effective matrix-diffusion coefficient and matrix porosity, and inversely proportional to the flow velocity and fracture aperture. $D_e$ in Eq. (II.B.1) is not the diffusion coefficient within a pore, which may be approximated by the free aqueous-diffusion coefficient in large pores, but includes at least the effects of the tortuosity of the pores and porosity. Additional factors controlling the magnitude of the matrix diffusion will be discussed later.

   Numerous models have been presented to describe the functional relationship between the free aqueous- or free gaseous-diffusion coefficients and effective-diffusion coefficients in natural or artificial porous media (e.g., Olsen and others, 1968; Saxena and others, 1974; van Brakel and Heertjes, 1974). Most of these models take the form of

$$D_e = \left\{ \phi_m \alpha / \tau^2 \right\} D_0 \qquad (II.B.2)$$

16

where

    $\tau$   is a tortuosity factor,

    $\alpha$   is a constrictivity factor, and

    $D_0$   is the free aqueous- or free-gaseous diffusion coefficient.


As used in Eq. (II.B.2), the tortuosity factor is taken to be the ratio of the actual path length through the porous medium divided by the macroscopic distance over which concentration gradients are measured.

If the pores in the tuff are relatively large, greater than about 10µm, then surface effects due to the solid phase should be negligible (Saxena and others, 1974) and the ratio of the effective matrix-diffusion ($D_e$) coefficient to the free-aqueous diffusion coefficient, $D_0$, is primarily a function of the tortuosity of the diffusion path and porosity. The term $L_e/L$ is squared because it is applied as a correction both to the concentration gradient and to the cross-sectional area perpendicular to the actual diffusion path. The tortuosity factor, $(L_e/L)^2$, can be estimated or experimentally determined from effective matrix-diffusion coefficients. Also, Wyllie and Spangler (1952) have shown that tortuosity is related to the formation factor, F, used by the petroleum industry, and so tortuosity can be determined by electrical-conductivity measurements. The electrical conductivity of the medium is a function of the tortuosity because the conductivity measurement requires that ions migrate through the medium in response to an imposed electrical potential, and the movement of the ions is impeded directly as a function of the tortuosity.

The discussion above applies only to large pores. For pores with diameters less than about 10$\mu$m, the effective-diffusion coefficient decreases to an extent which cannot be explained solely in terms of a geometrical tortuosity factor, hence the need for the constrictivity term in Eq. (II.B.2). Surface effects of the solid phase may act to decrease the effective matrix-diffusion coefficient. Kemper and others (1964) and Saxena and others (1974) have suggested that water near mineral surfaces may have a higher viscosity than the bulk fluid resulting in slower diffusion in this zone. A more important surface effect may be the interaction of ionic species with the electrical field extending from individual mineral surfaces.

In general, silicate mineral surfaces have a negative electrical charge. The potential field associated with this charge penetrates some distance into the fluid phase before it is neutralized by positive charges in solution. Anions do not penetrate as deeply into this field as do cations. The exclusion of anions from part of the cross-sectional pore area can result in a decrease in the matrix-diffusion coefficient. This effect becomes particularly important in very small pores where the electrical double layers of adjacent minerals overlap. Graham-Bryce (1963) has attributed anomalously low tracer-diffusion coefficients for iodide in clays to this phenomena. Blackmore (1976) and Banin (1972) have also explained seemingly irreversible diffusion in soil aggregates and clay pastes to this "salt-sieving" effect.

The concept of reduced mobility of anions in small pores has also been the basis for several models to explain the frequency dependence of bulk-rock electrical impedance (induced polarization effects) (Marshall and Madden, 1959; Anderson and Keller, 1964; Arulanandan and Mitchell, 1968). The theory of Marshall and Madden will be discussed in detail in a later section as it relates to the determination of tortuosity and constrictivity factors for the tuff. Van Brakel and Heertjes (1974) have explained the constrictivity factor in terms of the variation of cross-sectional area along the pore segments. Defined in this way, it can be related to the ratio of the maximum to cross-sectional area of the pore to the minimum cross-sectional. Estimates of the magnitude of the geometric-constrictivity factor for various pore geometrics (e.g., Michaels, 1959; Petersen, 1959), indicate that $\alpha$ should vary from 1 (no constrictions) to a minimum of about 0.2 (80% constriction).

Based on the above examination of the rock parameters controlling the effective matrix-diffusion coefficient, the following matrix properties have been experimentally determined for tuff samples from the NTS:

1) porosity,
2) pore size distribution,
3) effective diffusion coefficients, and
4) bulk resistivity at varying frequencies.

Details of the experimental procedures and the results will be presented in a later section.

## C. Chemical Factors Affecting Matrix Diffusion

Chemical processes may limit or enhance matrix diffusion in several ways. To see this, consider Fick's Law for an isothermal, multicomponent, aqueous solution

$$\underline{J}_i = -\sum_{j=1}^{N} D_{ij} \nabla c_j \tag{II.C.1}$$

or in matrix form

$$\underline{J} = -\overline{\overline{D}} \nabla \overline{c} \tag{II.C.2}$$

where

$D_{iv}$ is the diffusion coefficient,

single bar superscript is a column matrix, and

double bar superscript is a two-dimensional matrix.

The diffusion coefficients in Eq. (II.C.1) depend on the ionic strength and composition of the solution. Also, the off-diagonal diffusion coefficients, $D_{ij}$ where $i \neq j$, which couple the flux of one component to the gradients of the other components, are not zero. Thus, we can see immediately that predicting the diffusive flux of a given ionic specie requires a knowledge of the effect of solution composition and ionic strength on the diffusion coefficients, and the direction and magnitude of the concentration gradients of the coupled species.

In the general case of multicomponent solutions containing weak electrolytes, the causes of this coupling are both the electrostatic attractions between cations and anions, and formation of complex species due to ion association and complexation.

Inasmuch as many of the species of interest in radionuclide migration are weak electrolytes or form ion pairs and complexes, and the fact that some of the groundwater tracers are weak acids, consideration must be given to multicomponent-diffusion effects.

In Appendix II, multicomponent-diffusion equations based on the work of Wendt (1965), Toor (1964), and Anderson and Graf (1978) are derived which are suitable for numerical computation of these multicomponent effects. The data required to solve these equations are: (1) ionic conductances, (2) equilibrium constants for the complex and associated species, and (3) activity coefficients of the ions in solution. These data are already available for many species of interest, but were lacking for several of the tracers being used in this study. Consequently, the required missing parameters were measured as a part of this program. The results of the laboratory measurements are reported in section III of this report.

III.  EXPERIMENTAL INVESTIGATIONS

In order to evaluate the physical and chemical parameters which affect solute transport from fractures to the tuff matrix, various laboratory investigations were undertaken.  The methods and results of this work are described in this section.

## A.  Properties of the Tuff

Laboratory measurements have been made of the porosity and pore-size distribution of samples of the tuff from both G-Tunnel and drill holes on the Yucca Mountains at the NTS.  As qualitative verification for the porosimetry results, a series of scanning-electron micrographs were also taken of fractions of the tuff samples used in the porosimetry measurements. In addition, numerous measurements of effective-diffusion coefficients of samples of the tuff using various solutes have been made.  Measurements of bulk-electrical resistivity and induced-electrical polarization were also made on selected samples to support the diffusion studies.  These measurements were also used to evaluate the relative roles of the tortuosity and constrictivity factors in affecting the effective matrix-diffusion coefficients.

### 1.  Porosity and Pore-Size Distribution

The porosity of interest in this study is the diffusion porosity of the tuff matrix.  The diffusion porosity consists primarily of interconnected pores formed between mineral grains and rock aggregates, but ions may also diffuse into the crystal lattice of zeolite minerals.  Diffusion into the latter type of pore is generally considered as part of the kinetics of ion exchange and only the intergranular porosity will be considered here.  A

22

number of more or less standard techniques exist for measuring the various types of porosity associated with a rock sample but none is totally free from error and interpretational problems. Manger (1966) has discussed the various method-dependent errors associated with total- and effective-porosity measurements in tuff from the NTS.

For this study we are interested not only in the total-diffusion porosity, but also the size distribution of these pores. Four basic methods exist for estimating both porosity and pore-size distributions. These are nitrogen-adsorption techniques, mercury-infusion porosimetry (Gregg and Sing, 1967), successive granulation (Norton and Knapp, 1977), and microscopic examination using both optical- and scanning-electron microscopy. Mercury-infusion techniques are well developed and were used for routine measurements of porosity and pore-size distributions in this study. Grain-density measurements were used to estimate the total porosity of the samples.

A mercury-infusion porosimeter was constructed for porosity and pore-size distribution studies. A schematic drawing of the mercury-infusion apparatus is shown in Fig. III.A.1. The mercury porosimeter was constructed by modifying an existing Ruska mercury pump and pycnometer for use as a porosimeter by adding a polycarbonate mercury level observation tube to the top of the pycnometer and the necessary pressure and vacuum regulation and measurement system. System pressures are measured using a Setra 0-2000 psig pressure transducer and digital readout. The transducer also measures
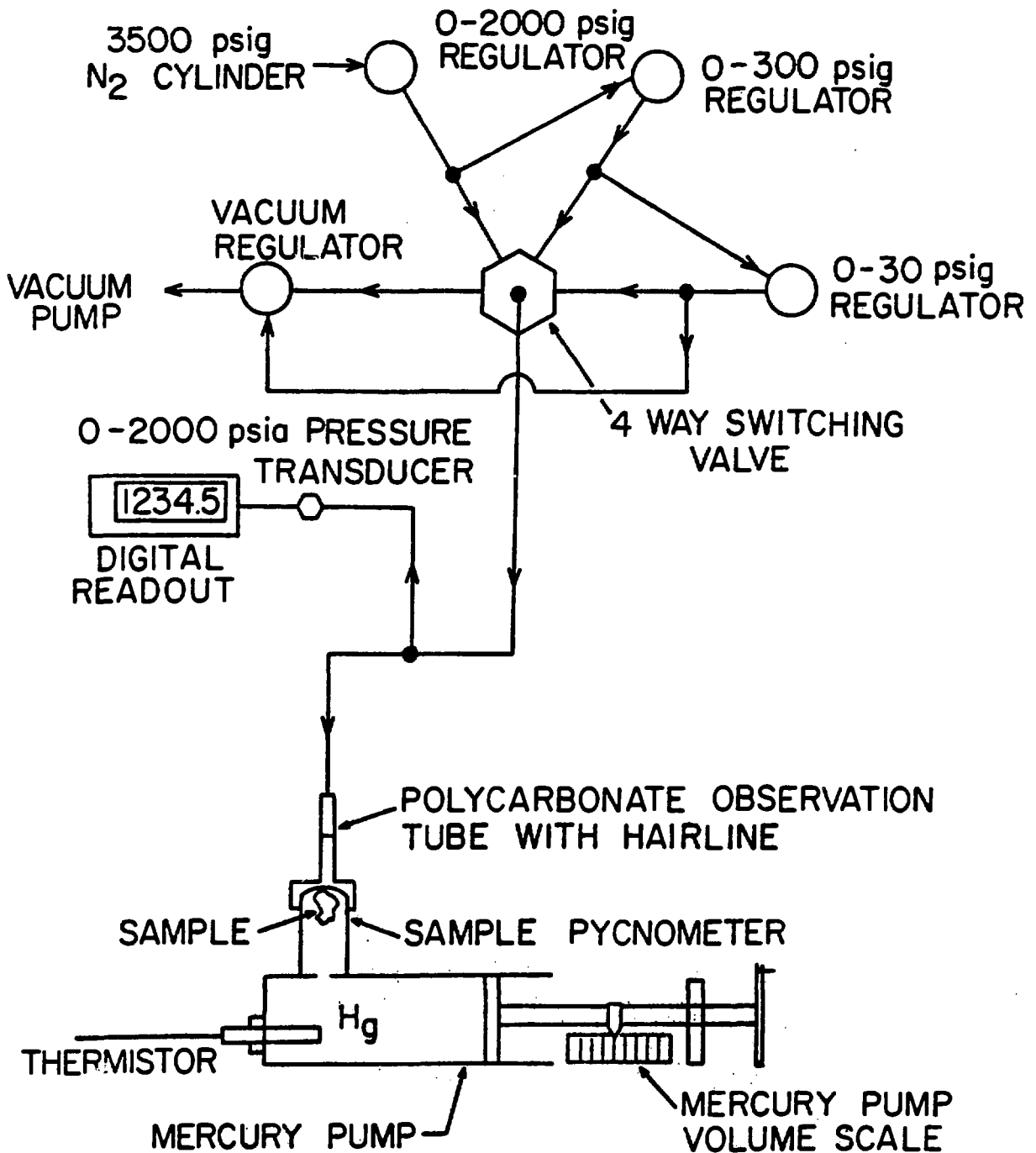
Fig. III.A.1.  Schematic drawing of the mercury infusion porosimeter.

partial vacuums. The porosimeter is capable of operating from pressures ranging from about 13 Pa (1 mm Hg) to $1.4 \times 10^6$ Pa (2000 psia). The porosimeter is thus capable of measuring pore-size distributions for pores with theoretical diameters between 0.1 cm and $10^{-5}$ cm. The porosimeter meets or exceeds the specifications of commercially available porosimeters and has a total system-expansion correction of less than 0.4 $cm^3$ at maximum pressure.

Initially, daily temperature fluctuations of several degrees Celsius in our laboratory caused problems in making accurate volume measurements. This problem has been partially corrected by repairs made to the lab cooling system and application of an ambient room temperature correction factor to the raw volume data. To more accurately measure the working temperature in the mercury reservoir, a thermistor-temperature probe was placed in the mercury reservoir and temperature was monitored during intrusion measurements.

Porosity and pore-size distribution measurements are made by placing a dried and weighed sample of tuff in the pycnometer and evacuating the system to less than 1 mm Hg. The mercury pump is used to force mercury into the pycnometer until the mercury level rises to a hairline in the observation tube. The displacement of the mercury-pump piston is then read to 0.001 $cm^3$. The total displacement from the zero position gives the bulk sample volume because at 1 mm Hg pressure, virtually none of the mercury will infuse into the sample.

After the bulk volume has been determined, the pressure in the
pycnometer is increased stepwise by releasing vacuum and applying $N_2$ gas
pressure. After each step increase in pressure, the system is maintained at
that pressure for several minutes to allow the mercury to infuse into the
sample. The cumulative-volume change is then measured by bringing the
mercury level back to the hairline with the pump. Typically, 10 to 20 steps
are used per order of magnitude change in pressure.

The pressure-volume data are analyzed by subtracting the system-volume
expansion at each pressure from the cumulative volume change during the
sample run and correcting for temperature changes. The system-expansion
correction is determined at low pressure using a semi-log regression of the
blank run pressure-volume data. Above about $3.5 \times 10^4$ Pa, a linear-
regression equation is used for the system-expansion correction. A P-V
curve with the regression line for a typical blank run is shown in
Fig. III.A.2.

To date, pore-size distribution measurements have been made on a number
of samples from G-Tunnel and from Yucca Mountain. The theoretical pore
diameters were calculated using the Washburn equation

$$d_T = \frac{4\tau \cos \theta}{P} \qquad\qquad\qquad (III.A.1)$$

where

    $d_T$ is the theoretical pore diameter,

    $P$ is the pressure,

    $\tau$ is the surface tension of mercury, and

    $\theta$ is the contact angle for mercury (140°).
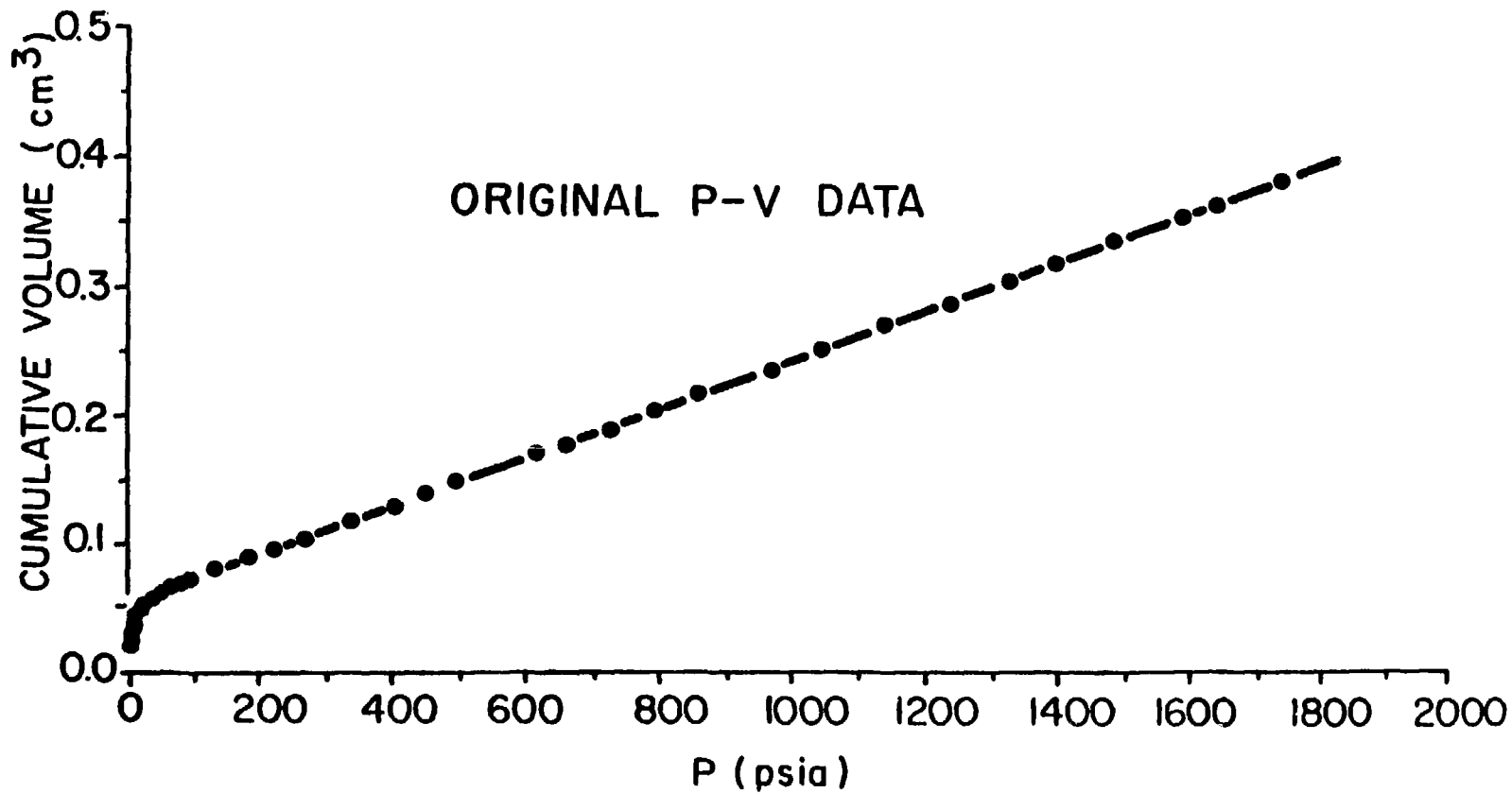
Fig. III.A.2.  Blank run P-V curve of the mercury infusion porosimeter.

The grain densities were determined using the pycnometer procedure described in Procedure ASTM D 854-58 (ASTM, 1973). Briefly, the procedure consisted of crushing a sample of tuff and drying it at approximately 95°C for several days. The crushed sample was then placed in a preweighed 25-ml pycnometer. The wetting fluid (water or kerosene) was added to the pycnometer until the sample was completely covered. The pycnometer was attached to a vacuum pump and evacuated for several hours to remove trapped air. The pycnometer was filled and weighed. The specific gravity, SpG, was computed from

$$SpG = W_0/[W_0 + (W_a - W_b)] \qquad (III.A.2)$$

where

$W_0$ is the weight of the oven-dry sample,

$W_a$ is the weight of the pycnometer filled with fluid, and

$W_b$ is the weight of the pycnometer filled with fluid and rock.

The specific gravities were corrected for temperature and fluid density to obtain the grain densities.

The total porosities were computed using the grain density of the crushed sample and the bulk volume of the sample used for mercury infusion measured under vacuum.

The grain densities, total porosities, porosities for pores greater than 0.1 μm diameter, and median pore diameters are listed in Table III.A.1. Because of the destructive nature of the grain-density measurement and the irreversibility of mercury infusion, both measurements could not be made on the same piece of tuff. Due to heterogeneities in the core chips from individual sections of core, an intrinsic uncertainty exists in the total

TABLE III.A.1.  GRAIN DENSITY POROSITY RESULTS FOR NTS TUFF SAMPLES

| Sample | Run | Grain Density g/cm$^3$ (mean) | Method[a] | Total Porosity | Porosity[b] >0.1 μm | Median Pore Diameter (μm) |
|---|---|---|---|---|---|---|
| G1-1292 | 1 | ND | | | ND | |
| G1-2233 | 1 | 2.24 | K | 0.353 | 0.279 | |
| G1-2290 | 2 | 2.35 | K | 0.331 | 0.195 | 0.21 |
| G1-2333 | | 2.65 | K | 0.364 | 0.292 | 1.17 |
| G1-2476 | | ND | | | ND | |
| G1-2539 | 1 | ND | | | 0.204 | |
|  | 2 | | | | 0.111 | |
| G1-2698 | | ND | | | 0.143 | |
| G1-2790 | 1 | 2.54 | K | 0.198 | 0.241 | |
|  | 2 | | | 0.201 | 0.160 | 0.1* |
|  | 3 | | | 0.146 | 0.225 | |
| G1-2840 | | 2.65 | K | 0.269 | 0.173 | 0.30 |
| G1-2901 | | 2.50 | K | 0.194 | 0.162 | 0.55 |
| G1-3116 | 1 | 2.43 | K | 0.268 | 0.238 | 0.79 |
|  | 2 | 2.48 | K | 0.076 | 0.103 | |
|  | 3 | 2.49 | K | | | |
|  | 4 | 2.48 | W | | | |
|  | | (2.47) | | | | |
| G1-3423 | | ND | | | ND | |
| G1-3802 | | ND | | | 0.180 | |
| G1-4411 | | ND | | | ND | |
| G1-4750 | | ND | | | ND | |
| YM-30 | | ND | | | ND | |
| YM-45 | | ND | | | 0.187 | |
|  | | | | | 0.311 | |
| YM-46 | | ND | | | 0.049 | |

TABLE III.A.1 -- Continued

| Sample | Run | Grain Density g/cm$^3$ (mean) | Method[a] | Total Porosity | Porosity[b] >0.1 μm | Median Pore Diameter (μm) |
|--------|-----|------------------------------|-----------|----------------|---------------------|---------------------------|
| U12G-RNM#9 (5.96 ft to 6.4 ft) | | ND | | | 0.154 | |
| U12G-RNM#9 (16.2 ft to 17.5 ft) | | 2.18 2.21 | K W | 0.405 | 0.229 | 0.1* |
| HF23 | | 2.74 2.50 | K W | 0.469 | 0.105 | 0.5* |

[a]K indicates that kerosine was used as the wetting fluid.
 W indicates that water was used as the wetting fluid.

[b]From volume of mercury intruded at 2000 psia.

*From distribution curve extrapolated to 50% to porosity.

ND - Not done to date.

porosity values.

Data on the pore-size distributions are shown in Fig. III.A.3. In Fig. III.A.3 the log-pore diameter in microns is plotted versus the cumulative percent of the total porosity intruded on the probability axis. Fig. III.A.3 is useful for estimating the statistical properties of the data on the pore-size distributions because a log-normal distribution will plot as a straight line. As can be seen, although some of the size-distribution curves are approximately log-normal, many are not.

### 2. Diffusion Experiments on the Tuffs

Direct measurements of the effective-diffusion coefficients of various ionic species through samples of the tuff have been made using a diaphragm-diffusion cell modified from the original design of Stokes (1950). A drawing of the diaphragm-diffusion cell is shown in Fig. III.A.4. The diffusion experiments are performed by cementing a 1-inch diameter by 1/4-inch thick tuff disc in the membrane-holding disc of the cell. A solution high in concentration of the diffusing species is placed in the lower reservoir and a solution of lower concentration is placed in the upper reservoir. The resulting concentration gradient causes molecular diffusion through the tuff disc. All the solutions used in the tuff-diffusion experiments are prepared using water from well J-13 as the solvent.

Two techniques have been used for monitoring the concentration in the upper reservoir. In the first technique, the concentration of the diffusing specie is continuously monitored in the upper reservoir using the pumping and detection system show in Fig. III.A.5. For the initial sodium-bromide

31
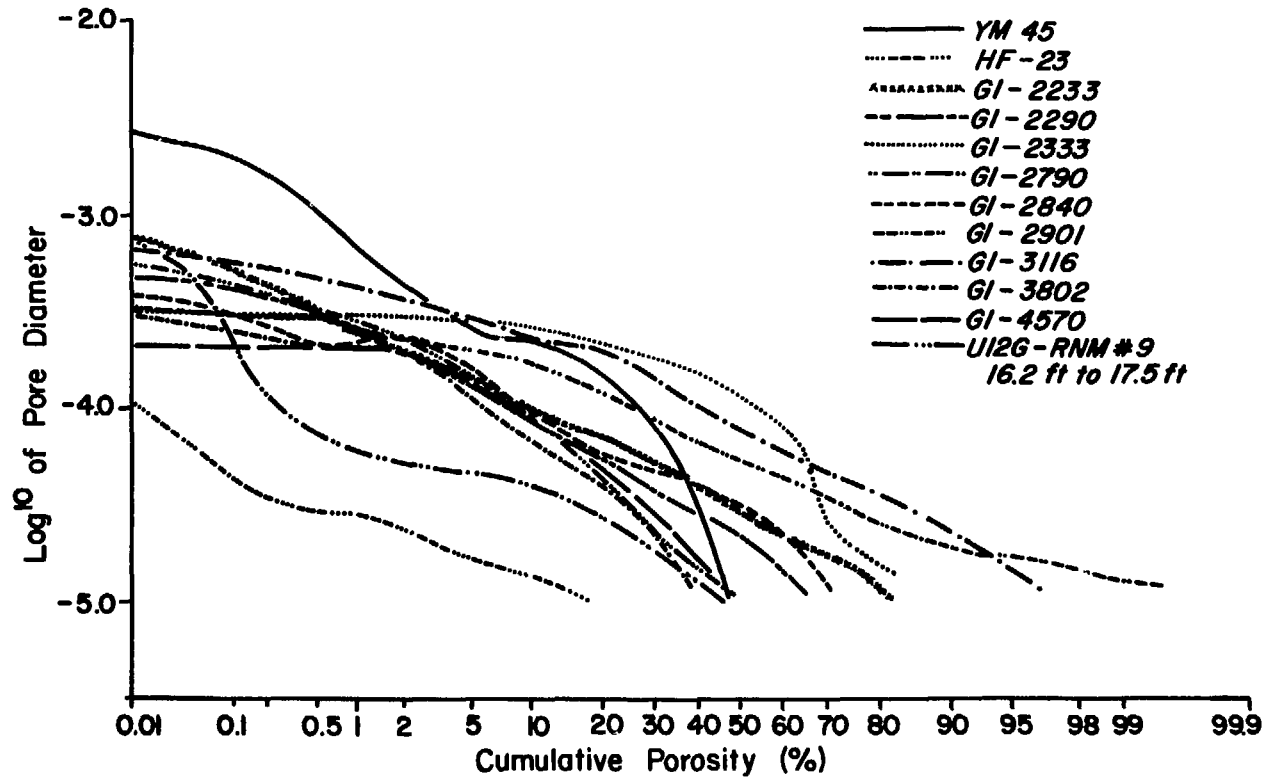
Fig. III.A.3. Log-Probability plot of cumulative porosity versus pore diameter for tuff samples.
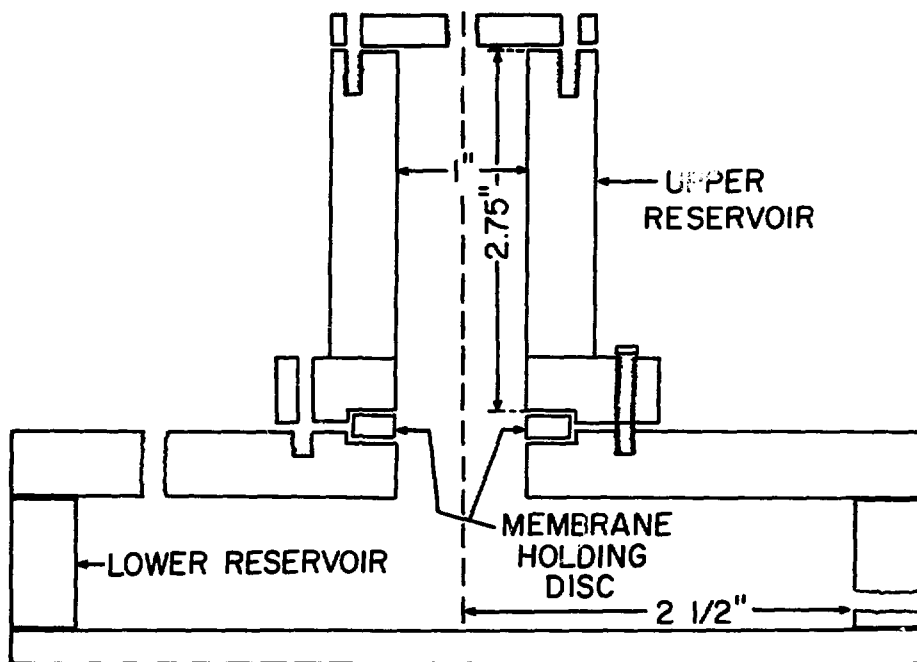
Fig. III.A.4. Plexiglas diaphram diffusion cell.
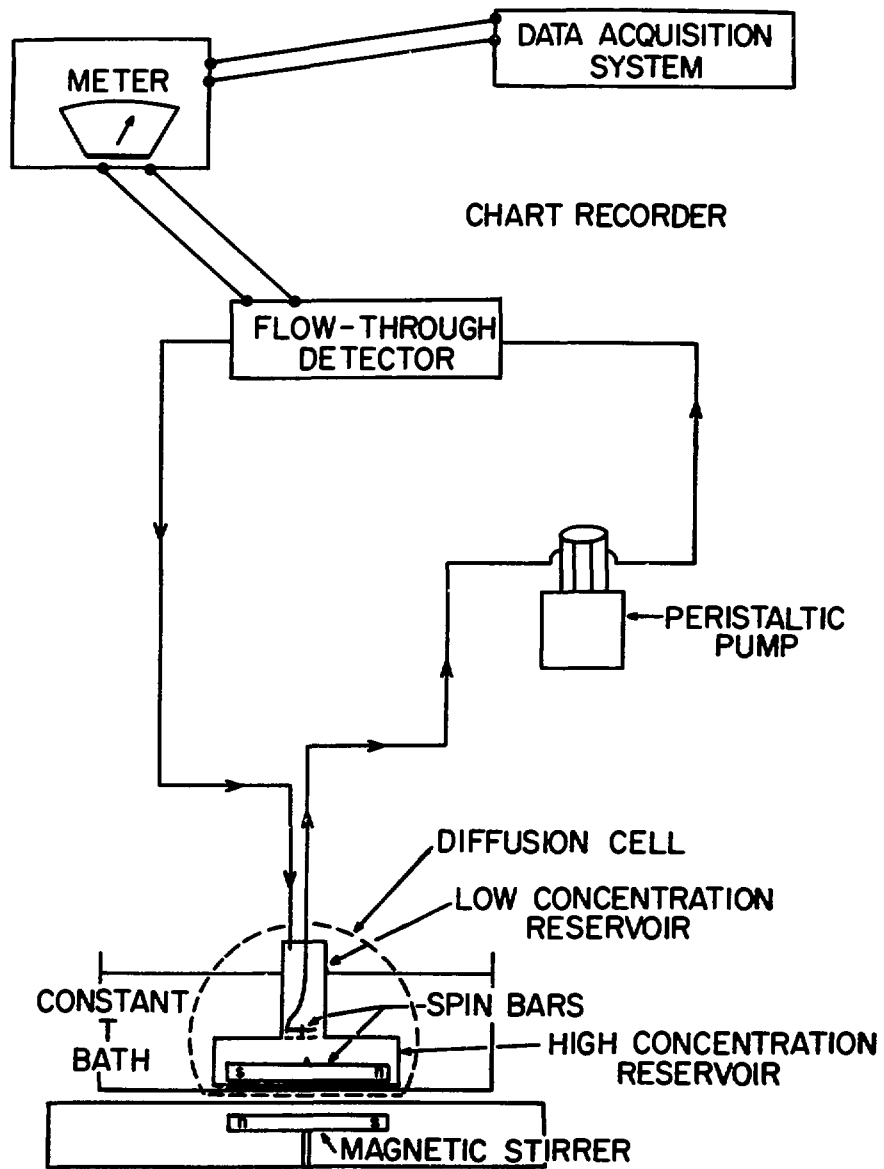
Fig. III.A.5.  Schematic drawing of the diffusion experiment pumping and
detection system.

and sodium-iodide tests, the detector for the tuff-diffusion studies consisted of a Plexiglas flow-through cell into which an ion-selective electrode and a reference electrode are inserted. In later tests, and tests using other species, a Wescan flow-through conductivity detector was used. The upper-reservoir solution was pumped through the cell using a peristaltic pump. The data-collection system used in the tests is shown in Fig. III.A.6. The output from the detector goes to a signal scanner which sequentially switches the output from up to three diffusion cells, or two diffusion cells and a digital thermometer to a Hewlett-Packard 3390A peak integrator. The scanning rate is such that a given diffusion cell is sampled once every 3 to 5 minutes, with a 30-second "on" and "off" mV signal which the integrator receives; it interprets these as chromatographic peaks which it integrates and stores.

The integrator transmits the stored peak areas and run times to a Hewlett-Packard 85A computer where they are stored on magnetic tape. All data reduction and computation of diffusion coefficients is then performed by programs written for the HP85A.

The second technique for monitoring the concentration in the upper reservoir consisted of discrete measurements using an Altex RC-20 conductivity bridge or a Schoeffel ultraviolet absorption detector. The conductivity bridge was used as a check on the results of the flow-through conductivity detector. The UV detector was used to selectively monitor the concentrations of the fluorobenzoate tracers.
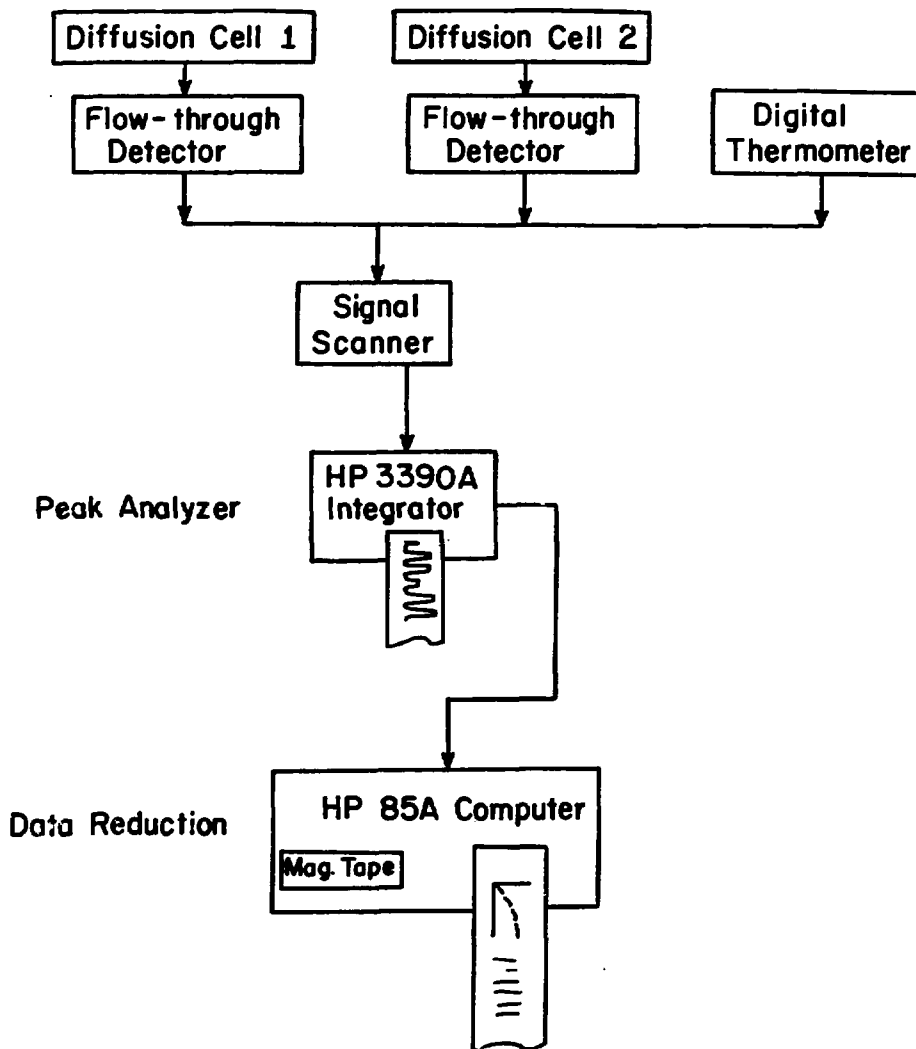
Fig. III.A.6. Data acquisition system for diffusion experiments.

The diffusion experiments were performed using solutions of a given sodium salt dissolved in J-13 well water. Prior to the tests, the tuff discs were soaked in the tracer solution for several days. To start the tests, the lower reservoir was filled with the tracer solution and the tuff sealed in place in the diffusion cell. Vacuum was then applied to the lower reservoir to degas the solution. For discs not previously saturated, vacuum was then applied to the upper reservoir to remove air from the disc and to initiate a flow of solution through the disc. Several hours were required to draw a few ml of solution through the discs. The cell was then placed in a constant temperature bath at 25 ± 0.1°C or 30 ± 0.1°C for several hours prior to the test. This procedure was designed to assure that the fluid in the tuff disc was in equilibrium with the solution in the lower reservoir at the start of the test. The tests were initiated by placing a known volume of either J-13 water or a solution with one-hundreth of the lower-reservoir concentration in the upper-reservoir.

The resulting time-concentration data are analyzed using the so-called steady-state method (Robinson and Stokes, 1959). This method uses only the data after a sufficient time has elapsed for an approximately linear-concentration gradient to be established across the disc. When such a gradient has been established, the time-average diffusion coefficient is given by

$$\overline{D}_e = [ \frac{At}{L} (\frac{1}{V_u} + \frac{1}{V_L}) ]^{-1} \ln \Delta C^* \qquad \text{(III.A.3)}$$

where

$D_e$ is the time-average effective diffusion coefficient,

A is the disc surface area of the disc,

L is the thickness of the disc,

$V_u$ is the volume of the upper reservoir,

$V_L$ is the volume of the lower reservoir,

$$\Delta C^* = \frac{C_L(0) - C_u(0)}{C_L(t) - C_u(t)}$$

$C_u(o)$ and $C_L(o)$ are the concentrations in the upper and lower reservoirs respectively when a linear concentration gradient exists, and

$C_u(t)$ and $C_L(t)$ are the concentrations at time t.

To compute $\bar{D}_e$, both the upper- and lower- reservoir concentrations must be known. The upper-reservoir concentration is measured and the lower-reservoir concentration is computed from the change in upper-reservoir concentration. In practice, the lower-reservoir concentration changed by less than 1% during the course of our experiments.

To apply the steady-state method, a time must be selected after which a linear-concentration gradient is assumed. We determine this time by plotting $\ln \Delta C^*$ versus time as shown in Fig. III.A.7 for sample U12G-RNM#9. From this figure we see that the $\ln \Delta C^*$ becomes linear in t after about 400 minutes. Regression analysis is then used to compute $\bar{D}_e$ from the linear portion of the curve. The error in the diffusion coefficient is computed from the variance of the regressive slope. Admittedly, the selection of the linear portion of the curve is somewhat subjective. The data-analysis program is written so that the operator can interactively perform the regression on various portions of the curve until the error in the computed-diffusion coefficient is minimized. Usually about three tries are needed to select a linear portion after which no further improvement in the error can be made.

Typical results of the diffusion experiments are shown in Fig. III.A.7 a, b, and c. Fig. III.7a shows results of a test using the Br⁻ selective electrode. Fig. III.A.7b shows a result using the conductivity bridge, and Fig. III.A.7c shows the results using the flow-through conductivity detector. The tests usually lasted about 24 hours, but some were as short as 12 hours and as long as 5 days.

Approximately 50 diffusion experiments were performed on 9 different discs of tuff from G-Tunnel and the G-1 test hole at Yucca Mountain. Many of the tests were unsuccessful, either because of failures in the detection system or because the resulting time-concentration results were clearly not the result of diffusion. In the latter case, the anomalous results were usually traced to a failure of the cement sealing the tuff disc into the diffusion cell. The results of tests which were considered to be successful, based on the criterion that the time-concentration curves were consistent with molecular diffusion, are listed in Table III.A.2.

Although the results of the diffusion experiments will be analyzed in detail in a later section, a few comments on the quality of the results are in order. As can be seen from Table III.A.2, the effective-diffusion coefficients so far measured were from $16.8 \times 10^{-2}$ down to $2.5 \times 10^{-7}$ cm$^2$/s. In general, these results fall within the range of values that would be expected based on reasonable, prior estimates of tortuosity and constrictivity (e.g., van Brakel and Heertjes, 1974).

As for the results for individual rocks on which multiple-diffusion experiments have been performed, obtaining reproducibility has been a persistent problem. For example, tests on G1-2840 (sample B) using
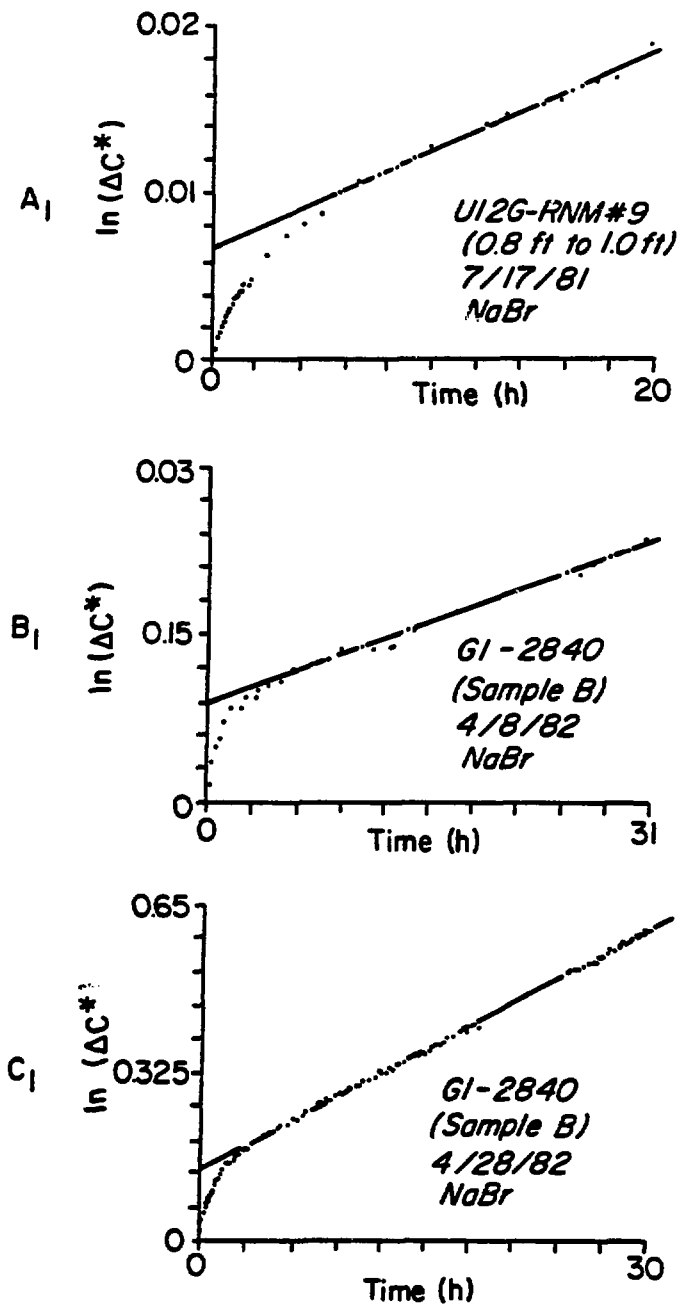
Fig. III.A.7. Typical diffusion test results for NaBr using:
A) Br⁻ electrode, B) conductivity bridge, and
C) conductivity detector.

TABLE III.A.2.  RESULTS OF DIFFUSION TESTS PERFORMED ON NTS TUFFS

| Sample | Date | Specie | $C_0$Conc. (M) | Detector | De $(10^{-7} cm^2/s)$ | T (°C) | Remarks |
|---|---|---|---|---|---|---|---|
| U126-RNM#9 0.8 ft to 1 ft | 7/17/81 | NaBr | 0.02 | ISE | 4.7 ± 0.1 | 25 | good fit to data |
| U12G-RNM#9 5.9 ft to 6.4 ft (side B) | 10/10/81 | NaBr | 0.05 | ISE | 10.8 ± 0.4 | 25 | good fit to data |
| U12G-RNM#9 5.9 ft to 6.4 ft (side A) | | | | | | | sample broken |
| U12G-RNM#9 16.2 ft to 17.5 ft (sample A) | 10/8/81 | NaI | 0.013 | ISE | 10.8 ± 0.3 | 25 | early part of test suspicious |
| U12G-RNM#9 16.2 ft to 17.5 ft (sample B) | | | | | | | to be run |
| G1-2290 | 8/21/82 | NaBr | 0.05 | ISE | 6.2 ± 0.4 | 25 | much scatter in data |
| G1-2333 (sample 1) | 3/17/82 | NaBr | 0.05 | CD | 11 ± 2 | 30 | cond. detector oscillate, scatter in data |
| G1-2333 (sample 2) | 3/11/82 | NaBr | 0.05 | CD | 16.8 ± 0.1 | 30 | good fit to data |
| G1-2840 (sample A) | 2/18/82 | NaBr | 0.05 | CD | 2.5 ± 0.4 | 30 | spin bar in lower reservoir stopped after 10 hours |
| | 2/24/82 | NaI | 0.05 | CD | 5.45 ± 0.02 | 30 | fairly good fit |
| | 3/24/82 | NaPFB | 0.01 | CD | 7.23 ± 0.07 | 30 | fairly good fit |
| | 4/01/82 | NaSCN | 0.05 | CB | 6.3 ± 0.2 | 30 | good fit to data |
| | 5/01/82 | NaPFB | 0.05 | CD | 2.48 ± 0.01 3.89 ± 0.01 | 30 | slope changes after 20 hrs, first number is early data, sec. is late data. |

Table III.A.2.--Continued

| Sample | Date | Specie | $C_o$Conc. (M) | Detector | $D_e$ $(10^{-7} cm^2/s)$ | T (°C) | Remarks |
|--------|------|--------|------|----------|------|--------|---------|
| | 5/11/82 | NaPFB | 0.05 | CD | 4.75 ± 0.05 | 30.5 | slope changes after 20 hrs probably due to pump malfunction-ing, late time data analyzed |
| | 5/11/82 | NaPFB | 0.05 | UV | 2.2 ± 0.1 | 30.5 | some scatter in data, fair fit to data |
| G1-2840 (sample B) | 2/18/82 | NaI | 0.05 | CD | 3.98 ± 0.04 | 30 | good fit to data |
| | 4/8/82 | NaBr | 0.05 | CB | 4.46 ± 0.07 | 30 | data oscillates, fairly good fit |
| | 4/14/82 | NaPFB | 0.05 | CB | 5. ± 1. | 30 | scatter in data |
| | 4/20/82 | NaSCN | 0.05 | CB | 5.01 ± 0.04 | 30 | good fit to data |
| | 4/28/82 | NaBr | 0.05 | CD | 5.37 ± 0.01 | 30 | good fit to data |
| | 4/29/82 | NaBr | 0.05 | CD | 5.68 ± 0.01 | 30 | restarted from 4/28 test, good fit to data |
| | 5/4/82 | NaBr | 0.05 | CD | 7.7 ± 0.2 | 30 | good fit to data |
| G1-2901 | 3/2/82 | NaBr | 0.05 | CB | 3.14 ± 0.05 | 30 | good fit to data |
| | 3/2/82 | NaSCN | 0.05 | ISE | 4.5 ± 0.5 | 30 | poor calibration and electrode response |
| | 3/11/82 | NaSCN | 0.05 | CD | 4.92 ± 0.04 | | good fit to data |
| | 4/28/82 | NaPFB | 0.05 | CB | 2.82 ± 0.06 | 30 | early part of test question-able, analyzed data from 10 to 30 hours |

*CB is the Altex conductivity bridge
CD is the Wescon conductivity detector
ISE is an ion-selective electrode
UV is a Schoeffel U-V absorption detector

NaBr, give a medium effective-diffusion coefficient of $5.8 \times 10^{-7}$ cm$^2$/s, but the range of values is rather large (4.5 to $7.7 \times 10^{-7}$ cm$^2$/s). Similar results were obtained for Na-pentafluorobenzoate on sample G1-2840 (sample A), where the measured diffusion coefficient ranges from 7.2 to $2.2 \times 10^{-7}$ cm$^2$/s.

An exhaustive search for the causes of these inconsistencies has indicated that they are associated with the diffusion apparatus or the tuff disc, not with the detection and data analysis system. The differences are too large to be accounted for by errors in the calibration of the detector, or other uncertainties in the data.

Another aspect of the diffusion tests is revealed in the 5/11/82 test using NaPFB on disc G1-2840 (sample A) in which the concentration change in the upper reservoir was monitored using both the conductivity detector and the UV detector. The analysis of the conductivity results yielded an effective-diffusion coefficient of $4.75 \times 10^{-7}$ cm$^2$/s while the UV detector results yield a value of $2.2 \times 10^{-7}$ cm$^2$/s. This difference may be attributable to the fact that the conductivity detector measures the total salt content while the UV detector measured essentially only the concentration of the PFB anion. Because concentration gradients existed only for Na and PFB, the results of this test imply that Na and PFB diffused independently of each other. The reasons for such behavior are discussed in a later section of this report.

Although leaks in the cement holding the tuff discs in the diffusion cell are a possible source of anomalously high values, the resulting time-concentration curves show no evidence of convective transport through these holes. On the other hand, air may have entered some of the discs,

43

either during degassing of the lower-reservoir solution or when they were dried to allow touching up of the cement.

Lastly, blank runs performed by soaking the discs in J-13 water and monitoring the change in conductivity have shown a perceptible increase in the dissolved salt content of the water. Although this drift is not sufficient to account for the variance in the diffusion coefficients, it does indicate that the rocks are not in chemical equilibrium with J-13 water. This disequilibrium implies that the tuff discs may change their properties after months of soaking in J-13 water. Additional tests are still in progress to further improve the reproducibility of the diffusion tests.

### 3. Osmosis Experiments

Preliminary tests were performed to determine if osmotic pressure differences can develop across the tuff discs used in the diffusion studies. If such pressure differences exist, they indicate selective transport of water relative to dissolved ionic species and may imply that finite concentration gradients can exist in the tuff without resulting in diffusive transport.

The osmosis experiment consisted of placing a disc of the tuff in a diffusion cell and attaching Tygon tubes to the upper and lower reservoir for measuring pressure differences (as cm of $H_2O$), as shown in Fig.III.A.8. The two tubes are connected by a short circuit through valve 1 so that the pressures in the two reservoirs can be equalized at the start of the test. The tests are started by placing identical salt solutions in the upper- and lower-reservoirs. The diffusion cell was placed in the temperature bath
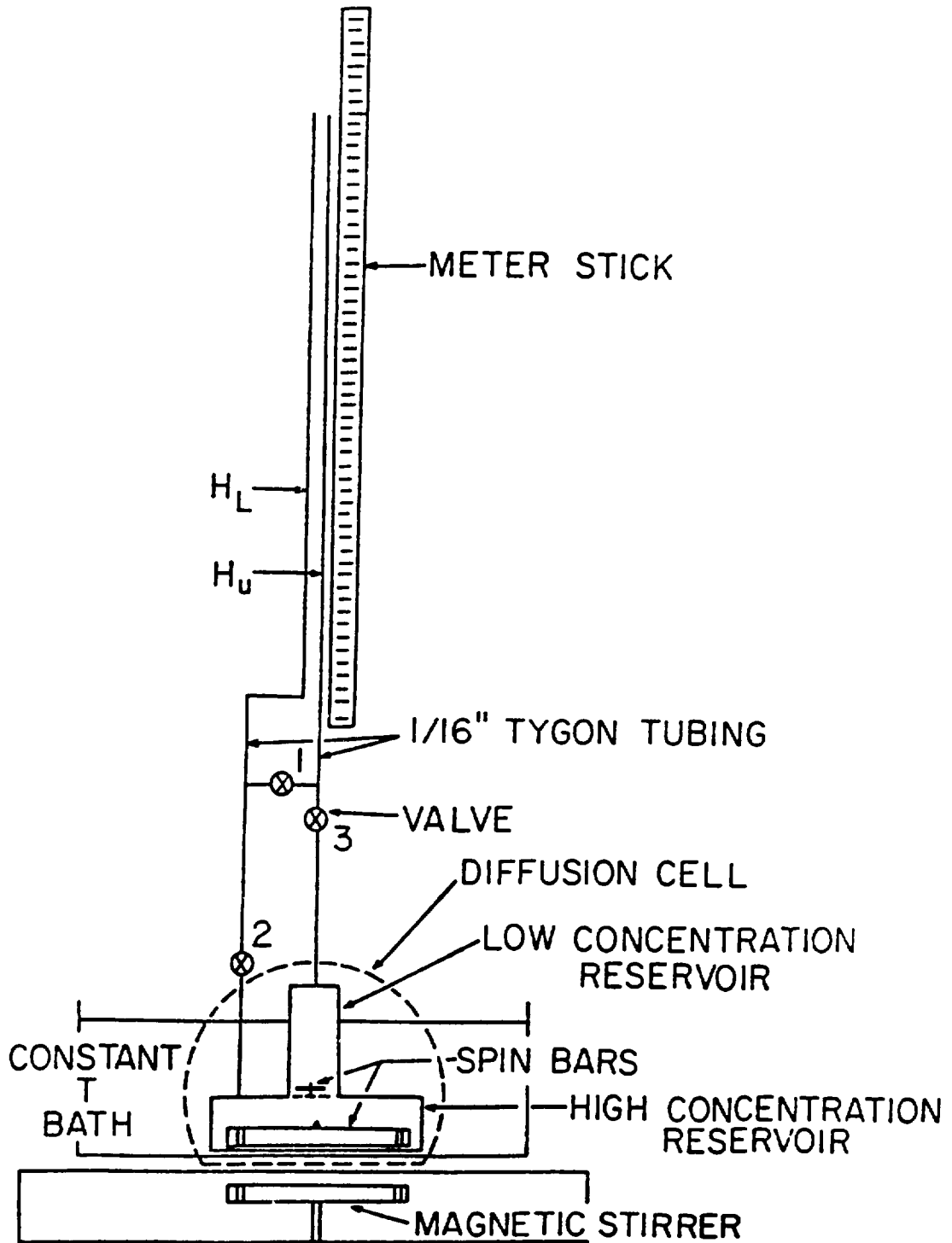
Fig. III.A.8. Apparatus used for osmosis experiments.

and allowed to equilibrate for a day with valve 1 open. The second stage of the osmosis experiment was begun by removing an aliquot of solution from the upper reservoir and replacing it with an equal volume of well J-13 water to create a concentration gradient. Valve 1 was closed to isolate the reservoirs, and the pressure difference between the reservoirs was monitored with time. This process was repeated to create successively greater concentration gradients. Some problems have been observed with air bubbles developing in the Tygon manometer tubes and in anomalous pressure fluctuations.

Results for disc U12G-RNM#9 (0.8 ft to 1.0 ft) and a 0.05 M NaI initial solution are shown in Figs. III.A.9 and III.A.10. Fig. III.A.9 shows the head differences between the two reservoirs that were developed for various differences in initial concentration gradients ($\Delta C$). In all cases, the pressure increases in the lower reservoir. Although the curves in Fig. III.A.9 are somewhat erratic, the head difference also increases with the concentration gradient which is consistent with an osmotic process. In Fig. III.A.10, the head difference after 45 h is plotted versus the initial concentration gradient by extrapolating the C = 0.035 curve to 45 h. The vertical-dashed line indicates the initial lower-reservoir concentration and the maximum concentration gradient which could be developed.

This result suggests that the tuffs can act as membranes and that osmotic pressures may exist between fractures and the tuff matrix. We are, however, attempting to refine the experiment to eliminate the erratic pressure fluctuations shown in Fig. III.A.9 and to eliminate all possible external sources of head differences between the reservoirs.

46
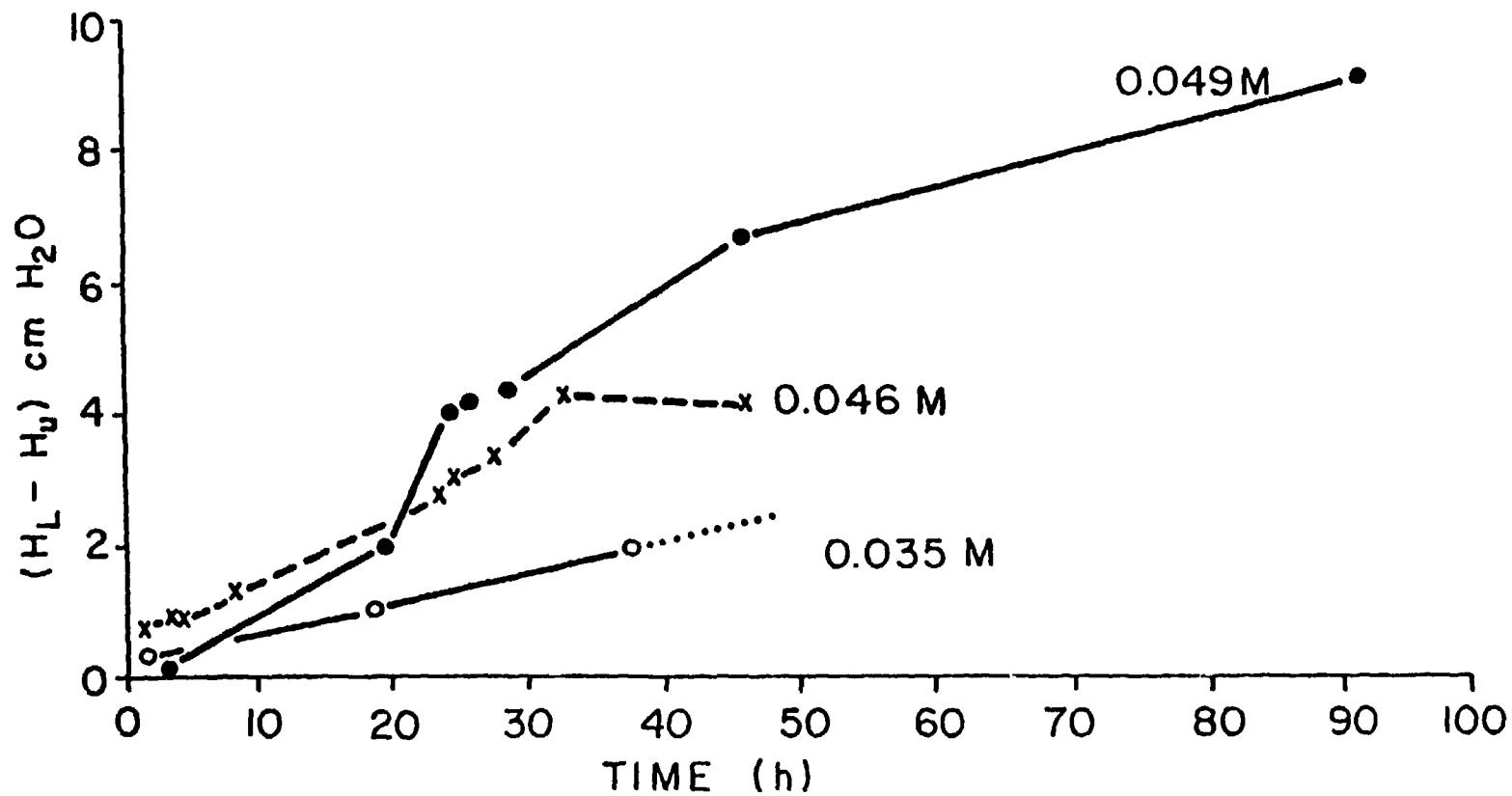
Fig. III.A.9. Head difference between upper and lower reservoirs vs time for various initial concentration differences.
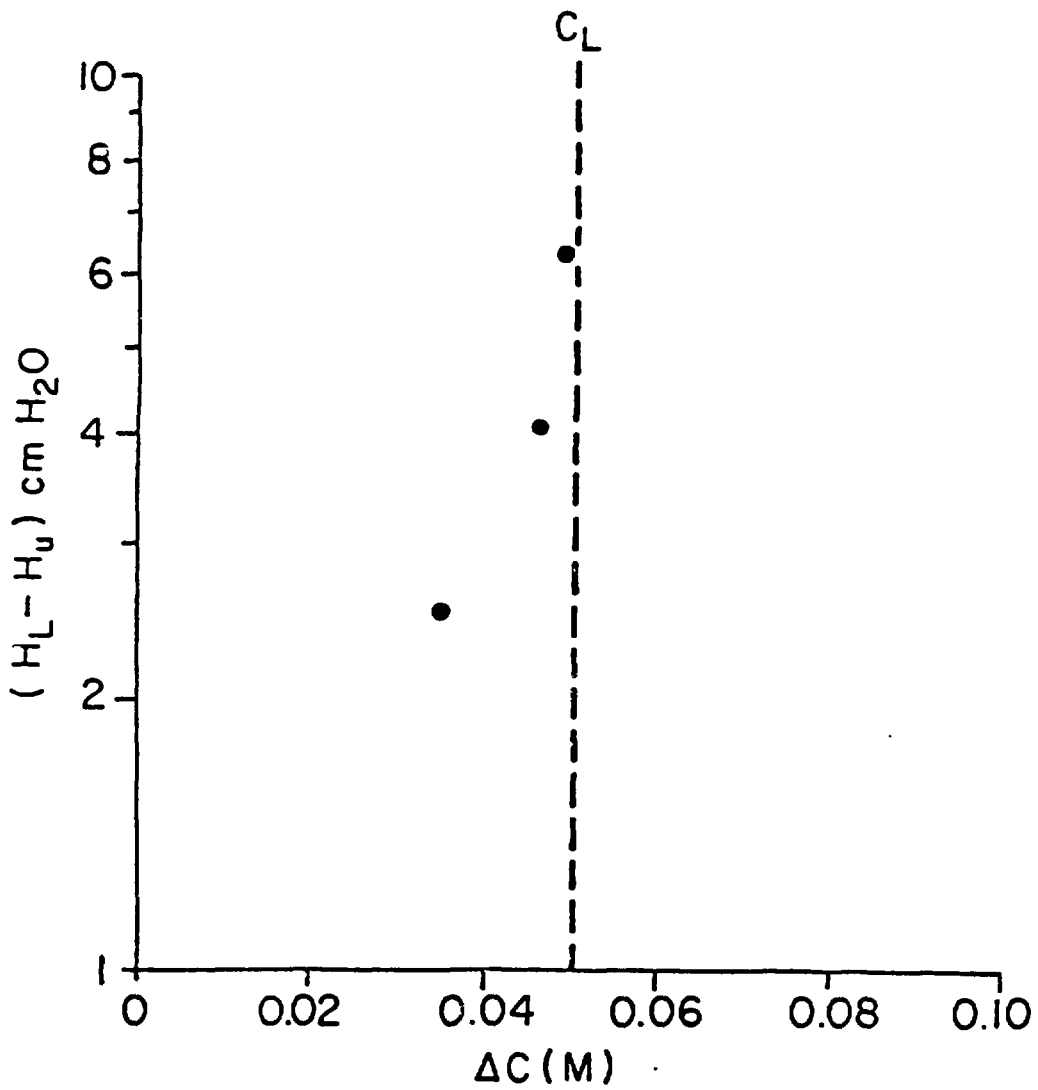
Fig. III.A.10. Head difference between upper and lower reservoirs vs
initial concentration difference after 45 h.

## 4. Electrical Properties of the Tuff

The fundamental similarity between molecular diffusion and electrical conductance through electrolyte solutions allows the use of measurements of the electrical resistance of saturated tuffs as a check on the results of the diffusion experiments. In addition, some properties of the tuffs which affect molecular diffusion may be measured more effectively using electrical methods. To these ends, six tuff discs used in the diffusion experiments were sent to Zonge Engineering of Tucson, Arizona, for measurements of their direct-current resistivity (d-c) and alternating-current (a-c) impedance at frequencies from 0.01 to 100 Hz.

Prior to measurement of their electrical properties, the tuff discs were soaked in J-13 water for several weeks, however, most of the samples had previously been used in diffusion experiments and were already saturated. The electrical measurements were performed using procedures described by Zonge (1972). In essence, the procedure consists of placing the rock sample in the sample holder shown in Fig. III.A.11 where each end of the rock is in contact with water presumed to be typical of the pore fluid. A constant current, square wave of alternating polarity is then passed through the rock, and the induced polarization effects are computed from the impedance and phase shift of the wave as modified by its passage through the sample.

The measured values of bulk-rock resistance $(\rho_a)$ determined from the impedance at 0.01 or 0.1 Hz are shown in Table III.A.3. These values are essentially equivalent to the d-c resistance. The changes in impedance with increasing frequency are shown in Fig. III.A.12 in terms of the ratio of the impedance at the lowest frequency measured to that at each increasing frequency.
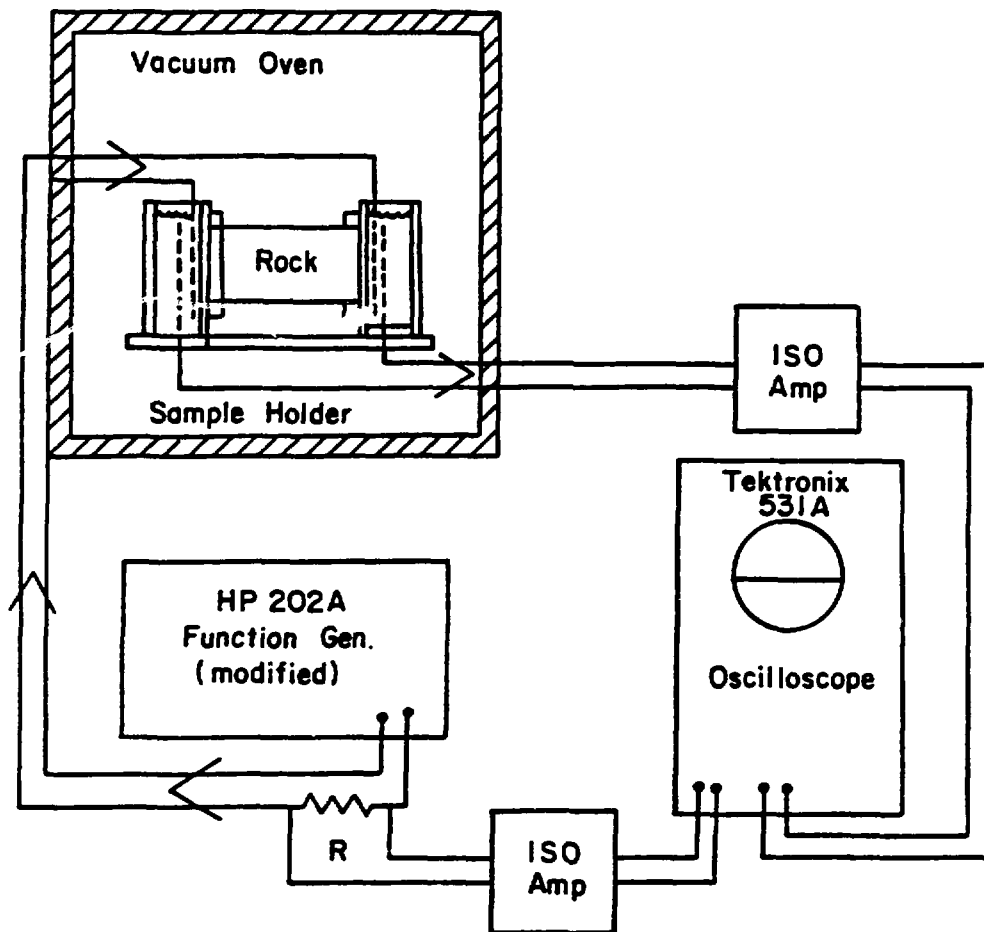
Fig. III.A.11.  Schematic drawing of the apparatus used for induced-
polarization measurements (Zonge, 1972).

TABLE III.A.3.  TORTUOSITIES OF SELECTED TUFF SAMPLES COMPUTED FROM BULK RESISTANCES (PORE-FLUID RESISTANCE) $\rho c$ = 13.5 ohm-m.

| Sample | Bulk Resistance (ohm-m) | Total Porosity | Tortuosity (T) |
|---|---|---|---|
| U12G-RNM#9 0.8 ft to 1.0 ft (sample A) | 43.3 | 0.35* | 1.26 |
| U12G-RNM#9 5.9 ft to 6.4 ft (side B) | 60.2 | 0.33 | 2.17 |
| U12G-RNM#9 16.2 ft to 17.5 ft (sample A) | 31.7 | 0.40 | 0.88 |
| G1-2290 | 133.7 | 0.31 | 9.42 |
| G1-2333 (sample 2) | 60.4 | 0.37 | 2.74 |
| G-2901 | 134.5 | 0.19 | 3.58 |

*estimated
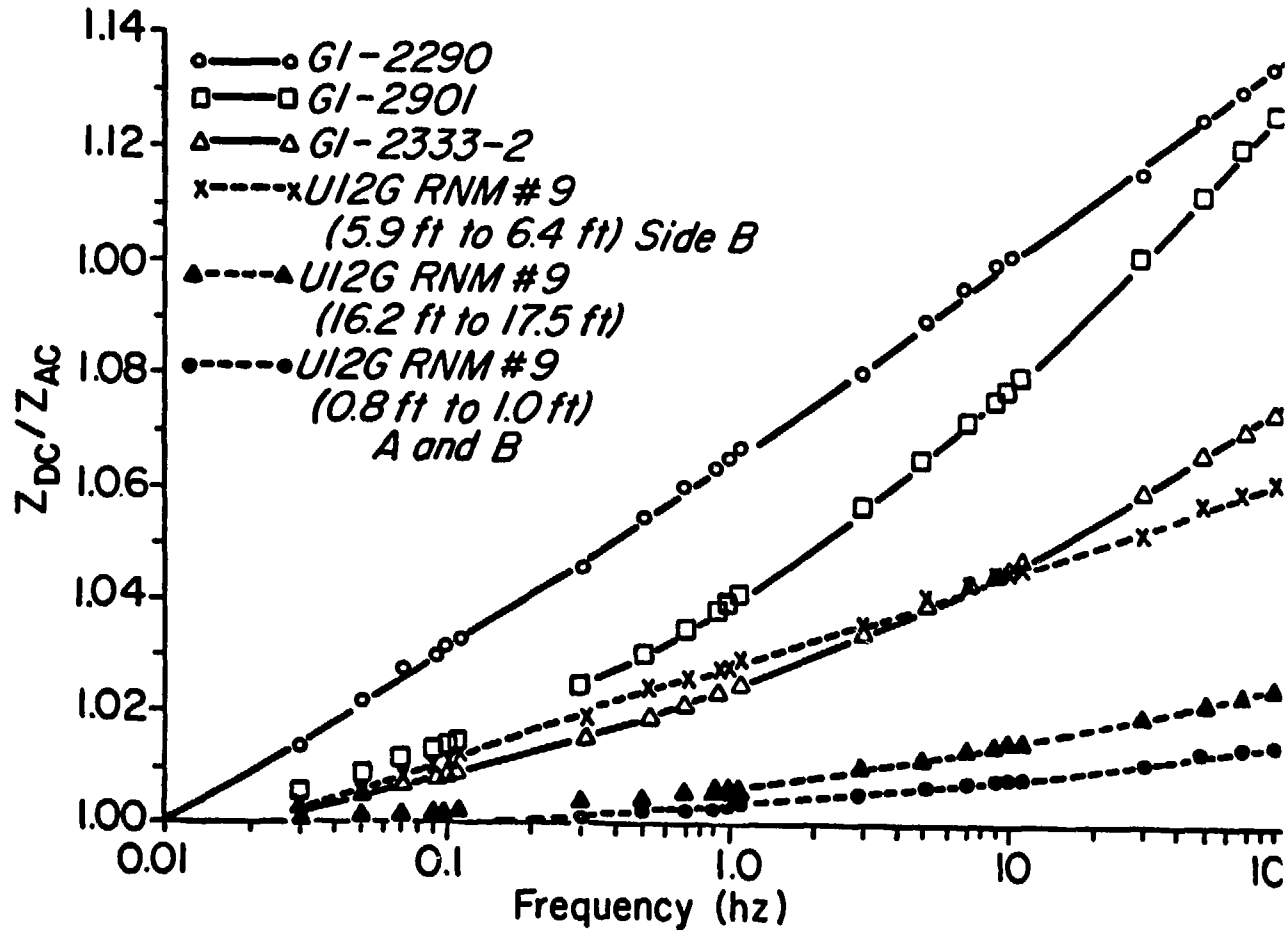
**Fig. III.A.12.** Ratio of d-c impedance to a-c impedance versus frequency for tuff samples.

The bulk-rock resistances shown in Table III.A.3 provide an independent check on the parameter $\alpha/\tau^2$ which was introduced as an empirical coefficient which, along with porosity, relates the effective-diffusion coefficient to the free aqueous-diffusion coefficient. For a rock which does not contain highly conductive minerals and is fully saturated, Wyllie and Spangler (1952) have related the bulk resistance to the resistance of the pore fluid, $\rho_c$, by

$$\rho_a = (T^{1/2}/\phi)\, \rho_c \qquad\qquad\qquad (III.A.4)$$

where

T is an empirical parameter often called "tortuosity" but not necessarily identical to $\tau$.

To the extent that the same factors which control molecular diffusion through the tuffs also control electrical conduction, we may equate T in Eq. (III.A.4) with $\tau$ in Eq. (II.B.2).

Given this assumption, the values of $\ell_a$ and the porosities of the tuff discs estimated from porosities measured from other samples from the same core section were used to compute the values of T shown in Table III.A.3. In making these calculations, the pore fluid in the disc was assumed to have the same specific resistance as J-13 which was measured to be 13.50 ohm-m. The computed value of T for U12G-RNM#9 (16.2 ft to 17.5 ft, sample A) is obviously incorrect because T must be greater than 1. This anomaly may be due to any of the following causes: 1) short circuit in the resistance cell, 2) a pore fluid more conductive than J-13 water, or 3) an erroneous value for porosity.

The change in impedance with frequency (Fig. III.A.12) can also be used to gain additional insights into the factors affecting conduction and diffusion through the tuffs. Marshall and Madden (1959) proposed a model describing IP effects in rocks containing no metallic minerals based on the membrane properties of the rock. Their model is based on the assumption that a porous rock may contain zones where the mobility of anions is less than that of cations due to the electrical surface charge on the mineral grains.

A schematic drawing of these zones in a granular rock is shown in Fig. III.A.13 where the constrictions between the grains are zones of low anion mobility due to overlapping electrical double layers. As discussed previously, the reduced anion mobility in the constrictions is at least one factor which contributes to the constrictivity factor, $\alpha$, in the relationship between the effective matrix-diffusion coefficient and the free aqueous-diffusion coefficient.

Based on this conceptual model, Marshall and Madden developed the following expression for the impedance of the rock at a given frequency and a pore solution containing a single monovalent salt

$$Z_i = \frac{\Delta x^h}{\mu_p^H mF} \quad t_p^H + \frac{B}{A} t_p^L$$

$$+ \frac{(S^L - S^H)^2}{\dfrac{\Delta x^H S^H}{(t_p^L)^2 (t_p^H) \tanh X^L} + \dfrac{A}{B} \dfrac{\Delta x^L S^L}{t_p^L (t_p^H)^2 \tanh X^H}}$$

(III.A.5)
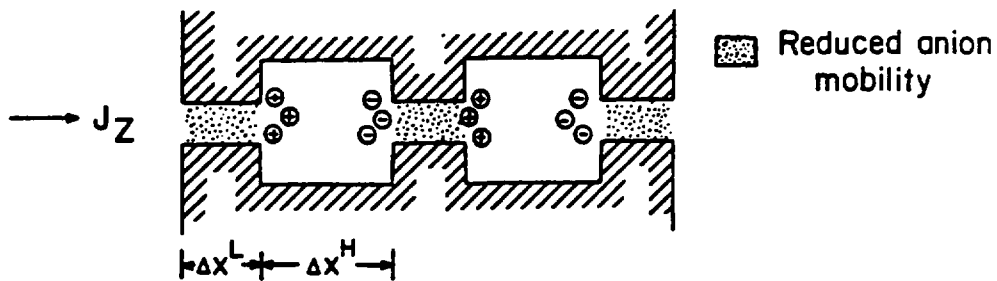
Fig. III.A.13.   Conceptual model of reduced anion mobility zones in
a porous rock (after Marshall and Madden, 1959).

where

$$X^j \text{ is } \left(\frac{i\omega}{2D_p^j t_n^j}\right)^{1/2} \frac{\Delta x^j}{2},$$

$A \text{ is } \Delta x^L/\Delta x^H,$

$B \text{ is } D^H/D_p^L,$

$S_i \text{ is } t_n^i/t_p^i,$

$\omega$ is the angular frequency,

$i$ is the $\sqrt{-1}$

$m$ is the total molar salt concentration,

$F$ is Farraday's constant,

$\mu_p^H$ is the mobility of the cation in the ion selective zone,

$t_p^H$, $t_p^L$ is the transport numbers for the cation is the high and low mobility zones, respectively,

$D_p$ is the diffusion coefficient of the cation, and

$T_n$ is the transport number for the anion.

For the steady-state direct-current conductance, Marshall and Madden have also derived the following equation

$$\sigma_{dc} = \frac{F u_p^H m}{\Delta x^H} \frac{\frac{1}{t_n^L} + \frac{A}{B}\frac{1}{t_n^H}}{S^H (1 + \frac{B}{A}) + S^L (1 + \frac{A}{B})} S^H S^L \qquad \text{(III.A.6)}$$

Multiplying Eq. (III.A.5) and Eq. (III.A.6) and taking the inverse gives the IP response at each frequency

$$Z_{dc}/Z_{ac} = \frac{S^H \left(1 + \frac{B}{A}\right) + S^L \left(1 + \frac{A}{B}\right)}{S^H S^L \frac{1}{t_n^L} + \frac{A}{B} \frac{1}{t_n^H}}$$

$$\left[ t_p^H + \frac{B}{A} t_p^L + \frac{(S^L - S^H)^2}{\frac{X^H S^H}{(t_p^L)^2 (t_p^H) \tanh X^L} + \frac{A}{B} \frac{X^L S^L}{t_p^L (t_p^H) \tanh X^H}} \right]^{-1}$$

In order to simplify further discussion, it is convenient at this point to replace the transport numbers by diffusion coefficients using the following definition

$$t_p = \frac{\lambda_p}{\lambda_p + \lambda_n} = \frac{D_p}{D_p + D_n}$$

Substituting Eq. (III.A.8) into Eq. (III.A.7) then gives

$$Z_{DC}/Z_i = \frac{\left[ \frac{D_n^H}{D_p^H} \left(1 + \frac{D_p^H}{D_p^L} \frac{\Delta X^L}{\Delta X^H}\right) + \frac{D_n^L}{D_p^L} \left(1 + \frac{D_p^L}{D_p^H} \frac{\Delta X^H}{\Delta X^L}\right) \right]}{\frac{D_n^H D_n^L}{D_p^H D_p^L} \left( \frac{D_p^L + D_n^L}{D_n^L} + \frac{D_p^L}{D_p^H} \frac{\Delta X^H}{\Delta X^L} \frac{D_p^H + D_p^H}{D_n^H} \right)}$$

$$\cdot\left\{\left[\frac{D_P^H}{(D_P^H+D_n^H)} + \frac{D_P^H}{D_P^L}\frac{\Delta X^L}{\Delta X^H}\frac{D_P^L}{(D_P^L+D_n^L)}\right.\right.$$

$$+\left(\frac{D_n^L}{D_P^L} - \frac{D_n^H}{D_P^H}\right)^2\cdot\left[\frac{\Delta X^H D_n^H}{D_P^H\left(\dfrac{D_P^L}{D_P^L+D_n^L}\right)^2\left(\dfrac{D_P^H}{D_P^H+D_n^H}\right)\tanh X_H}\right.$$

$$\left.\left.\left. +\left(\frac{X_H}{X^L}\frac{D_P^L}{D_P^H}\right)\frac{X^L D_n^L}{D_P^L\left(\dfrac{D_P^L}{D_P^L+D_n^L}\right)\left(\dfrac{D_P^H}{D_P^H+D_n^H}\right)^2\tanh X^L}\right]^{-1}\right\}^{-1}\right.$$

(III.A.9)

The model described by Eq. (III.A.9) has the property that as the frequency increases, the impedance decreases. This effect is largely due to fact that when frequencies become sufficiently high, the distance traveled by an ion during a half cycle is comparable or less than the length of the high mobility zone. At and above this frequency, the anions no longer see the effect of the constrictions and the impedance decreases very rapidly. Fig. III.A.14 shows a set of impedance curves computed from Eq. (III.A.9) for a range of parameters applicable to the tuffs. We had hoped to compare these curves with the experimental impedance curves shown in Fig. III.A.12 in order to estimate zone lengths and transport numbers in the tuffs. Obviously, the measured curves do not match any of the experimental curves. This is probably due to the fact that Eq. (III.A.9) assumes uniform zone lengths and transport numbers, while each tuff sample contains a range of zone lengths. This nonuniformity results in a dispersion of the impedance effect over a broad range of frequencies. Nevertheless, the impedance
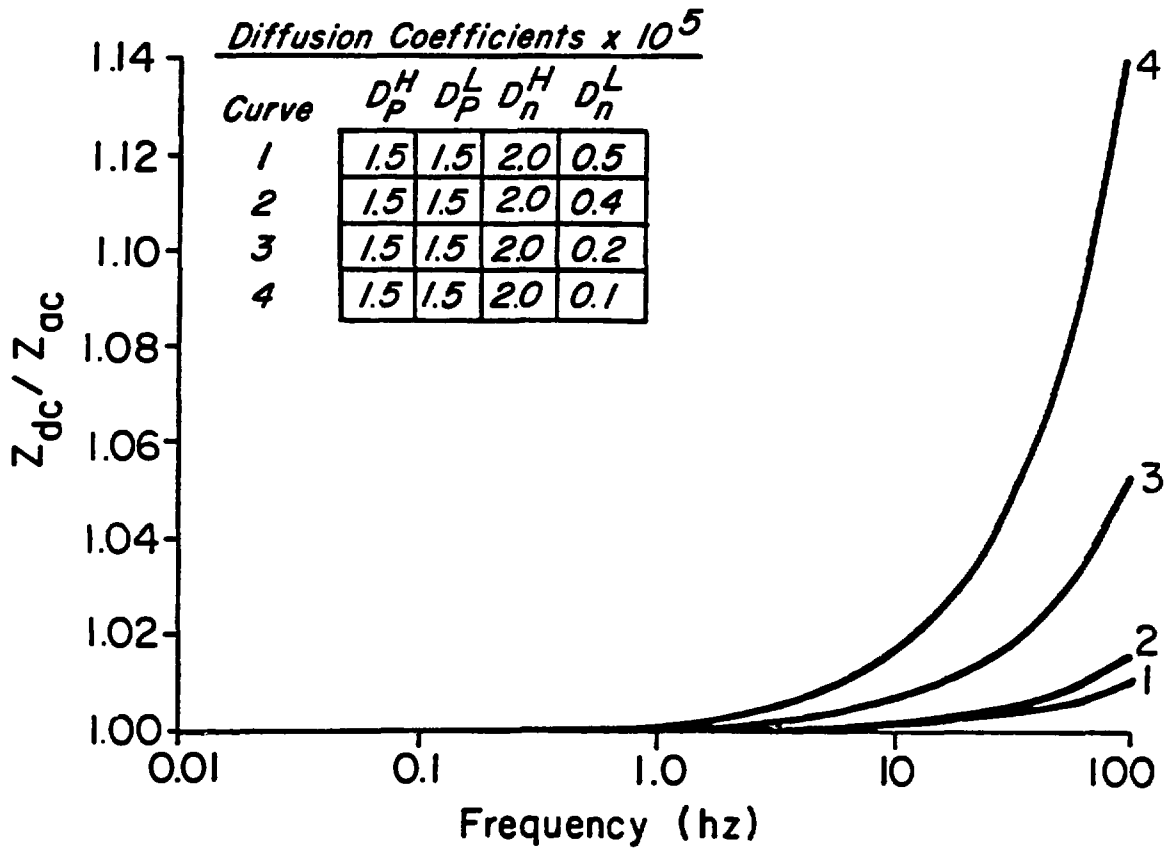
Fig. III.A.14. Theoretical changes in a-c impedance with frequency for a typical NTS tuff.

effects and frequencies predicted by Eq. (III.A.9) using reasonable guesses at zone length and diffusion coefficients, support the proposition that the observed frequency effects are due to restricted ion mobility.

Despite the failure of the theoretical curves to match the observed impedance curves, some information can still be gleaned from these data. In theory, when the frequency becomes very high, the impedance ratio in Eq. (III.A.9) will reach a plateau value at which point the effect of the constrictions on ion mobility will no longer be seen. At this point, the apparent "tortuosity" factor, $T$, in Eq. (III.A.4) should approach the true tortuosity, $\tau$, and we can rewrite Eq. (III.A.4) as

$$\rho_{AC} = (T^{1/2}/\phi)\rho_c \qquad\qquad (III.A.10)$$

Assuming that $\alpha$ goes to 1 as the frequency increases, Eq. (III.A.10) can be rewritten as

$$\rho_{AC} = (\tau/\phi)\rho_c \qquad\qquad (III.A.11)$$

and Eq. (III.A.4) becomes

$$\rho_{DC} = \frac{\tau}{\alpha^{1/2}\phi}\,\rho_c \qquad\qquad (III.A.12)$$

Equating the a-c impedances with resistance (Marshall and Madden, 1959) we divide Eq. (III.A.12) by Eq. (III.A.11) to get

$$z_{DC}/z_{AC} = \frac{\rho_{DC}}{\rho_{AC}} = \alpha^{-1/2} \qquad\qquad (III.A.13)$$

60

Using Eq. (III.A.13) we can estimate the minimum contribution of restricted anion mobility to the constrictivity factor from the maximum frequency effect in Fig. III.A.12. This value then gives a maximum estimate of the constrictivity because the maximum frequency effects had not been reached at 100 Hz. The values for $\alpha$ computed in this way are shown in Table III.A.4.

### 5. Discussions of Results

The primary purpose of the experimental measurements described above was to measure the rock properties which must be known to model matrix diffusions in the tuffs. In addition, the experimental results provide a basis for evaluating the extent to which effective matrix-diffusion coefficients can be predicted from free aqueous-diffusion coefficients and the properties of the rock as defined by

$$D_e = (\theta\alpha/\tau^2)D_0 \qquad\qquad (III.A.14)$$

To accomplish this, we will consider the rock properties listed in Table III.A.5 for tuff samples on which porosity, pore-size distributions, effective diffusion coefficients, and electrical resistance have been measured. The values of total porosity and median pore diameter were determined by methods described above and need no comment. The values of the effective-diffusion coefficient are those measured for sodium-halide salts as indicated by the comment numbers.

The values for $\alpha/\tau^2$ were computed by dividing the effective-diffusion coefficient by the total porosity and a free aqueous-diffusion coefficient of $1.5 \times 10^{-5}$ cm$^2$/s for sodium- halide salts. The use of a single sodium-

TABLE III.A.4.  MAXIMUM FREQUENCY EFFECT AND MAXIMUM $\alpha$ FROM IP MEASUREMENTS.

| Sample | Maximum $(Z_{DC}/Z_{AC})$ | $\alpha$ |
|---|---|---|
| U12G-RNM#9<br>0.8 ft to 1.0 ft<br>(sample A) | 1.015 | 0.97 |
| U12G-RNM#9<br>5.9 ft to 6.4 ft<br>(side B) | 1.063 | 0.88 |
| U12G-RNM#9<br>16.2 ft to 17.5 ft<br>(sample A) | 1.015 | 0.97 |
| U12G-RNM#9<br>16.2 ft to 17.5 ft<br>(sample B) | 1.025 | 0.95 |
| G1-2333<br>(sample 2) | 1.077 | 0.86 |
| G1-2290 | 1.140 | 0.76 |
| G1-2901 | 1.132 | 0.78 |

TABLE III.A.5. POROSITY DIFFUSION AND PORE-SIZE DATA FOR
SELECTED SAMPLES OF NTS TUFFS

| Sample | Total Porosity | $D_e$ (x10$^7$ cm$^2$/s) | Comment | $\alpha/\tau^2$ | $\tau$ | Median Pore Diameter ($\mu$m) |
|---|---|---|---|---|---|---|
| G1-2290 (sample 1) | 0.331 | 6.2 ± .4 | e | 0.12 | 2.5 | 0.21 |
| G1-2333 (sample 1) | 0.364 | 11 ± 2 | e | 0.20 | 2.1 | 1.17 |
| G1-2333 (sample 2) | 0.364 | 16.8 ± .1 | e | 0.31 | 1.7 | 1.17 |
| G1-2840 (sample A) | 0.269 | 5.9 | a | 0.15 | NA | 0.30 |
| G1-2840 (sample B) | 0.269 | 5.4 | b | 0. 13 | NA | 0.30 |
| G1-2901 | 0.194 | 4.2 | c | 0.14 | 2.4 | 0.55 |
| U12G-RNM#9 (16.2 ft-17.5 ft) (sample A) | 0.405 | 10.8 | d | 0.18 | 2.3 | 0.1 |

a   mean of NaI and NaSCN
b   mean NaBr, NaI, NaSCN
c   mean NaSCN, NaBr
d   NaI
e   NaBr

halide diffusion coefficient is an acceptable approximation because the sodium salts of halides and pseudohalides such as thiocyanate have free aqueous-diffusion coefficients which differ by less than 5%.

The values of $\tau$ shown in the second to the last column in Table III.A.5 were obtained by correcting $\alpha/\tau^2$ using the values of constrictivity ($\alpha$) estimated from the a-c impedance of these rock and listed in Table III.A.4.

The measured effective-diffusion coefficients are plotted versus total porosity in Fig. III.A.15. Only a fair correlation (r = 0.75) exists betweeen these parameters. If the anomalously high value for G1-2333 (sample 2) is ignored, the regression coefficient rises to 0.90. The regression line shown in Fig. III.A.14 was determined by ignoring the G1-2333 (sample 2).

As for the parameter $\alpha/\tau^2$, a fair correlation (r = 0.75) seems to exist between this parameter and the median pore diameter as shown in Fig. III.A.16. This correlation probably exists because the variance $\alpha/\tau^2$ is primarily due to the constrictivity which is a function of pore diameter. As can be seen in Table III.A.5, the estimated values for the tortuosity ($\tau$) are rather uniform.

With regard to these values of tortuosity, they are somewhat higher than one would predict. For example, theoretical values for tortuosity computed from packed-sphere porous-media models range from 1.4 to 1.7 (Van Bratel and Heertjes, 1974). This discrepancy may in part be due to the fact that the values of constrictivity computed from the impedance measurements are maximum values and the true constrictivities are almost certainly lower. Also, scanning-electron photomicrographs of samples of the tuff show that their pore structures are very tortuous and differ significantly from the
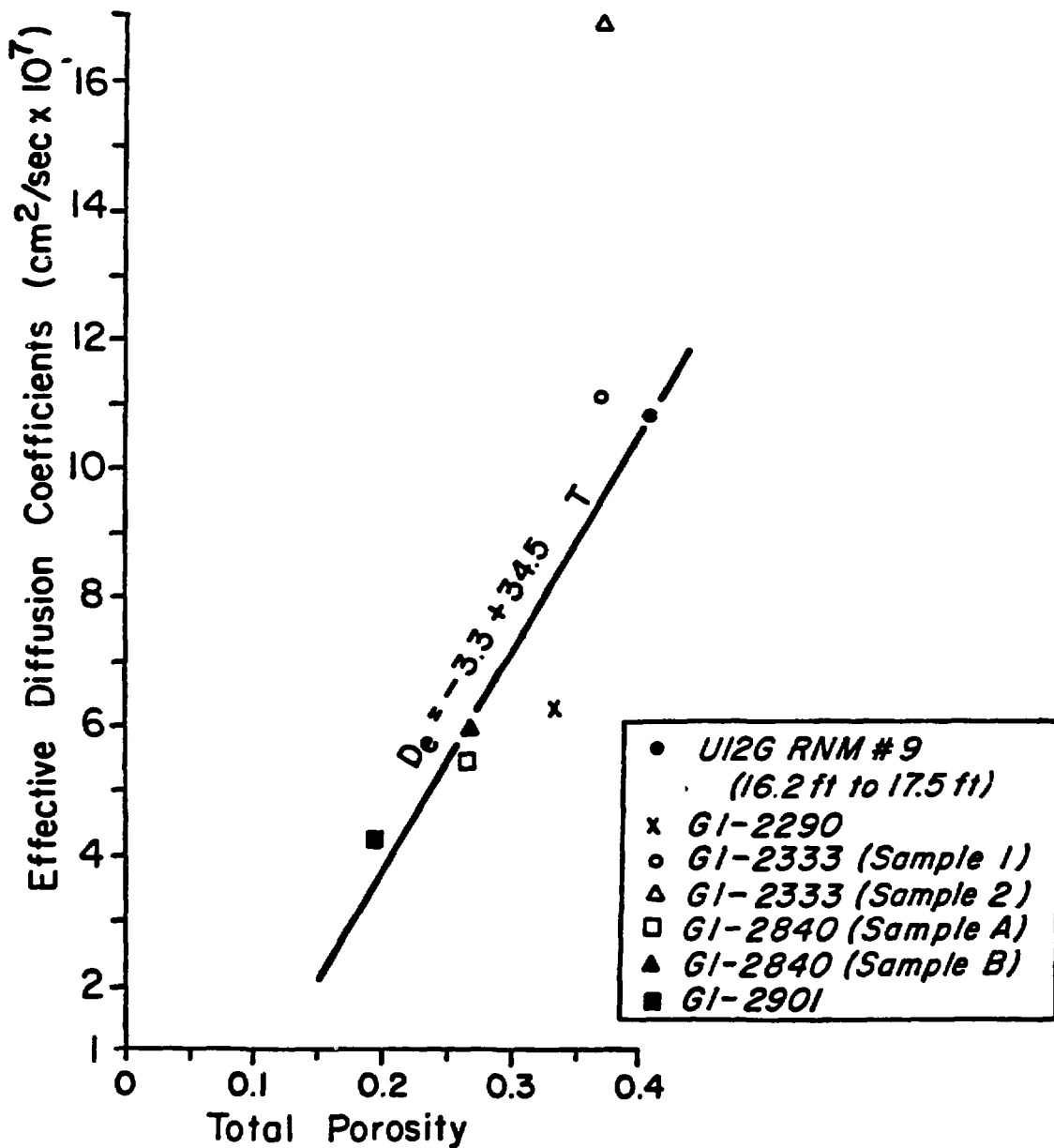
Fig. III.A.15. Effective sodium halide diffusion coefficients versus total porosity.

● *U12G RNM #9 (16.2 ft to 17.5 ft)*
× *GI-2290*
○ *GI-2333 (Sample 1)*
△ *GI-2333 (Sample 2)*
□ *GI-2840 (Sample A)*
▲ *GI-2840 (Sample B)*
■ *GI-2901*

$$\alpha/\gamma^2 = 0.12 + 0.11\,d_m$$

$\alpha/\gamma^2$

0.3
0.2
0.1
0

0   0.2   0.4   0.6   0.8   1.0   1.2

Median Pore Diameter ($\mu$m)
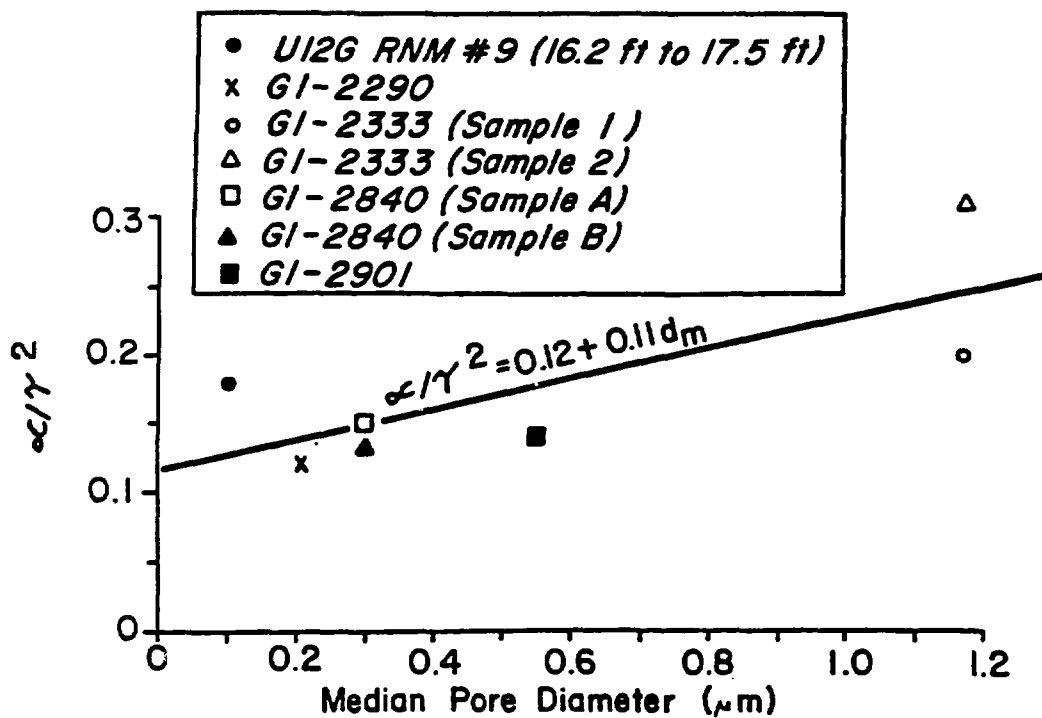
Fig. III.A.16.   The parameter $\alpha/\tau^2$ versus median pore diameter.

structure of a packed-sphere porous media. Selected photomicrographs are shown in Appendix D.

## B. TRACER CHARACTERIZATION

In addition to evaluating the diffusion properties of the tuff, an important aspect of this project is to characterize the physical and chemical properties of the fluorobenzoate tracers which affect their use in matrix-diffusion experiments. Experiments were conducted to determine the acid dissociation constants of the fluorobenzoic acids, their complexation behavior, their free aqueous-diffusion coefficients, and their sorption behavior with respect to the tuffs.

### 1. Acid Dissociation Constants

The dissociation constants of the five fluorinated benzoic acid tracers were determined by potentiometric titrations using an Altex PHI 71 pH meter and double-junction glass-membrane electrode. Accurate values for the pKa's of these tracers are necessary to predict their diffusion properties.

All titrations were performed using a $9.700 \times 10^{-3}$ M NaOH solution prepared with water distilled over $KMnO_4$ and degassed with nitrogen. Potassium chloride was added to the solution to adjust the ionic strength to 0.1. The base solution was stored in a 5 L polyethylene bottle wrapped with aluminum foil. The base was stored under a nitrogen atmosphere. Solutions of primary-standard potassium-acid phthalate and the fluorinated benzoic acids were prepared in a similar manner with their ionic strengths adjusted to 0.1 using KCl. The concentrations of the acids ranged from $4 \times 10^{-3}$ M for the weakest and least soluble acid to $10^{-2}$ M for the strongest.

The titrations were performed under a nitrogen atmosphere using the apparatus shown in Fig. III.B.1. The pH electrode was standardized with
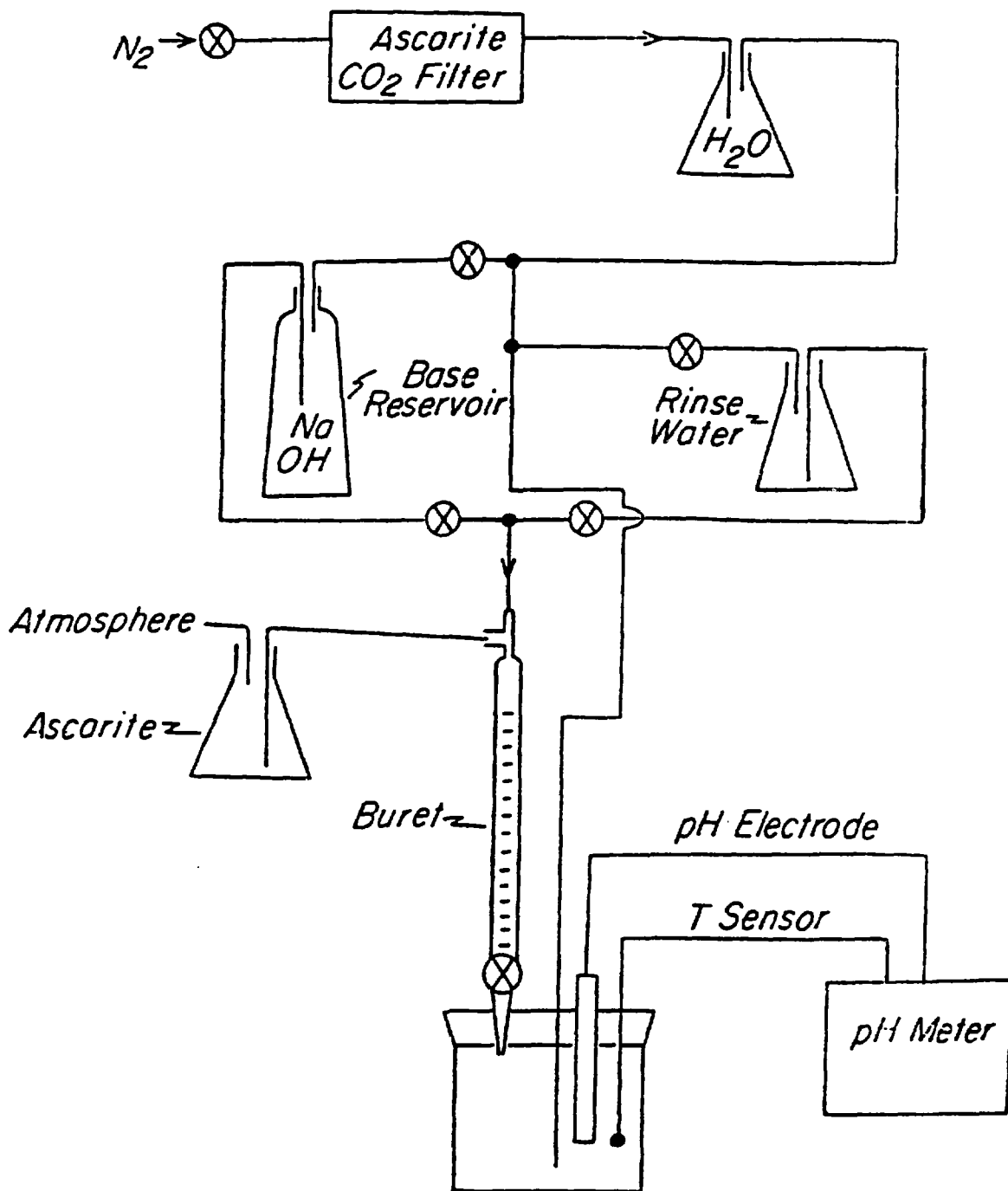
Fig. III.B.1. Apparatus for performing pH titrations under nitrogen atmospheres.

Curtin Matheson pH 4 and pH 7 buffer solutions. The base solution was standardized against the potassium-acid phthalate solutions.

The dissociation constants for the acids were then determined from the titration curves using the following mass-balance and mass-action equations

$$K_a = \frac{a_{H+} \, a_{A-}}{a_{HA}} \qquad\qquad (III.B.1)$$

$$m_{HA} = F_{HA} - m_{H^+} + m_{OH^-} - F_{B^-} \qquad\qquad (III.B.2)$$

$$m_{A^-} = F_{B^-} + m_{H^+} - M_{OH^-} \qquad\qquad (III.B.3)$$

$$a = \gamma m \qquad\qquad (III.B.4)$$

where

        a is the activity,

        m is the molarity,

        F is the formal concentrations,

        $\gamma$ is the the activity coefficient,

        HA is the undissociated acid,

        $H^+$ is the hydrogen ion,

        $A^-$ is the acid anion,

        $B^-$ is the base, and

        OH is the hydroxide ion.

Eq. (III.B.1,2,3 and 4) are combined to give

$$K_a = \frac{a_{H^+} \, \gamma_{A^-} \, (F_B + a_{H^+}/\gamma_{H^+})}{\gamma_{HA} \, (F_{HA} - a_{H^+}/\gamma_{H^+} - F_{13^-})} \qquad\qquad (III.B.5)$$

The activity coefficients $\gamma_{H^+}$, $\gamma_{A^-}$, and $\gamma_{HA}$ used in the calculations were 0.83, 0.77 and 1.0, respectively (Kielland, 1928). The dissociation constants were determined by solving Eq. (III.B.5) for four to five points in the buffer region of the titration curve. The computed pKa's are given in Table III.B.1 with their standard errors and the reported values. The relative strengths of the acids can be qualitatively predicted from the expected stability of the respective anions, or the ability of each to accommodate the negative charge. The charge of the benzoate ion is distributed over most of the molecule through resonant stabilization. All the possible resonant structures can be represented by the hybrid shown in Figure III.B.2.

When an electron-withdrawing fluorine is added to the ring, the ability of the ring to accept the charge from the carboxyl group is enhanced. The effect of electron-withdrawing substituents diminishes with distance and this tendency is observed with the o, m, and p isomers. The three fluorines attached to the m-methyl group in m-trifluoromethylbenzoic acid produce an electron-deficient carbon which in turn withdraws electrons from the ring about the same as the single fluorine. As expected, the fully substituted pentafluorobenzoic acid is the strongest acid by two orders of magnitude. The pKa of pentafluorobenzoic acid is lower than previously reported possibly because of poor standardization of the electrode below pH 4. The reproducibility of values at different points in the titration was less than for the weaker acids. The only explanation of the disagreement between repeated and measured values for the orthofluorobenzoic acid is impurities in the acid.

71
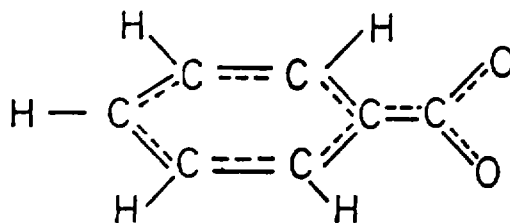
Fig. III.B.2. Resonance hybrid structure for benzoate anion.

## TABLE III.B.1. MEASURED AND REPORTED pKa's
## FOR FLUOROBENZOIC ACIDS

| Acid | pKa Reported (25°C) | pKa Measured (23°C) |
|------|---------------------|---------------------|
| Benzoic | 4.19[a] | 4.18 ± .01 |
| p-fluorobenzoic | 4.04[b] | 4.13 ± .01 |
| m-fluorobenzoic | 3.85[b] | 3.82 ± .01 |
| o-fluorobenzoic | 2.90[b] | 3.42 ± .02 |
| m-trifluoromethylbenzoic | - | 3.79 ± .01 |
| pentafluorobenzoic | 1.73[c] | 1.49 ± .02 |

[a]Handbook of Chemistry and Physics.

[b]Kuhn and Wasserman (1928).

[c]Ryan and Berner (1969).

## 2. Complexation Behavior

To evaluate the possibility of complexation between the fluorobenzoate tracers and transition metals, a series of titrations were performed where solutions of the sodium and potassium salts of the fluorobenzoates were added to solutions of $Cu^{+2}$, $Ag^+$, and $Pb^{+2}$. During the titrations, the metal-ion activities were monitored with their respective ion-selective electrodes. A complex series of reactions was observed which resulted in either precipitation of metal fluorobenzoate or metal hydroxides depending on the pH of the solution. We also observed that the solubility of the metal fluorobenzoates increased with the acidity of the corresponding fluorobenzoic acid. We did not, however, observe changes in the metal-ion activities which might be interpreted as complexation or ion pairing. For this reason we have discontinued these studies.

## 3. Free Aqueous Diffusion Coefficients

Given the accuracy with which we can measure the effective matrix-diffusion coefficients, calculation of the free aqueous-diffusion coefficients of the fluorobenzoate tracers from their limiting ionic conductances was determined to be sufficiently accurate. At the pH's and concentrations under consideration, the tracers are completely dissociated and behaved as strong 1:1 electrolytes. Based on data and calculations given by Robinson and Stokes (1959) and our own calculations, free aqueous-diffusion coefficients computed from ionic conductances differ by no more than 5% from directly measured diffusion coefficients.

The limiting ionic conductance of an ion is defined as its equivalent ionic conductance at infinite dilution. These values for the fluorobenzoate anions were determined by measuring the molar conductances of their sodium

and potassium salts at various concentrations. For strong electrolytes such as these, the molar conductance is described by the empirical equation (Moore, 1972)

$$\Lambda = \Lambda_0 - k_c \, c^{1/2} \qquad\qquad \text{(III.B.6)}$$

where

$\Lambda$ is the molar conductance,

$\Lambda_0$ is the molar conductance at infinite dilution,

$k_c$ is an experimental constant, and

$c$ is the molar concentration.

The sodium and potassium salts of the fluorobenzoic acids were prepared by titrating the acids with the appropriate base to the equivalence points. The resulting salt solution was then used to prepare more dilute solutions. The conductivities of these solutions were measured using the apparatus shown in Fig. III.B.3. The temperature bath was set at $25 \pm .05°C$ and the values of $\Lambda_0$ for the salt solutions were determined by regression techniques. The limiting ionic conductance of the anion was then computed from the Kohlrausch's Law of the Independent Migration of Ions

$$\Lambda_0 = \Lambda_0^+ + \Lambda_0^- \qquad\qquad \text{(III.B.7)}$$

where $\Lambda_0^+$ for sodium and potassium ions are known.

The resulting values for the limiting ionic conductances and computed diffusion coefficients are listed in Table III.B.2. Based on the differences between the measured values and the published values for benzoate and p-fluorobenzoate, the error in the other measured values may be about 7%. We do not know the source of this error, but this level of accuracy seems

75
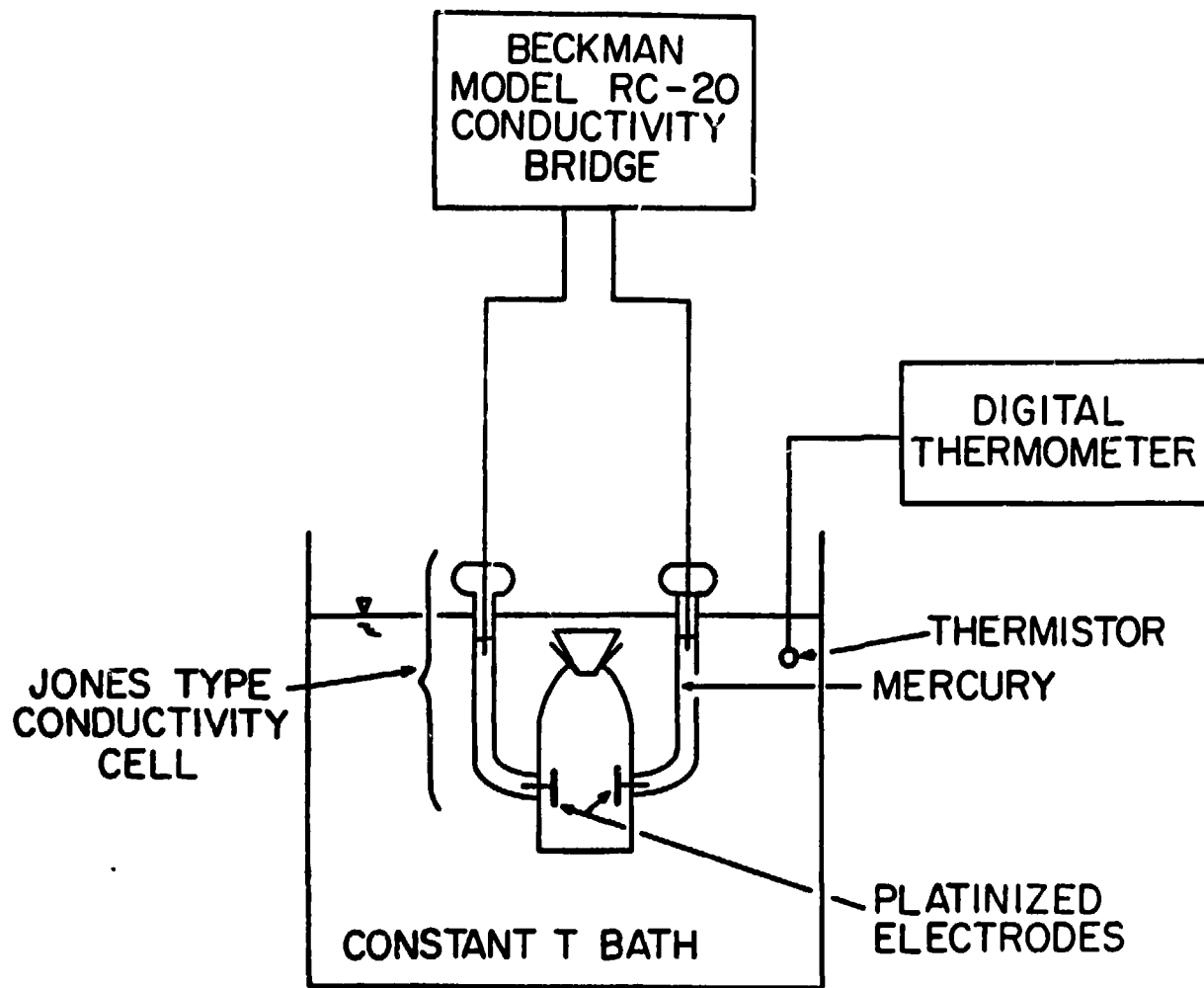
Fig. III.B.3.  Schematic drawing of apparatus used for electrical conductivity measurements.

adequate for our purposes. The resulting values for the free aqueous-diffusion coefficients at infinite dilation are also shown in Table III.B.2. These values were computed by the Nernst expression (Robinson and Stokes, 1959)

$$D_0 = \frac{RT\lambda_0}{|Z|F^2} \tag{III.B.8}$$

where

$R$ is the gas constant,

$T$ is absolute temperature,

$\lambda_0$ is the limiting ionic conductance,

$Z$ is ionic change, and

$F$ is Faraday's constant.

TABLE III.B.2.  LIMITING IONIC CONDUCTANCES FOR BENZOATE AND
FLUOROBENZOATES WITH COMPUTED DIFFUSION COEFFICIENTS ($D_o$).

| Species | Published | Measured | $D_o$ |
|---|---|---|---|
| | | $\Lambda_o \dfrac{cm^2}{(ohm\text{-}eq.)}$ | |
| benzoate | 32.38 | 30.8 | $0.82 \times 10^{-5}$ |
| p-fluorobenzoate | 33.00 | 35.0 | $0.93 \times 10^{-5}$ |
| m-fluorobenzoate | - | 30.0 | $0.80 \times 10^{-5}$ |
| o-fluorobenzoate | - | 30.5 | $0.81 \times 10^{-5}$ |
| m-trifluoromethylbenzoate | - | 27.9 | $0.74 \times 10^{-5}$ |
| pentafluorobenzoate | - | 27.1 | $0.72 \times 10^{-5}$ |

## 4. Sorption Properties of the Fluorobenzoate Tracers

The adsorption of benzoate, m-trifluoromethylbenzoate, pentafluoro-
benzoate, bromide, o-, m-, and p-fluorobenzoate on tuff sample HF23 at a
concentration of 8.3 x $10^{-5}$ M in J-13 water was investigated.
The adsorption studies were performed in 50 ml jars with screw cap lids.
Each jar contained 14 g of the tuff, ground and sieved through a 270 mesh
screen. The void space was then evacuated and 30 mls of solution was added
(Fig. III.B.4) under low vaccuum (~4 in Hg). Each jar was then shaken and a
1/2 ml sample was withdrawn, filtered, and injected through a 10 ml sample
loop The LC column was 25 cm x 1/4 in packed with partisil-10 SAX. The
detector was a Hitachi model 1040 at 200 mm. The mobile phase was a 0.01 M
$H_3PO_4$, $H_2PO_4$ buffer at pH 4.

Two batch solutions were used. One contained p-, m-, and pentafluoro-
benzoate and the other contained bromide, benzoate, o-fluorobenzoate and
m-trifluoromethylbenzoate. Each batch was compared to an identical
solution with only the tuff excluded after each injection. Samples were
collected and analyzed at 10, 100, 1000, and 10,000 minutes. Excluding the
first sampling, each solution was shaken thoroughly for 30 minutes before
sampling.

No adsorption greater than the reproducibility of the analytical
technique was observed. An increase in the peak area of the first eluting
peak relative to the blank was observed for each batch and attributed to the
increased background. Peak heights above a corrected base line remained
constant. Incidental to the adsorption studies, nitrate concentrations were
also measured. In each batch a three-fold increase in the nitrate
concentration relative to the blank was also observed. The pH was observed
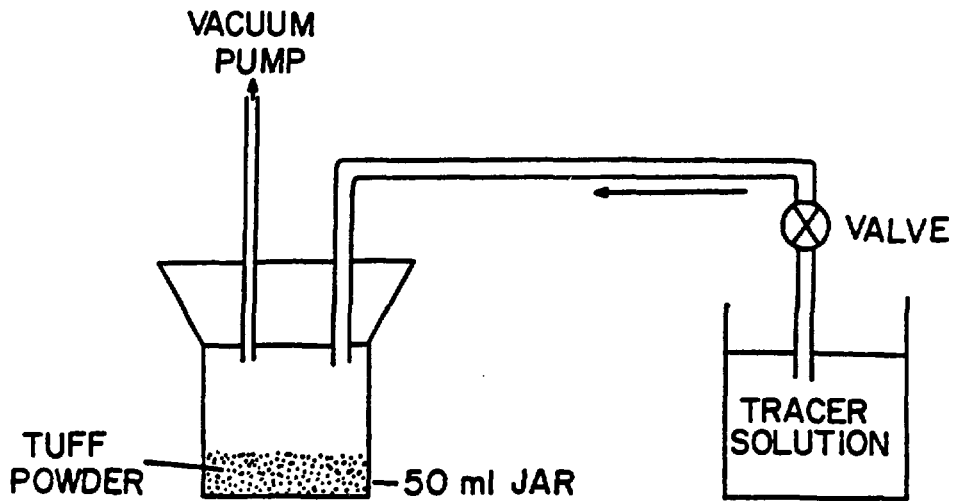
Fig. III.B.4.  Apparatus for filling and degassing tuff sample used
              in batch sorption tests.

to remain constant during the test.

## 5. Tracer development

Two bacteriophages, F2 and MS2, are being investigated to use as groundwater tracers in fractured rock. This work is being done with the aid of the laboratory of Dr. C. Gerba and D. Zink in the Department of Nutrition and Food Science at the University of Arizona.

The choice of phages MS2 and F2 as likely candidates stems from previous sand-column experiments testing the mobility of viruses and from recently completed laboratory experiments that used polystyrene columns to test the relative charges of several viruses. These two bacteriophages are negatively charged. Initial stability tests have shown that both viruses are viable for several days in groundwater having a pH between 7.0 and 8.0 and containing sodium, calcium, chloride, silica, carbonate species, and other minor constituents (total dissolved solids, ~400 ppm). The phage F2 has been shown to be extremely mobile, even more so than MS2. However, the MS2 phage might have a slightly greater half life in a groundwater environment. These phages are tailless, symmetrical polyhedrons having an approximate diameter of 30 nm. They are RNA bacteriophages and are not pathogenic.

An initial quantity of the F2 bacteriophage was prepared and purified, which yielded a small volume (~20 ml) of $10^{12}$ plaque-forming units per millileter (pfu/ml). This volume is a measure of the amount of viable virus present in a preparation. Starting with this preparation of F2 phage, antibodies specific to the F2 phage were prepared using rabbits. The purified rabbit sera yielded an extremely active antibody titer. The activity of this rabbit sera antibody preparation is approximately 1:5,000,000. One milliliter of sera will inactivate 5000 liters of water

containing $10^7$ pfu/ml of the F2 phage.

The rabbit sera antibodies are to be used in two techniques for the detection and quantification of the bacteriophage F2. One technique will be the ELISA test. This well-documented, antigen-antibody reaction utilizes a visible dye marker that can be covalently bonded to the antibody so that when any antigen bacteriophage is present, the test solution will become yellow. The ELISA test requires a considerable amount of sample handling but can be easily adapted for use in the field. The ELISA test can be performed with small sample volumes (100 μl).

The other use for the F2 specific antibodies will involve high performance liquid chromatography, which should be faster than the ELISA test, more easily performed, and also enable greater ease in quantification of the bacteriophage in a sample. A fluorescent compound will be covalently bound to the antibody, and the antibody will react with the bacteriophage to produce a fluorescent bacteriophage-antigen complex. This complex will be detected and measured by high performance liquid chromatography using a fluorescence detector. The chromatographic technique will allow quantification of the amount of the specific bacteriophage present in a test volume without interference from the unreacted antibody-fluorescent dye complexes. Chromatographic columns packed with 40-μm glass beads should provide enough separation, as bacteriophages readily change their retention on glass as a function of pH.

## IV. THEORETICAL AND NUMERICAL EVALUATION OF MULTICOMPONENT EFFECTS

As mentioned in section II, multicomponent diffusion effects add a complexity to the problem of matrix diffusion which has not been addressed in previous models. The purpose of this section is to develop multicomponent diffusion-flux equations in a form suitable for incorporation into a model of matrix diffusion of reactive, ionic species.

### A. Multicomponent Diffusion Equation

Consider molecular diffusion in an isothermal, aqueous solution with no external electric potentials consisting of N component ions which may combine to form M binary complexes or ion pairs according to Eq. (IV.A.1)

ith reaction $(C_{j\nu_{ij}} A_{k\nu_{ik}})^{Z_i} =$

$$\sum_{j=1}^{J} \nu_{ij} C_j + \sum_{k=1}^{k} \nu_{ik} A_k; \quad i = 1 \text{ to } M, \ J + K = N \qquad (IV.A.1)$$

where

$C_j$ is the $j^{th}$ cation component,

$A_k$ is the $k^{th}$ anion component,

$\nu_{ij}$ is the stoichiometric coefficient of the $j^{th}$ component in the $i^{th}$ complex, and

$Z_i$ is the charge of the $i^{th}$ complex.

Following the development of Wendt (1965), the chemical potentials of the complexes are given by

$$\mu_i = \sum_{n=1}^{N} \nu_{in} \mu_n \qquad (IV.A.2)$$

or in matrix form

$$\overline{\mu}_c = \overline{\overline{\nu\mu}}_I \qquad (IV.A.3)$$

83

where

$\overline{\mu}_c$ is the column vector of complex chemical potentials,

$\overline{\mu}_I$ is the column vector of ionic components, and

$\overline{\nu}$ is a square matrix of stoichiometric coefficients.

In defining $\nu$ to be a square matrix, it is to be understood that terms for non-existent complexes are zero.

Using Eq. (IV.A.3), the potential gradients of the complexes are related to the gradients of the component ions by

$$\nabla \overline{\mu}_c = \overline{\nu} \; \nabla \; \overline{\mu}_I \tag{IV.A.4}$$

For conservation of charge, we also require that

$$\overline{z}_c = \overline{\nu} \; \overline{z}_I \tag{IV.A.5}$$

Now, the molar diffusion fluxes of the species (component ions and complexes) in the solvent-fixed reference frame are given by (Wendt, 1965)

$$\underline{J}^* = \overline{L}^* \{ \nabla \overline{\mu}^* + F \overline{z}^* \nabla E \} \tag{IV.A.6}$$

where

L* is the matrix of phenomenological coefficients,

F is Faraday's constant,

E is the electrical potential gradient due to the charge of each specie, and

z* is the column vector of charges.

For the case of no external electrical fields, the condition for no electrical current is

$$\overline{z}^{*T} \underline{J}^* = 0 \tag{IV.A.7}$$

Multiplying both sides of Eq. (IV.A.6) by $z*^t$ we obtain

$$\bar{z}*^T \underline{J}* = \bar{z}*^T \bar{L}* \nabla\bar{\mu}* + \nabla E \, \bar{z}*^T \bar{L}* \bar{z}* \tag{IV.A.8a}$$

and by Eq. (IV.A.7) we have

$$0 = \bar{z}*^T \bar{L}* \nabla\bar{\mu}* + F\nabla E \, \bar{z}*^T \bar{L}* \bar{z}* \tag{IV.A.8b}$$

Rearranging Eq. (IV.A.7) gives

$$F\nabla E = \frac{-\bar{z}*^T \bar{L}* \nabla\bar{\mu}*}{\bar{z}*^T \bar{L}* \bar{z}*} \tag{IV.A.8c}$$

where we note that both the numerator and denominator in Eq. (IV.A.8) are scalars. Substituting Eq. (IV.A.8) into Eq. (IV.A.6) then gives

$$\underline{J}* = \bar{L}* \quad \nabla\bar{\mu}* - \frac{\bar{z}* \, \bar{z}*^T \bar{L}* \, \nabla\bar{\mu}*}{\bar{z}*^T \bar{L}* \, \bar{z}*} \tag{IV.A.9}$$

Applying the associative law to the last term in Eq. (IV.A.9) we obtain

$$\underline{J}* = \left[ \bar{L}* - \frac{\bar{L}* \bar{z}* \bar{z}*^T \bar{L}*}{\bar{z}*^T \bar{L}* \bar{z}*} \right] \nabla\bar{\mu}* \tag{IV.A.10}$$

which is a relatively simple equation for the specie fluxes.

In order to reduce the number of flux equations which must be solved, we now rearrange Eq. (IV.A.10) to obtain the total component fluxes, $\underline{J}_t$. By conservation of mass, we know that

$$\underline{J}_T = \underline{J}_I + \overset{=}{\nu}{}^T \underline{J}_c \tag{IV.A.11}$$

Now if we define the vectors of complex fluxes and free-ionic fluxes as

$$\underline{J}_c = \begin{matrix} 0 \\ \cdot \\ \cdot \\ \cdot \\ 0 \\ J_1 \\ \cdot \\ \cdot \\ J_N \end{matrix} \quad \text{and} \quad \underline{J}_I = \begin{matrix} J_1 \\ \cdot \\ \cdot \\ J_N \\ 0 \\ \cdot \\ \cdot \\ 0 \end{matrix}$$

then the vector of species fluxes is

$$\underline{J}^\star = \underline{J}_I + \underline{J}_c \tag{IV.A.12}$$

and

$$\underline{J}^\star - \underline{J}_I = \underline{J}_c \tag{IV.A.13}$$

By similarly filling out $\nabla\bar{\mu}_I$ and $\nabla\bar{\mu}_c$ so that $\nabla\bar{\mu}^\star = \nabla\bar{\mu}_I + \nabla\bar{\mu}_c$, we can rewrite Eq. (IV.A.10) as

$$\underline{J}^\star = \left[ \overset{=}{L}{}^\star - \frac{\overset{=}{L}{}^\star \, \bar{z}^\star \, \bar{z}^{\star T} \, \overset{=}{L}{}^\star}{\bar{z}^{\star T} \, \overset{=}{L}{}^\star \, \bar{z}^\star} \right] \nabla\bar{\mu}_I + \left[ \overset{=}{L}{}^\star - \frac{\overset{=}{L}{}^\star \, \bar{z}^\star \, \bar{z}^{\star T} \, \overset{=}{L}{}^\star}{\bar{z}^{\star T} \, \overset{=}{L}{}^\star \, \bar{z}^\star} \right] \nabla\bar{\mu}_c \tag{IV.A.14a}$$

In the absence of any complex formation, Eq. (IV.A.14a) becomes

$$\underline{J}^\star = \underline{J}_I = \left[ \overset{=}{L}{}^\star - \beta \right] \nabla\bar{\mu}_I \tag{IV.A.14b}$$

where

$$\beta = \left\{ \frac{\overset{=}{L}* \; \overline{z}* \; \overline{z}*^T \; \overset{=}{L}*}{\overline{z}*^T \; \overset{=}{L}* \; \overline{z}*} \right\}$$

We may substitute the first term on the RHS of Eq. (IV.A.14a) into
Eq. (IV.A.11) for $J_I$ and the second term for $J_C$ to give

$$\underline{\overset{=}{J}}_T = \{\overline{L}* - \beta\} \, \nabla\overline{\mu}_I + \overset{=}{\nu}^T \, \{\overset{=}{L}* - \beta\}\nabla\overline{\mu}_C \tag{IV.A.15}$$

Using Eq. (IV.A.4) for $\nabla\overline{\mu}_C$ in Eq. (IV.A.15) yields

$$\underline{\overset{=}{J}}_T = \{\overset{=}{L}* - \beta + \overset{=}{\nu}^T \overset{=}{L}* \overset{=}{\nu} - \overset{=}{\nu}^T \overset{=}{\beta\nu}\} \, \nabla\overline{\mu}_I \tag{IV.A.16}$$

or

$$\underline{J}^T = \overset{=}{A}* \, \nabla\overline{\mu}_I \tag{IV.A.17}$$

where
$\overset{=}{A}*$ is a symmetric matrix (see Appendix B).

87

The chemical potential gradients in Eq. (IV.A.17) can now be eliminated by
the transformation (Cullinan, 1965)

$$\nabla \overline{\mu}_I = \overline{\overline{n}}_I \, \nabla \, \overline{m}_I \; ; \; n_{ij} = \frac{\partial \mu_i}{\partial m_j} \bigg|_{T,P,m_k} \; ; \; k \neq j \qquad \text{(IV.A.18)}$$

given by Cullinan (1965)


where

   $m_j$ is the molal concentration of the $j^{th}$ ion, and

   $n_I$ is a real symetric matrix.

Substituting Eq. (IV.A.18) into Eq. (IV.A.17) then gives


$$\underline{J}_T = \overline{\overline{A}}^\star \, \overline{\overline{n}}_I \, \nabla \, \overline{m}_I \qquad \text{(IV.A.19)}$$


or


$$\underline{J}_T = \overline{\overline{D}} \, \nabla \, \overline{m}_I \qquad \text{(IV.A.20)}$$


At this point it is useful to consider the properties of the matrices $A^\star$, $\mu_I$
and D. As has been shown, $A^\star$ is a real, symetrical matrix. As for $n_I$,
it can be shown to be diagonally dominant by considering its terms. By
definition the actual chemical potential of the $i^{th}$ component ion is


$$\mu_i = \mu^\circ_i + RT \ln \gamma_i \, m_i \qquad \text{(IV.A.21)}$$

where

$\gamma_i$ is the activity coefficient of i, and

$\mu^{\circ}_i$ is the chemical potential of i in its standard state.

Differentating Eq. (IV.A.21), we have

$$d\mu_i = \frac{RT}{\gamma_i} d\gamma_i + \frac{RT}{m_i} dm_i \tag{IV.A.22}$$

and the partial with respect to $m_j$ is

$$\frac{\partial \mu_i}{\partial m_j}\bigg|_{T,P,m_k} = RT \frac{\partial \ln \gamma_i}{\partial m_j}\bigg|_{T,P,m_k} + \frac{RT}{m_i} \frac{\partial m_i}{\partial m_j}\bigg|_{T,P,m_k} \tag{IV.A.23}$$

We can evaluate the first term on the right hand side of Eq. (IV.A.23) for dilute solutions by considering the Debye-Huckel Equation

$$\ln \gamma_i = \frac{-A z_i^2 \sqrt{I}}{1 + a_i B \sqrt{I}} \tag{IV.A.24}$$

where

$$I = 1/2 \sum_{\ell = 1}^{n} m_\ell Z_\ell^2, \text{ and}$$

A, $a_i$ and B are constants.

Differentiating Eq. (IV.A.24), we have

$$d \ln \gamma_i = \frac{-2 A z_i^2}{\sqrt{I} (1 + aB \sqrt{I})^2} dI \tag{IV.A.25}$$

From the definition of I, we have for constant $m_\ell$

$$dI = 1/2 Z_j^2 dm_j \tag{IV.A.26}$$

and substituting Eq. (IV.A.26) into Eq. (IV.A. 25) and rearranging, we obtain

$$\frac{\partial \ln \gamma_i}{\partial m_j} = \frac{-A z_i^2 z_j^2}{\sqrt{I}\,(1 + a_i B \sqrt{I})} \qquad (IV.A.27)$$

For very dilute solutions, Eq. (IV.A.27) is approximated by

$$\frac{\partial \ln \gamma_i}{\partial m_j} = \frac{-A z_i^2 z_j^2}{\sqrt{I}} \qquad (IV.A.28)$$

and so

$$\frac{\partial \ln \gamma_i}{\partial m_j} = \frac{\partial \ln \gamma_j}{\partial m_i} \qquad (IV.A.29)$$

Now considering the second term on the right hand side of Eq. IV.A.23), since $m_i$ is the actual molal concentration of the ith ion (and not its stoichiometric or analytic concentration), $m_i$ is not a function of $m_j$ and

$$\frac{\partial m i}{\partial m j} = 0 \; ; \; \frac{\partial m i}{\partial m i} = 1 \qquad (IV.A.30)$$

Thus from Eq. (IV.A.28) and Eq. (IV.A.30), the coefficients of $\overline{n}_i$ are

$$\eta_{ij} = \delta_{ij} \frac{RT}{m_i} - \frac{A z_i^2 z_j^2}{\sqrt{I}} \qquad (IV.A.31)$$

where

$\delta_{ij}$ is the Kronecher delta, and

$\overline{\alpha}$ is symmetric.

Eq. (IV.A.20) describes the diffusion fluxes within an individual pore of the matrix and is not appropriate for describing the macroscopic matrix-diffusion fluxes. Numerous models have been presented to account for the fact that observed diffusion fluxes through saturated porous media are less than free water-diffusion fluxes for equivalent concentration gradients (e.g., Porter and others, 1966; Saxena and others, 1974). VanBrakel and Heertjes (1974) point out that in all of these models the relationship between the free aqueous-diffusion coefficient and the effective-diffusion coefficient for the porous medium takes the form of

$$D_{ei} = \phi \gamma^n \alpha_i D_{oi} \qquad\qquad (IV.A.32)$$

where

De is the effective macroscopic-diffusion coefficient,

$\phi$ is the porosity,

$\gamma$ is a tortuosity factor,

$\alpha$ is a constrictivity factor, and

n is an exponent.

While $\phi$, $\gamma$ and n are generally regarded as solely properties of the porous medium, $\alpha$ may be dependent on both the medium and on the colligative and compositional properties of the solution. For these reasons let us focus our attention on $\alpha_i$ and make the assumption that $\alpha_i$ affects the equivalent conductivity of an ionic specie in the same way that it affects its diffusion coefficient.

Anderson and Graf (1978) reviewed and tested various methods to compute the coefficients of $\bar{L}^*$ (equivalent to $\ell$ in their Eq. (IV.A.5)).

In particular, they discuss and refine the models of Lane and Kirkaldy (1965), and Wendt (1965). Although the kinetic models of Lane and Kirkaldy are more accurate then Wendt's model, Anderson and Graf doubt that the site-exchange mechanism postulated by Lane and Kirkaldy is applicable to solutions of weak electrolytes. For this reason we will use Wendt's more simplistic model.

Assuming that the off-diagonal coefficients in $\bar{\bar{L}}*$ are zero, then the diagonal terms for ionic species are given by

$$L*_{ii} = \lambda_i \, m_i / (/Z_i \, / \, F^2 \times 10^7) \qquad \text{(IV.A.33)}$$

where

$\lambda_i$ is the limiting ionic conductivity of i, and

$m_i$ is the molar concentration of i.

Following our assumption about $\alpha_i$, we may now define a phenomenological coefficient for each specie in the porous medium as

$$L_{ii}^m = \alpha_i \, \lambda_i m_i / (|z_i| \, F^2 \times 10^7) \qquad \text{(IV.A.34)}$$

or

$$\bar{\bar{L}}^m = \bar{\alpha}^T \, \bar{\bar{L}}* \qquad \text{(IV.A.35)}$$

where we note that $L^m$ is diagonal we can now define a new matrix $A^m$ as

$$\bar{\bar{A}}^m = \bar{\bar{L}}^m - \frac{\bar{\bar{L}}^m \bar{z}* \bar{z}*^T \bar{\bar{L}}^m}{\bar{z}*^T \bar{\bar{L}}^m \bar{z}*} + \bar{\bar{\nu}}^T \bar{\bar{L}}^m \bar{\bar{\nu}} - \qquad \text{(IV.A.36)}$$

$$\frac{\bar{\bar{\nu}}^T \bar{\bar{L}}^m \bar{z}* \bar{z}*^T \bar{\bar{L}}^m \bar{\bar{\nu}}}{\bar{z}*^T \bar{\bar{L}}^m \bar{z}*}$$

92

The set of equations represented by Eq. (IV.A.37) are the multi-component, diffusion flux equation which can be incorporated into a model of matrix diffusion.

### 1. Numerical Calculation of Multicomponent Effects

In order to make a preliminary estimate of the multicomponent effects, Eq. (IV.A.19) was used to calculate the free aqueous, diffusion coefficient matrix applicable to the conditions of our laboratory diffusion experiments. The matrix for the NaBr tests is shown in Table IV.A.1. This diffusion-coefficient matrix was computed using the J-13 water composition reported by Wolfsberg and others (1979), and a NaBr concentration of 0.03M, the approximate average during a diffusion test. The diffusion coefficients were computed from limiting ionic conductances tabulated in Landoft-Bornstein (1960). For this calculation we have assumed that all ions (except $HCO_3^-$) are completely dissociated.

As can be seen, complete coupling exists between all the ions, although concentration gradients exist only for Na and Br. The results for a similar calculation using Na sodium pentafluorobenzoate (NaPFB) as the tracer ion are shown in Table IV.A.2. This coupling behavior may explain the results of 5/11/82 diffusion test on G1-2840 (sample A) where the effective diffusion coefficient computed using the UV detector results for PFB was $2.2 \times 10^{-5}$ $cm^2$/s while that computed from the conductivity detector was $4.8 \times 10^{-5}$ $cm^2$/s. These results imply that PFB diffused at less than half the rate of the salts causing the increase in conductivity. In order to maintain electrical neutrality, other anions must have diffused across the disc under the influence of the Na and PFB gradients. Further tests and analysis are planned to verify this interpretation.

TABLE IV.A.1.   FREE AQUEOUS-DIFFUSION COEFFICIENT MATRIX
FOR NaBr IN J-13 WATER.

|     | Na | K | Ca | Mg | Cl | $HCO_3$ | $SO_4$ | F | PFB |
|-----|------|------|------|------|------|------|------|------|------|
| Na | 2.165 | 1.193 | 0.957 | 0.860 | -1.240 | -0.722 | -1.306 | -0.893 | -0.440 |
| K | 0.005 | 1.962 | 0.005 | 0.005 | -0.007 | -0.004 | -0.007 | -0.005 | -0.002 |
| Ca | 0.010 | 0.014 | 0.796 | 0.010 | -0.015 | -0.008 | -0.015 | -0.010 | -0.005 |
| Mg | 0.002 | 0.003 | 0.003 | 0.707 | -0.003 | -0.002 | -0.003 | -0.002 | -0.001 |
| Cl | -0.008 | -0.012 | -0.010 | -0.009 | 2.045 | 0.007 | 0.013 | 0.009 | 0.004 |
| $HCO_3$ | -0.054 | -0.079 | -0.063 | -0.057 | 0.082 | 1.232 | 0.086 | 0.059 | 0.029 |
| $SO_4$ | -0.009 | -0.013 | -0.010 | -0.009 | 0.013 | 0.008 | 1.085 | 0.009 | 0.005 |
| F | -0.003 | -0.004 | -0.003 | -0.003 | 0.004 | 0.002 | 0.004 | 1.466 | 0.001 |
| PFB | -0.411 | -0.603 | -0.484 | -0.435 | 0.627 | 0.365 | 0.661 | 0.451 | 0.944 |

## TABLE IV.A.2.  FREE AQUEOUS-DIFFUSION COEFFICIENT MATRIX FOR Na PENTAFLUOROBENZOATE IN J-13 WATER

|     | Na | K | Ca | Mg | Cl | HCO$_3$ | SO$_4$ | F | Br |
|-----|------|------|------|------|------|------|------|------|------|
| Na | 1.848 | 0.755 | 0.606 | 0.545 | -0.785 | -0.457 | -0.827 | -0.565 | -0.802 |
| K | 0.003 | 1.960 | 0.003 | -0.003 | -0.004 | -0.003 | -0.005 | -0.003 | -0.004 |
| Ca | 0.006 | 0.009 | 0.792 | -0.006 | -0.009 | -0.005 | -0.010 | -0.007 | -0.009 |
| Mg | 0.001 | 0.002 | 0.002 | 0.707 | -0.002 | -0.001 | -0.002 | -0.001 | -0.002 |
| Cl | -0.005 | -0.008 | -0.006 | -0.005 | 2.041 | 0.005 | 0.008 | 0.006 | 0.008 |
| HCO$_3$ | -0.034 | -0.050 | -0.040 | -0.036 | -0.052 | 1.214 | 0.054 | 0.037 | 0.053 |
| SO$_4$ | -0.005 | -0.008 | -0.006 | -0.006 | 0.008 | 0.005 | 1.080 | 0.006 | 0.008 |
| F | -0.002 | -0.002 | -0.002 | -0.002 | 0.002 | 0.001 | 0.002 | 1.465 | 0.002 |
| Br | -0.749 | -1.099 | -0.883 | -0.793 | 1.143 | 0.666 | 1.204 | 0.883 | 3.242 |

## B. Numerical Modeling

A numerical model is under development to handle single-fracture flow problems with multicomponent diffusion of reactive solutes. Confining the model to convective flow in a single fracture greatly simplifies solving the transport part of the problem. The transport modeling technique will be similar to that used by Grisak and Pickens (1980) in their studies of matrix diffusion, except that it will include the nonlinear effects of multicomponent diffusion.

The mathematical problem to be solved is governed by the following partial differential equation

$$\frac{\partial \bar{m}}{\partial t} = \nabla \cdot \bar{J}_T - \underline{v} \cdot \nabla \bar{m} + \bar{S}_I \qquad \text{(IV.B.1)}$$

where

   $c$ is the solute concentration,

   $\nabla$ is the gradient operator,

   $\bar{J}_T$ is the diffusive flux, and

   $\bar{S}_I$ is a source/sink term including homogeneous reactions and sorption.

As described in a previous section, Eq. (IV.A.37), the diffusion flux is

$$\bar{J}_T = \bar{D}_e \nabla \bar{m}_I \qquad \text{(IV.B.2)}$$

Although Eq. (IV.B.2) could be substituted into Eq. (IV.B.1) for the diffusion flux, this would greatly complicate formulating the numerical problem. Toor (1964a, 1964b) has shown that the form of Eq.(IV.B.1) can be preserved if the diffusion coefficient matrix, $D_e$, can be diagonalized. This can be done if $D$ is independent of concentration and the Onsager

relationships hold, by finding a nonsingular matrix $\bar{\bar{P}}$ such that

$$\bar{\bar{P}}^{-1} \ \bar{\bar{D}} \ \bar{\bar{P}} = \bar{\bar{D}}' \qquad\qquad\qquad (IV.B.3)$$

where

$\bar{\bar{D}}'$ is a diagonal matrix.

Cullinan (1965) showed from thermodynamic arguments that this can always be done if $\bar{\bar{D}}'$ is defined in the mean volume reference frame. By operating on on Eq. (IV.B.1) by $\bar{\bar{P}}^{-1}$, we obtain

$$\frac{\partial \psi_i}{\partial t} = \nabla \cdot \underline{v} \ \psi_i - \nabla \cdot D'_{ii} \ \nabla \ \psi_i + \phi_i \qquad\qquad (IV.B.4)$$

In Eq. (IV.B.4), $\psi_i$ is the $i^{th}$ member of the vector given by

$$\bar{\psi} = \bar{\bar{P}}^{-1} \ \bar{m} \qquad\qquad\qquad (IV.B.5)$$

and $\phi_i$ is the $i^{th}$ member of the vector given by

$$\bar{\phi} = \bar{\bar{P}}^{-1} \ \bar{S}_I \qquad\qquad\qquad\qquad (IV.B.6)$$

A Fortran program has been developed to accomplish the above trans-formations. The program has been tested on diffusion coefficient matrices generated for various tracers in J-13 water, including those for NaBr and NaPFB shown in Tables IV.B.1 and IV.B.2, and these matrices were success-fully diagonalized.

The transformed flux equations represented by Eq. (IV.B.4) are in a form which can readily be solved by various numerical techniques. For cases where all the aqueous components are completely ionized and do not form ion pairs or complexes, the fictitious components whose concentrations are represented by $\psi_i$ in Eq. (IV.B.4) diffuse independently of each other. In this case, each equation can be solved independently by any suitable

analytical or numerical technique. The solutions in terms of the fictitious component concentrations can then be backtransformed into concentrations of the original components by

$$\overline{m} = \overset{=}{P} \overline{\psi} \tag{IV.B.7}$$

For situations where complexation or ion pairing reactions between the components of interest are important, the solution procedure is more complex. Because the flux equations are written in terms of the actual concentrations of the component ions (rather than their total or analytical concentrations), these concentrations must be computed before governing equation can be solved. To do this, a computer program based on the mono-tone sequences method of Wolery and Walters (1975) was developed which can be incorporated into a numerical model of matrix diffusion. The original procedure of Wolery and Walters was modified in the program to enhance convergence of the iterative scheme. These modifications are described in Appendix C.

Work is in progress to adopt an existing integrated finite difference model (Walter and Kidd, 1979) to solve problems of matrix diffusion from a single fracture. This work involves modifications to incorporate the diagonalization and chemical-equilibrium procedures into the computer code.

# V. SUMMARY AND CONCLUSIONS

In theory, the various physical/chemical transport processes discussed in section II may cause non-convective solute transport from fractures into the unfractured tuff matrix at the NTS. In the absence of artifically induced electrical or thermal potential gradients, molecular diffusion, and possibly osmosis, appear to be the dominate processes. Although the tuffs have some membrane properties as illustrated by the electrically induced potential effects and the osmosis experiment, assessment of these properties is still preliminary. More and better osmosis experiments are needed to verify them.

Extensive measurements of the total porosity and pore-size distribution have revealed that the sample porosities vary from about 10 to 40%. Much of this porosity is present as pores less than 1 μm in diameter. In some samples, the median pore diameter is less than 0.1 μm. The pore diameter and size distribution seems to affect the effective matrix-diffusion coefficients.

The effective matrix-diffusion coefficients determined from diffusion experiments using sodium halide salts range from about $2 \times 10^{-7}$ to $17 \times 10^{-7}$ $cm^2$/s. These values are in a range which would be predicted from an educated guess about the porosity and constrictivity/tortuosity factor for the tuffs. The data in this report basically support a relationship between the effective-diffusion coefficient and the free aqueous-diffusion coefficient of the form

$$D_e = \phi\, (\alpha/\tau^2) D_0 \qquad\qquad\qquad (V-1)$$

The correlation between the total porosity and the effective-diffusion coefficient for the samples studied was very good (r = 0.90) and the total porosity accounts for most of the variation in diffusion coefficients from sample to sample. A fair correlation (r = 0.75) was found between the constrictivity/tortuosity factor and the median pore diameter. The reasons for the correlation are not certain, but may be due to ion exclusion from the smaller pores. These results indicate that reasonably accurate effective matrix-diffusion coefficients may be made based on porosity and pore-size distributions. Electrical measurements such as bulk-rock resistance and changes in bulk impedance with current frequency may also be used to estimate the effective-diffusion coefficients.

The results of the experimental work all indicate that the tuffaceous rocks from the NTS have sufficient porosity and large enough effective-diffusion coefficients to make matrix diffusion an important transport process. For some species, such as those which form ion pairs or complexes, multicomponent diffusion effects may complicate the simple single-component diffusion models on which previous theoretical studies have been based (e.g., Neretniks, 1981; Grisak and Pickens, 1980). The multicomponent diffusion-coefficients reported here are certainly large enough to cause coupled ionic fluxes under some conditions. Additional work is in progress to estimate the extent to which multicomponent diffusion will affect the matrix-diffusion process.

Lastly, the tracer development and characterization work performed under this contract indicates that halide, pseudo-halides ($SCN^-$), and the fluorobenzoate tracers will be useful in future fracture-flow experiments.

100

The halides and pseudo-halides behaved nearly identically in diffusion experiments. Fracture-flow experiments using halides and the fluorobenzoates as tracers may be useful for verifying matrix diffusion effects based on their differing diffusion coefficients. At least in our experiments, pentafluorobenzoate diffused at measurably different rates. Even more useful may be the bacteriophage-particulate tracers which we will begin testing shortly.

## ACKNOWLEDGEMENTS

## VI.  REFERENCES

ASTM, Annual Handbook of ASTM Standards.  Part 11.  Phila., Pa. (1973)
    pp. 321-323.

Anderson, D. E., and D. L. Graf, "Ionic Diffusion in Naturally-Occurring
    Aqueous Solutions:  Use of Activity Coefficients in Transition State
    Models," Geochim. Cosmochim. Acta 42, 251-262 (1978).

Anderson, L. A. and G. V. Keller, "A Study in Induced Polarization,"
    Geophysics 29(5), 848-864 (1964).

Arulanandan, K. and J. K. Mitchell, "Low Frequency Dielectric dispersion of
    Clay-Water-Electrolyte Systems, Clays Clay, (1968).

Banin, A., "Transfer Properties and Friction Coefficients for Salt Land
    Water Flow through Clays, Funda. Transport Phenomena in Porous Media,
    Elsevier, Amsterdam (1972) pp.212-220.

Blackmore, A. V., "Salt Sieving within Clay Soil Aggregates," Austral. J.
    Soil Res. 14, 149-158, (1976).

Cullinan, H. T. Jr., "Analysis of the Flux Equations of Multicomponent
    Diffusion," A. I. Chem. Eng. J. 4(2), 133-138 (1965).

Chemical Rubber Co., CRC Handbook of Chemistry and Physics, CRC Press Boca
    Raton, Florida (1980-81).

Garrels, R. M., R. M. Dreyer, and A. L. Howland, "Diffusion of Ions through
    Intergranular Spaces in Water Saturated Rocks," Bull. Geol. Soc. Am.
    60, 1809-1828 (1949).

Graham-Bryce, F. J., "Self Diffusion of Ions in Soils. II.  Anions," J. Soil
    Sci. 14, 195-200 (1963).

Gregg, S. J. and K. S. W. Sing, Adsorption, Surface Area, and Porosity,
    Academic Press, London (1967).

Grisak, G. E. and J. F. Pickens, " An Analytical Solution for Solute
    Transport through Fractured Media with Matrix Diffusion," J. Hydrology
    52, 47-57 (1981).

Grisak, G.E. and J. F. Pickens, "Solute Transport through Fractured Media:
    1.  The Effect of Matrix Diffusion," Water Resour. Res. 16,
    719-730 (1980).

Grisak, G. E., J. F. Pickens, and J. A. Cherry, "Solute Transport through
    Fractured Media: 2.  Column Study on Fractured Till," Water Resour.
    Res. 16, 731-739 (1980).

Groenevelt, P. H. and G. H. Bolt, "Non-equilibrium Thermodynamics of the Soil-Water System,"J. Hydrology 7, 358-388 (1969).

Haase, R., Thermodynamics of Irreversible Processes, Addison-Wesley, Reading, Mass. (1969).

Kemper, W. D., D. E. L. Maasland, and L. K. Porter, "Mobility of Water Adjacent to Mineral Surfaces," Proc. Soil Sci. Soc. Am. 28, 164-167 (1964).

Kielland, J., Kuhn, R. and A. Wasserman, "Die Dissoziations-Konstanten der Halogenbenzoesauren," Helvetica Chimica, Acta II, 31-41 (1928).

Kuhn, R. and A. Wassermann, "Die Dissoziationskonstanten der Halogen benzoesouren", Helvetica Chimica Acta, 11, 31-41 (1928).

Landolt-Bornstein Zahlenwerte und Funktionen aus Physik, Chemie, Astronomie, Geophysik Technik: Electrische Eigenschaften II, v. 5, 258-263 (1969).

Lane, J. E. and J. S. Kirkaldy, "Diffusion in Multicomponent Aqueous Systems," Can. J. Chem., 4, 477-485 (1965).

Lasaga, A. C., "The Treatment of Multicomponent Diffusion and Ion Pairs in Diagnostic Flutes," Am J. Science 279, 324-346 (1979).

Lerman, A., "Maintenance of Steady State in Oceanic Sediments," Am. J. Sci. 275, 609-635 (1975).

Manger, G. E., "Method Dependent Values of Bulk, Grain, and Pore Volume as Related to Observed Porosity," U.S. Geol. Surv. Bull. 1203D (1966).

Marshall, D. J. and T. R. Madden, "Induced Polarization, A Study of its Causes," Geophysics 24(4), 790-816 (1959).

Michaels, A. S., "Diffusion in a Pore of Irregular Cross Section - A Simplified Treatment," A. I. Chem. Eng. J. 5, 270-271 (1959).

Moore, W. J., Physical Chemistry, Prentice-Hall, Englewood Cliffs, N. J. (1972).

Neretniks, I., "Age Dating of Groundwater in Fissured Rocks: Influence of Water Volume in Micropores," Water Res. Res. 17(2), 421-422 (1981).

Norton, D. and R. Knapp, "Transport Phenomena in Hydrothermal Systems: The Nature of Porosity," Am. J. Sci. 277, 913-936 (1977).

Olsen, S. R. and W. D. Kemper, "Movement of Nutrients to Plant Roots," Adv. Agronomy 20, 91-151 (1968).

Petersen, E. E., "Diffusions in a Pore of Varying Cross Sections," A. I. Chem. Eng. 4(3), 343-345 (1959).

Porter, L. K., W. D. Kemper, R. D. Jackson, and R. C. Stewart, "Chloride Diffusion in Soils as Influenced by Moisture Content," Proc. Soil Sci. Soc. Am. 24, 460-463 (1966).

Robinson, R. A. and R. H. Stokes, Electrolyte Solutions, Butterworths, London (1959) p. 253.

Ryan, M. T. and K. J. Berner, "$\Lambda_{OH}$ and $pK_d$ Values of Pera Substituted Tetra Pluorobenzoic Acids," Spectrochimica Act 25A, 1155-1157 (1969).

Saxena, S. K., L. Boersma, F. T. Lindstrom, and L. Young, "Effect of Pore Size on Diffusion Coefficients in Porous Media," Soil Science 117, 80-86 (1974).

Stokes, R. H., "Improved Diaphragm-cell for Diffusion Studies and Same Tests of the Method," J. Am. Chem. Soc., 72, 763-676 (1950).

Stumm, W. and J. J. Morgan, Aquatic Chemistry, John Wiley and Sons, New York (1970).

Tang, D. E., E. O. Frind, and E. A. Sudicky, "Contaminant Transport in Fractured Porous Media: Analytical Solutions for a Single Fracture," Water Res. Res. 17(3), 555-564 (1981).

Toor, H. L., "Solution of the Linearized Equations of Multicomponent Mass Transfer: I," A. I. Chem. Eng. J. 10, 448-455 (1964a).

Toor, H. L., "Solution of the Linearized Equations of Multicomponent Mass Transfer: II," Matrix Methods," A. I. Chem. Eng. J. 10, 460-465 (1964b).

van Brakel, J. and P. M. Heertjes, "Analysis of Diffusion in Macroporous Media in Terms of a Porosity, a Tortuosity, and a Constrictivity Factor," Int. J. Heat Mass Transfer 17, 1093-1103 (1974).

van Genuchten, M. T. and P. J. Wierenga, Mass transfer studies in sorbing Porous Media. I. Analytical Solutions," J. Soil Sci. Soc. Am. 40, 473-480 (1976).

Walter, G. R. and R. E. Kidd, "Management Techniques for the Control of Salt Water Encroachment in Coastal Aquifers," Alabama Water Res. Research Center Project Rpt., (B-073-ALA) 1979.

Wendt, R. P., "The Estimation of Diffusion Coefficients for Ternary Systems of Strong and Weak Electrolytes," J. Phys. Chem. 69, 1227-1237 (1965).

Wolery, T. J. and L. J. Walters, "Calculations of Equilibrations Distributions of Chemical Species in Aqueous Solutions by Means of Monotone Sequences," Math. Geology 7(2), 99-114 (1975).

Wolfsberg, K., B. P. Bayhurst, B. M. Crowe, W. R. Daniels, B. R. Erdal, F. O. Lawrence, A. E. Norris, and J. R. Smyth, "Sorption-Desorption Studies on Tuff I. Initial studies with samples from the J-13 Drill Site, Jackass Flats, Nevada", Los Alamos National Laboratory Informal Rpt. LA-7480-MS (1979).

Wyllie, M. O. J., and H. B. Spangler, "Application of Electrical Resistivity Measurements to Problems of Fluid Flow in Porous Media," Bull. Am. Assoc. Pet. Geol. 36, 359-403 (1952).

Zonge, K. L., "Electrical Properties of Rocks as Applied to Geophysical Prospecting," Ph.D. Thesis, Univ. of Arizona (1972).

APPENDIX A

In order to rewrite Eq. (II.A.12, 13, and 14) in terms of an experimentally tractable set of forces and fluxes, consider first the case where $\nabla M_k = 0$, $F = 0$, and $(c^k g - n_k \nabla P) = 0$ for same k. We then have

$$\underline{J}_v = \sum_{i=1}^{N} \hat{V}_i \sum_{k=1}^{N} L_{ik}^*(c_k \underline{g} - \dot{n}_k \nabla P) \tag{A.1}$$

$$\underline{J}_{mi} = M_i \sum_{k=1}^{N-2} L_{ik}^*(c_k \underline{g} - \dot{n}_k \nabla P) \tag{A.2}$$

$$\underline{J}_z = \sum_{i=1}^{N} z_i \sum_{k=1}^{N} L_{ik}^*(c_k \underline{g} - \dot{n}_k \nabla P) \tag{A.3}$$

We can rewrite Eq. (A-1, A-2 and A-3) as

$$\underline{J}_v = \sum_{i=1}^{N} \dot{V}_i L_{ii}^*(c_i \underline{g} - \dot{n}_i \nabla P) + \sum_{i=1}^{N} \dot{V}_i \sum_{k \neq i}^{N} L_{ik}^*(c_k \underline{g} - \dot{n}_k \nabla P) \tag{A.4}$$

$$\underline{J}_{mi} = M_i L_{ii}^*(c_i \underline{g} - \dot{n}_i \nabla P) + M_i \sum_{k \neq 1}^{N} L_{ik}^*(c_k \underline{g} - \dot{n}_k \nabla P) \tag{A.5}$$

$$\underline{J}_z = \sum_{i=1}^{N} z_i L_{ii}^*(c_i \underline{g} - \dot{n}_i \nabla P) + \sum_{i=1}^{N} z_i \sum_{k \neq 1}^{N} L_{ik}^*(c_k \underline{g} - \dot{n}_k \nabla P) \tag{A.6}$$

Now, in Eq. (A-4) we add and subtract

$$\sum_{i=1}^{N} \dot{V}_i L_{ii}^* \sum_{k \neq 1}^{N} (c_k \underline{g} - \dot{n}_k \nabla P) \qquad (A.7)$$

to the RHS to obtain

$$\underline{J}_v = \sum_{i=1}^{N} \dot{V}_i L_{ii}^*(c_i \underline{g} - \dot{n}_i \nabla P) + \sum_{i=1}^{N} \dot{V}_i L_{ii}^* \sum_{k \neq i}^{N} (c_k \underline{g} - \dot{n}_k \nabla P)$$

$$(A.8)$$

$$+ \sum_{i=1}^{N} \dot{V}_i \sum_{k \neq 1}^{N} L_{ik}^*(c_k \underline{g} - \dot{n}_k \nabla P) - \sum_{i=1}^{N} \dot{V}_i L_{ii}^* \sum_{k \neq i}^{N} (c_k \underline{g} - \dot{n}_k \nabla P)$$

Then rearranging Eq. (A-8) we obtain

$$\underline{J}_v = \sum_{i=1}^{N} \dot{V}_i L_{ii}^* \sum_{k=1}^{N} (c_k \underline{g} - \dot{n}_k \nabla P)$$

$$(A.9)$$

$$+ \sum_{i=1}^{N} \dot{V}_i \sum_{k \neq 1}^{N} (L_{ik}^* - L_{ii}^*)(c_k \underline{g} - \dot{n} \nabla P)$$

107

Consider the summation over k in the first term in Eq. (A-9). Inasmuch as

$$\sum_{k=1}^{N} c_k \underline{g} = \rho_s \underline{g} \qquad (A.10)$$

where $\rho_s$ is the density of the solution (total mass of solution per unit volume) and

$$\sum_{k=1}^{N} \dot{n}_k \nabla P = \nabla P \qquad (A.11)$$

(remembering that $\dot{n}_k$ is the volume fraction of k and $\sum_{k=1} \dot{n}_\rho = 1$), then Eq. (A-9) can be written in terms of the total external force potential-per-unit volume and a "sedimentation term" (Groenvelt & Bolt, 1969)

$$\underline{J}_v = \sum_{i=1}^{N} \dot{V}_i L_{ii}^{\star} (\rho_s \underline{g} - \nabla P) + \sum_{i=1}^{N} \dot{V}_i \sum_{k \neq i}^{N} (L_{ik}^{\star} - L_{ii}^{\star})(c_k \underline{g} - \dot{n} \nabla P) \qquad (A.12)$$

Groenvelt and Bolt have shown that when gravity is the only external force, the sedimentation term is negligible for dissolved species and for the present discussion we will ignore it.

108

We can now perform similar rearrangements to Eq. (A-5 and A-6) to obtain

$$\underline{J}_{mi} = M_i L_{ii}^* \sum_{k=1}^{N} (c_k \underline{g} - \dot{n}_k \nabla P) + M_i \sum_{k \neq 1}^{N} (L_{ik}^* - L_{ii}^*)[c_k \underline{g} - \dot{n}_k \nabla P] \qquad (A.13)$$

and

$$\underline{J}_z = \sum_{i=1}^{N} z_i L_{ii}^* (\rho_s \underline{g} - \nabla P) + \sum_{i=1}^{N} z_i \sum_{k \neq 1}^{N} (L_{ik}^* - L_{ii}^*)[c_k \underline{g} - \dot{n}_k \nabla P) \qquad (A.14)$$

where the sedimentation terms in Eq. (A-13) and Eq. (A-14) should also be small.

Now, ignoring the sedimentation terms in Eq. (A-13, A-14 and A-15) the equations can be written as

$$J_v = L_{vv} (\rho_s \underline{g} - \nabla P)$$

$$J_{mi} = L_{iv} (\rho_s \underline{g} - \Delta P) \qquad (A-15)$$

$$J_z = L_{zv} (\rho_s \underline{g} - \Delta P)$$

where $L_{vv}$ is the coefficient relating the volume flux to the external force per unit volume (permeability). $L_{iv}$ relates the flux of i to the volume force (filtration coefficient) and $L_{zv}$ relates the charge flux to the volume force (streaming coefficient).

Now consider the case where $(C_{ig} - \Delta P) = 0$ for all $i$ and $F = 0$, then from Eq. (A-9, A-10, and A-11) we have

$$\underline{J}_v = \sum_{i=1}^{N} \dot{V}_i \sum_{k=1}^{N} L_{ik}^{*} (-m_k \nabla \mu_k) \qquad (A.16)$$

$$\underline{J}_{mi} = M_i \sum_{k=1}^{N} L_{ik}^{*} (-m_k \nabla \mu_k) \qquad (A.17)$$

$$\underline{J}_z = \sum_{i=1}^{N} z_i \sum_{k=1}^{N} L_{ik}^{*} (-m_k \nabla \mu_k) \qquad (A.18)$$

If we rearrange Eq. (A-16) by switching the order of summation we obtain

$$\underline{J}_v = \sum_{k=1}^{N} \dot{V}_k L_{k1}^{*}) (-m_i \nabla \mu_1) + \ldots + \left( \sum_{k=1}^{N} \dot{V}_k L_{ki}^{*} \right) (-m_i \nabla \mu_i)$$

$$(A.19)$$

$$+ \ldots + \left( \sum_{k=1}^{N} \dot{V}_k L_{kn}^{*} \right) (-m_N \nabla \mu_N)$$

or

$$\underline{J}_v = L_{v1}(-m_1 \nabla \mu_1 + \ldots + L_{vi}(-m_i \nabla \mu_i) + \ldots + L_{vN}(-m_N \nabla \mu_N) \qquad (A.20)$$

where each $L_{vi}$ relates the total-volume flux to the diffusion force of component i (osmotic coefficients). Rewriting Eq. (A-17) without rearranging gives

$$\underline{J}_{mi} = -M_i L_{i1}^* m_1 \nabla \mu_1 - \ldots - M_i L_{ik}^* m_k \nabla \mu_k - M_i L_{iN}^* m_N \nabla \mu_N \qquad (A.21)$$

or

$$\underline{J}_{mi} = -L_{i1} \nabla \mu_1 - \ldots - L_{ik} \nabla \mu_k - \ldots - L_{iN} \nabla \mu_N \qquad (A.22)$$

111

where each $L_{ik}$ relates the diffusion flux of i to diffusion force of k. Lastly, rearranging the charge flux given by Eq. (A-18) as we did for the volume flux gives

$$\underline{J}_z = \left( \sum_{k=1}^{N} z_k L_{k1}^* \right) (-m_1 \nabla \mu_1) + \dots + \left( \sum_{k=1}^{N} z_k L_{k1}^* \right) (-m_i \nabla \mu_i)$$

$$+ \dots + \left( \sum_{k=1}^{N} z_k L_{k1}^* \right) (-m_N \nabla \mu_N) \tag{A.23}$$

or

$$\underline{J}_z = L_{z1}(-m_1 \nabla \mu_1) + \dots + L_{zi}(-m_i \nabla \mu_i) + \dots + L_{zN}(-m_N \nabla \mu_N) \tag{A.24}$$

where each $L_{zi}$ relates the total-charge flux to the diffusion force on i (these may be called the "diffusion-current" coefficients.

Now consider the case where $(C_k g - \nabla P) = 0$ for all k and $\nabla \mu_k = 0$ for all k, but $F \neq 0$. Then the resulting fluxes are

112

$$\underline{J}_v = \sum_{i=1}^{N} V_i \sum_{k=1}^{N} L_{ik}^* m_k z_k F \nabla E$$

$$J_{mi} = M_i \sum_{k=1}^{N} L_{ik}^* m_k z_k F \nabla E \qquad\qquad (A.25)$$

$$\underline{J}_z = \sum_{i=1}^{N} z_i \sum_{k=1}^{N} L_{ik}^* m_k z_k F \nabla E$$

Without rearrangement we can write

$$J_v = L_{vz} \nabla E$$
$$J_{mi} = L_{iz} \nabla E \qquad\qquad (A.26)$$
$$J_z = L_{zz} \nabla E$$

where $L_{vz}$ relates the volume flux to the electric field strength (electro-osmotic permeability), $L_{iz}$ relates the mass flux of i to the field strength (electro-phoretic coefficient) and $L_{zz}$ is the electrical-conduction co-efficient.

APPENDIX B

That $\bar{A}*$ is symmetric can be seen by considering its expanded form in Eq. (IV.A.14b) term by term. First, $\bar{L}*$ is known to be symmetric. Considering the second term, we wish to show that

$$\frac{\bar{L}* \; \bar{z}* \; \bar{z}*^T \; \bar{L}*}{\bar{z}*^T \; \bar{L}* \; \bar{z}*} = \left[ \frac{\bar{L}* \; \bar{z}* \; \bar{z}*^T \; \bar{L}*}{\bar{z}*^T \; \bar{L}* \; \bar{z}*} \right]^T \tag{B.1}$$

Because the denominator in Eq. (B-1) is a scalar, we need only consider the numerator

$$(\bar{L}* \; \bar{z}* \; \bar{z}*^T \; \bar{L}*)^T = \bar{L}*^T \; \bar{z}* \; \bar{z}*^T \bar{L}*^T \tag{B.2}$$

and since $\bar{L}*$ is symmetric we have

$$(\bar{L}* \; \bar{z}* \; \bar{z}*^T \; \bar{L}*)^T = \bar{L}* \; \bar{z}* \; \bar{z}* \; \bar{L}* \tag{B.3}$$

Now, considering the third term

$$\left( \underset{\nu}{\overset{=T}{\nu}} \ \bar{L}\star \ \underset{\nu}{\overset{=}{\nu}} \right)^T = \underset{\nu}{\overset{=T}{\nu}} \ \bar{L}\star^T \underset{\nu}{\overset{=}{\nu}} = \underset{\nu}{\overset{=T}{\nu}} \ \bar{L}\star \underset{\nu}{\overset{=}{\nu}} \qquad (B.4)$$

Finally, for the last term we have

$$\left( \underset{\nu}{\overset{=T}{\nu}} \ \bar{L}\star \ \bar{z}\star \ \bar{z}\star^T \ \bar{L}\star \ \underset{\nu}{\overset{=}{\nu}} \right)^T = \left( \bar{z}\star^T \ \bar{L} \ \underset{\nu}{\overset{=}{\nu}} \right)^T \left( \underset{\nu}{\overset{=T}{\nu}} \ \bar{L}\star \ \bar{z}\star \right)^T$$

$$= \left( \bar{L}\star \ \underset{\nu}{\overset{=}{\nu}} \right)^T \left( \bar{z}\star^T \right)^T \left( \bar{L}\star \ \bar{z}\star \right)^T \left( \underset{\nu}{\overset{=T}{\nu}} \right)^T \qquad (B.5)$$

$$= \underset{\nu}{\overset{=T}{\nu}} \ \bar{L}\star \ \bar{z}\star \ \bar{z}\star \ \bar{L}\star^T \ \underset{\nu}{\overset{=}{\nu}}$$

Since the sum of symmetric matrices is symmetric, $\bar{A}\star$ is symmetric.

APPENDIX C

Consider an aqueous solution containing N cationic components and M anionic components which may combine to form S ion pairs or complexes. Further assume that the total molarity of each component is known.

The jth complexation reaction can be represented by

$$\nu_{j1}C_1 + \cdots \nu_{jN}C_N + \nu_{jN+1}A_1 + \nu_{jN+M}A_M = S_j \qquad (C-1)$$

where $\nu_{ji}$ are the stoichiometric coefficients of the ith reactant (component) in the jth reaction and in the jth complex. For each reaction there is a thermodynamic-equilibrium constant defined as

$$K_j = \frac{\gamma_j m_j}{\prod\limits_{i=1}^{N+M} \gamma_i m_i^{\nu_{ji}}} \qquad (C-2)$$

where $m_i$ is the molar concentration of the ith component and $\gamma_i$ is the activity coefficient of component i. This is the mass-action constraint.

To handle redox equilibria, we adapt the convention that all redox reactions be defined by the appropriate reduction half-reactions (Stumm and

116

Morgan, 1970) written in terms of an oxidized component, electrons, and a reduced product specie. Thus, the general reduction half-reaction is

$$\text{jth reduction:} \quad \sum_{j=1}^{N+M-1} \nu_{ji} C_i + \nu_{jN+M} e = R_j \qquad \text{(C-3)}$$
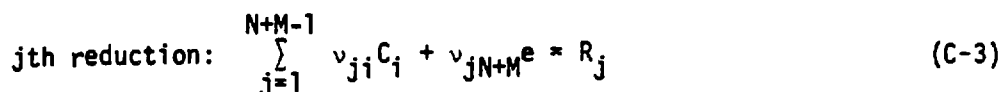
and the corresponding mass-action equation is

$$K_j = \frac{\gamma_j m_j}{\left( \prod_{i=1}^{N+M-1} \gamma_i m_i \right)^{\nu_{ji}} a_e^{\nu_{jN+M}}} \qquad \text{(C-4)}$$

Note that this convention requires that the fictitious free electron be treated as a component.

In the remainder of this section, the free electrons are treated in a manner exactly analogous to the treatment of free protons ($H^+$) (Stumm and Morgan, 1970).

Because the total molarity of the components is assumed to be known, we can also write a mass-balance constraint as

$$m_i^T = m_i + \sum_{j=1}^{S} \nu_{ji} m_i \qquad \text{(C-5)}$$

where $m_i^T$ is the total or analytic concentration of component i. An additional constraint on the system is that the solution must be electrically neutral so that

$$\sum_{i=1}^{N+M} z_i m_i + \sum_{j=1}^{S} z_j m_j = 0 \qquad \text{(C-6)}$$

Equations (C-2), (C-4), (C-5) and (C-6) are sufficient to completely define the actual distribution of aqueous species in the solution and our purpose here is to solve this system of equations for the molar concentrations of these species. Following the method of Wolery and Walters (1975), we solve Eq. (C-2) for the concentration of the jth complex so that

$$m_j = \frac{1}{\gamma_j} K_j \prod_{i=1}^{N+M} \gamma_i m_i^{\nu_{ji}} \qquad \text{(C-7)}$$

and substituting Eq. (C.7) into Eq. (C.5) we obtain

$$m_i^T = m_i + \sum_{j=1}^{S} \frac{\nu_{ji}}{\gamma_j} \prod_{k=1}^{N+M} \gamma_k m_k^{\nu_{jk}} \qquad \text{(C-8)}$$

which is mass-balance constraint expressed entirely in terms of the components. Also note that in Eq. (C.8) the subscript k is simply a dummy subscript for i and that $\gamma_k$, $m_k$ and $\nu_{jk}$ all refer to the components. We wish to solve Eq. (C-8) for the unknown concentration of i, $m_i$. Dividing Eq. (C-8) by $m_i$ gives

$$\frac{m_i^T}{m_i} = 1 + \sum_{j=1}^{S} \frac{\nu_{ji}}{\gamma_j} K_j \gamma_i m_i^{(\nu_{ji}-1)} \cdot \prod_{k=1}^{N+M} \gamma_k m_k^{\nu_{jk}} \qquad \text{(C-9)}$$

and rearranging Eq. (C-9) gives

$$m_i = m_i^T \left[ 1 + \sum_{j=1}^{S} \frac{\nu_{ji}}{\gamma_j} K_j \gamma_i m_i^{(\nu_{ji}-1)} \cdot \sum_{k=1}^{N+M} \gamma_k m_k^{\nu_{jk}} \right]^{-1} \tag{C-10}$$

Using Eq. (C-10) we can define an iterative solution algorithm for $m_i$ by writing

$$m_i^{(\ell+1)} = m_i^T \left[ 1 + \sum_{j=1}^{S} \frac{\nu_{ji}}{\gamma_j^{(\ell)}} K_j \gamma_i^{(\ell)} (m_i^{(\ell)})^{(\nu_{ji}-1)} \cdot \prod_{k=1}^{N+M} \gamma_k^{(\ell)} (m_k^{(\ell)})^{\nu_{jk}} \right]^{-1} \tag{C-11}$$

where the superscript ($\ell$) denotes the value at the lth iteration. Wolery and Walters (1975) have shown that this iterative procedure is convergent for physically meaningful values of the parameters and variables in Eq. (C-11).

As written, Eq. (C-11) has the form of a point Jacobi iteration in that the new values of the vector, $\overline{m}^{(\ell+1)}$ are computed only from the values of $\overline{m}$ at the previous iteration. We wish to consider the possibility of using a Gauss-Seidel iteration, that is, updating the values of $m_k$ as soon as they are available. In this way Eq. (C-11) becomes

$$m_i^{(\ell+1)} = m_i^T \left[ 1 + \sum_{j=1}^{S} \frac{\nu_{ji}}{\gamma_j} K_j \gamma_i (m_i^{(\ell)})^{(\nu_{ji}-1)} \right.$$

$$\left. \cdot \prod_{K=1}^{i-1} \gamma_k^{(\ell)} (m_k^{(\ell+1)})^{\nu_{jk}} \cdot \prod_{k=i+1}^{N+M} \gamma_k^{(\ell)} (m_k^{(\ell)})^{\nu_{jk}} \right]^{-1} \qquad (C-12)$$

Let us evaluate the convergence of Eq. (C-12) by following the procedure of Wolery and Walters (1975). First, by differentiating Eq. (C.12) with respect to any $m_p$ where $p \neq i$, we obtain

$$\frac{\partial m_i^{(\ell+1)}}{\partial m_p} = - \frac{(m_i^{(\ell+1)})^2}{m_i^T} \left[ \sum_{j=1}^{S} \frac{\nu_{ji}}{\gamma_j^{(\ell)}} K_{ji} (m_i^{(\ell)})^{\nu_{ji}-1} \right.$$

$$\cdot \gamma_p^{(\ell)} (m_p^{(\ell)})^{\nu_{jp}-1} \nu_{jp} \cdot \prod_{k=1}^{i-1} \gamma_{jk}^{(\ell)} (m_k^{(\ell+1)})^{\nu_{jk}}$$

$$\qquad (C-13)$$

$$\left. \cdot \prod_{k=i+1}^{N+M} \gamma_k^{(\ell)} (m_k^{(\ell)})^{\nu_{jk}} \right]^{-1}$$

For Eq. (C-13), since the summation term is nonnegative, we have

$$\frac{\partial m_i^{(\ell+1)}}{\partial m_p} \leq 0 \qquad\qquad (C\text{-}14)$$

If we differentiate Eq. (C-13) with respect to $m_i^{(1)}$ we obtain

$$\frac{\partial m_i^{(\ell+1)}}{\partial m_i^{(\ell)}} = -\frac{(m_i^{(\ell+1)})^2}{m_i^T} \left[ \sum_{j=1}^{S} \frac{\nu_{ji}}{\gamma_j^{(\ell)}} K_{ji}(\nu_{ji}-1) \right.$$

$$\cdot\ \gamma_j (m_i^{(\ell)})^{\nu_{ji}-2} \cdot \prod_{k=1}^{i-1} \gamma_k^{(\ell)} (m_k^{(\ell+1)})^{\nu_{jk}} \qquad (C\text{-}15)$$

$$\left. \cdot \prod_{k=i+1}^{N+M} \gamma_k^{(\ell)} (m_k^{(\ell)})^{\nu_{jk}} \right]^{-1}$$

so that

122

$$\frac{\partial m_i^{(\ell+1)}}{\partial m_i^{(\ell)}} \leq 0 \qquad \text{if } \nu_{ji} \geq 1 \text{ for at least one} \qquad (C-16)$$
$$\text{reaction}$$

Now consider the approximations to $m_i$ obtained from the iterative solution of Eq. (C.12). Letting the initial estimate of $\bar{m}$ be $\bar{m}^T$ and representing the right hand side of (C.12) by $\phi(\bar{x}^{(1)})$ we have

$$\phi(0) = \bar{m}^T > \bar{m}^* \qquad \text{where } \bar{m}^* \text{ is the exact solution.} \qquad (C-17)$$

Because of the decreasing nature of $\phi$ and

$$\bar{m}^{(1)} = \phi(\bar{x}^\circ) = \phi(\bar{m}^T) \qquad (C-18)$$

Inasmuch as $\bar{x}^\circ > \bar{m}^*$ the negative slope of the $\phi$ (specified by the nonpositive partial derivatives) requires that

$$m_i^{(1)} \leq m_i^* \qquad \text{(C-19)}$$

Similarly, for the second step

$$m_i^{(2)} = \phi(m_1^{(1)}, \ldots, m_{i-1}^{(1)}, m_i^T, \ldots, m_{N+M}^T) \qquad \text{(C-20)}$$

and, by the negative partial derivatives,

$$m_i^{(2)} \geq m_i^* \qquad \text{(C-21)}$$

By induction

$$\overline{m}(0) \geq \overline{m}(2) \geq \overline{m}(4) \ldots \geq \overline{m}*$$

$$\geq \ldots \geq \overline{m}(3) \geq \overline{m}(1) \tag{C-22}$$

The sequences

$$\overline{m}(0), \overline{m}(2)\ldots$$

and

$$\overline{m}(1), \overline{m}(3)\ldots$$

are bounded monotone sequences by Eq. (C-22) and are, therefore, convergent by the same arguments given in Wolery and Walters (1975).

The calculation of pH by the iterative procedure described above is accomplished by writing proton balance as

$$m_H^T = m_H^o - \sum_{j=1}^{S} \nu_{jH} m_j + m_{oH} \tag{C-23}$$

where $m_{OH}$ accounts of the production of protons by the dissociation of water and $m_{OH}$ is computed from

$$a_{H^+} a_{OH^-} = K_w \qquad \text{(C-24)}$$

By rearranging Eq. (C.23) in a manner similar to that described for the other components the same iterative procedure can be used. Convergence of the iterative procedure was found to be very slow for weak acids if the initial guess for the proton concentration is taken as

$$m_H^T = m_H^o \qquad \text{(C-25)}$$

with $m_H^T$ computed for the stoichiometry of any acids in solution. Convergence is greatly enhanced in this case if the initial estimates for the conjugate bases are used.

If required, activity coefficients are computed before each step in the iteration using the extended Debye-Huckel Equation if the ionic strength is less than 0.1 and the mean salt method if the ionic strength is greater than 0.1.

# APPENDIX D

A number of scanning-electron photomicrographs were made on portions of tuff samples used in the porosimetry and diffusion studies. The purpose of these samples was to provide qualitative verification of the extremely small pore diameters (median diameter 1 to 0.1 µm) computed from the mercury-intrusion porosimetry studies. These photomicrographs reveal that such small pores do exist in sufficient numbers to account for the mercury-infusion results. These photomicrographs also indicate that the pore structures of the tuff are very tortuous which may account for the abnormally high tortuosity factors computed from the diffusion tests. Selected photomicrographs are shown without comment on the following pages.
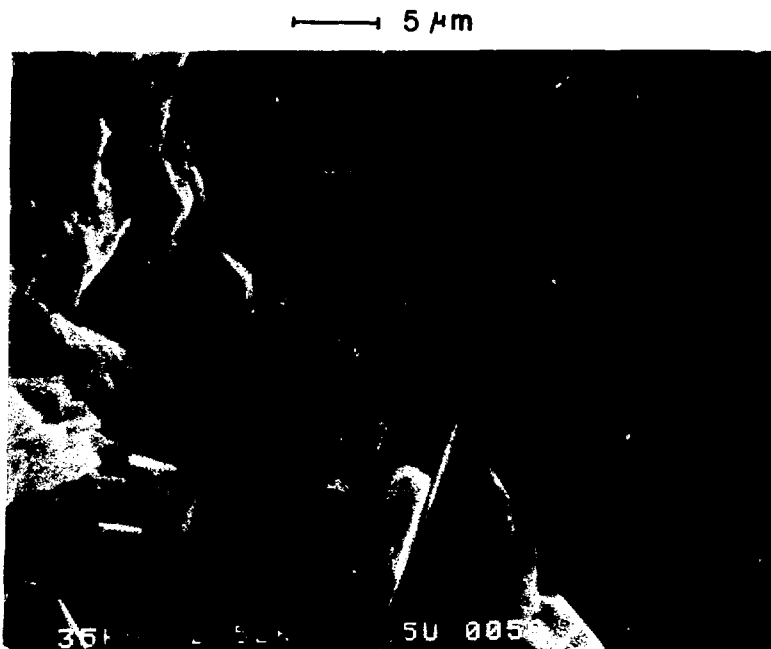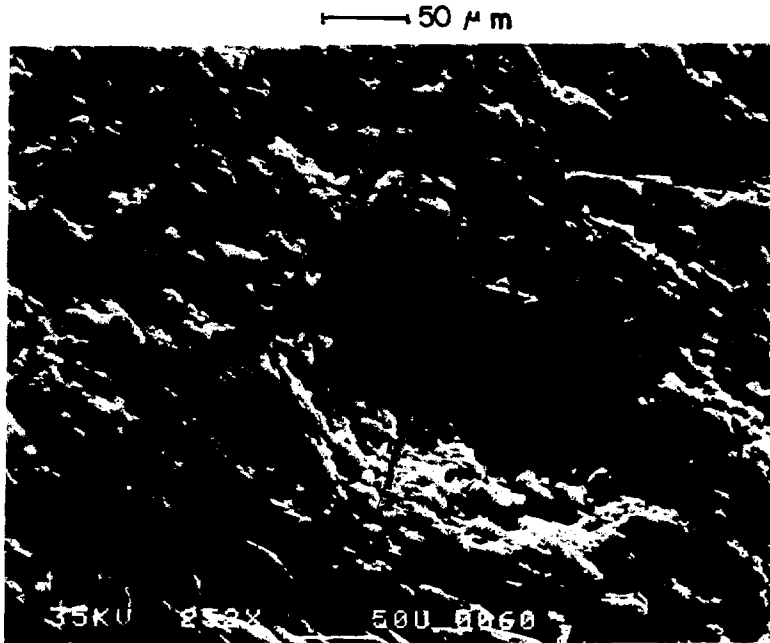
Fig. D.1.   G1-2233 at 252X and 2.52 x 10$^3$ X.
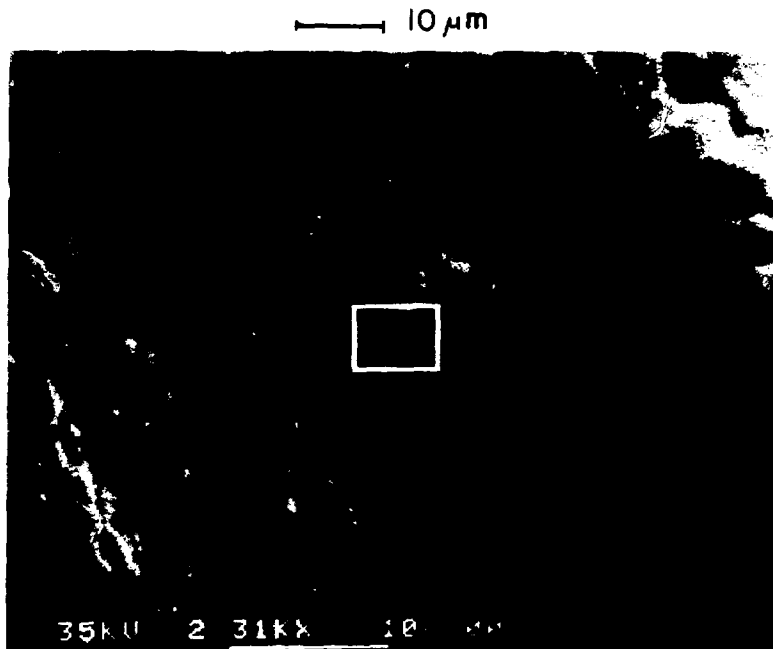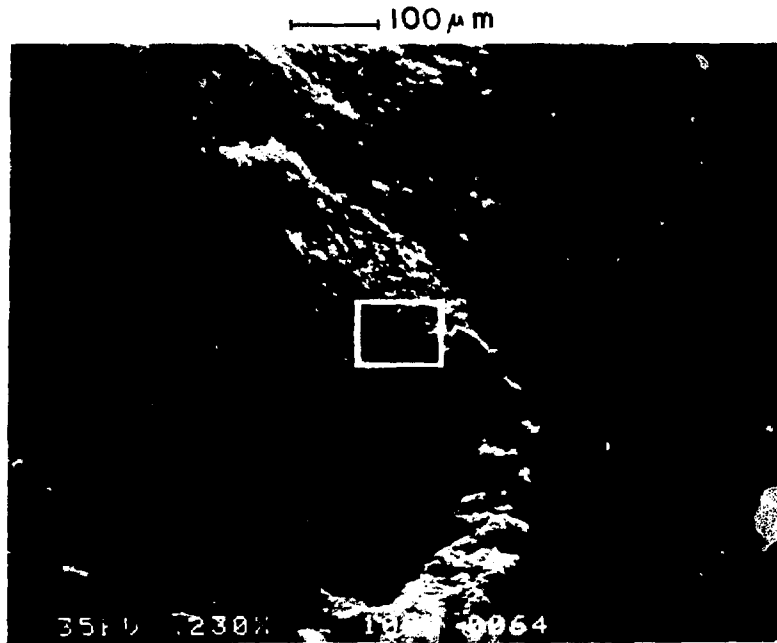
Fig. D-2.   G1-2539 at 230X and 2.31 x $10^3$ X.

50 μm



5 μm
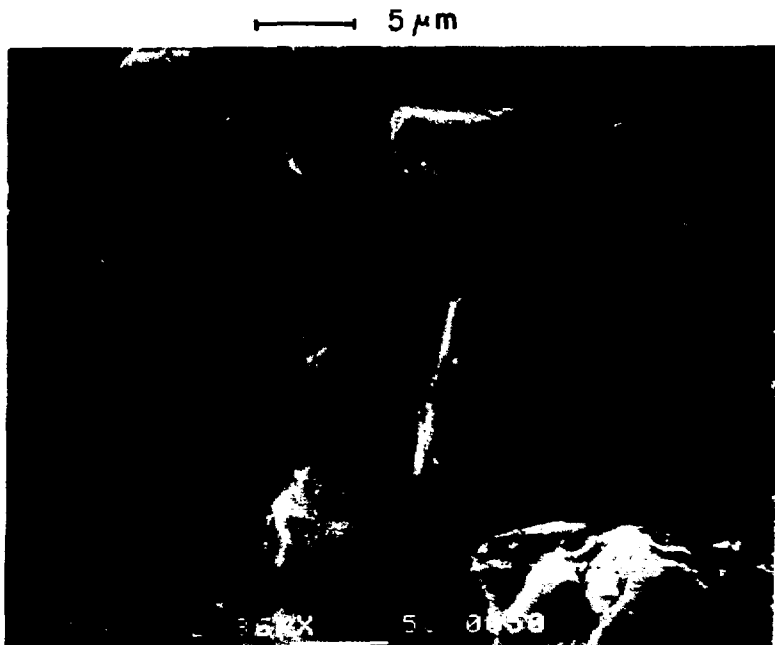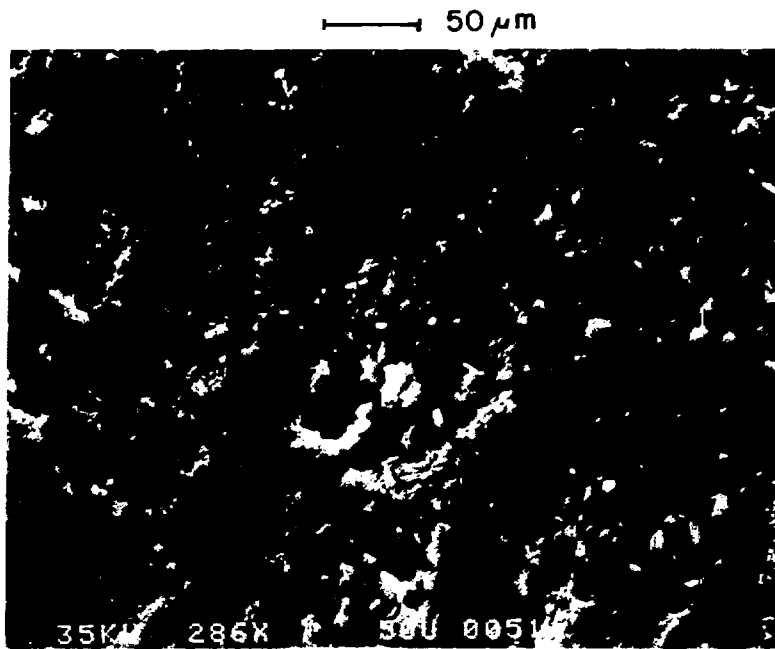
Fig. D.3.   G1-2698 x 286X and 2.86 x $10^3$ X.

50 μm

5 μm
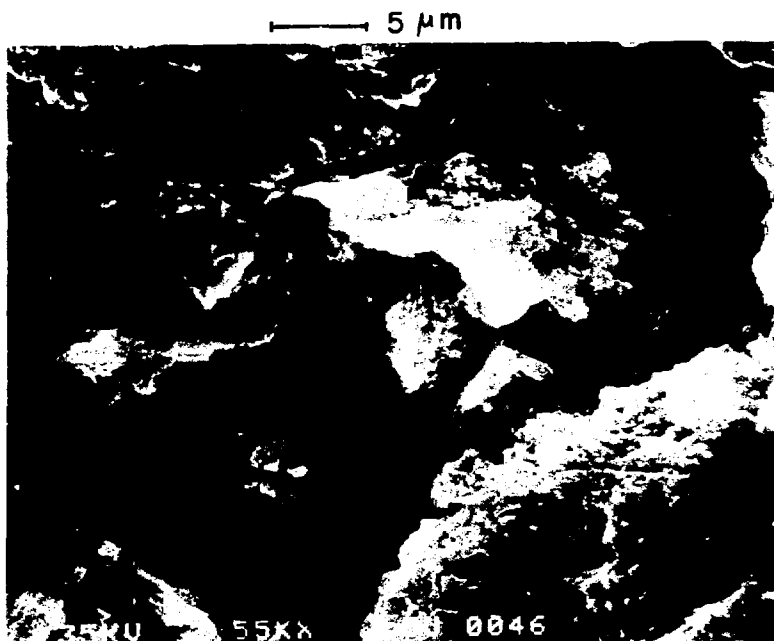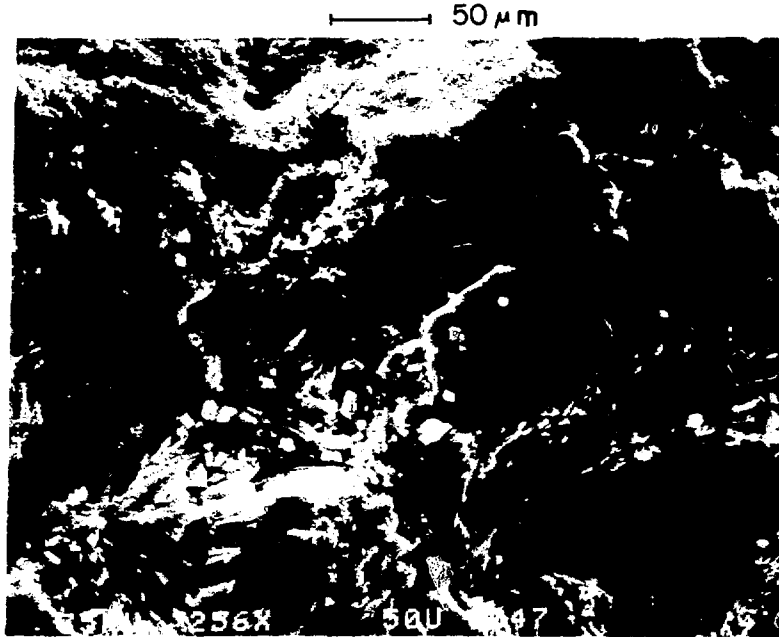
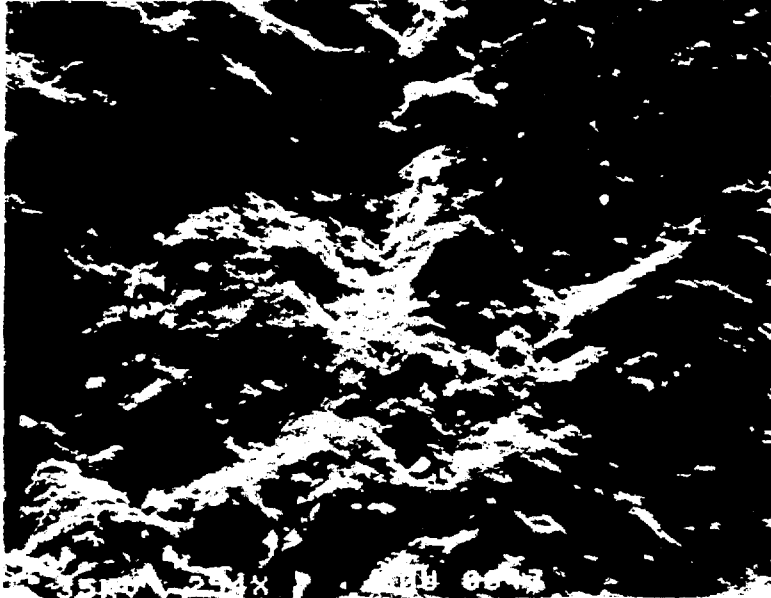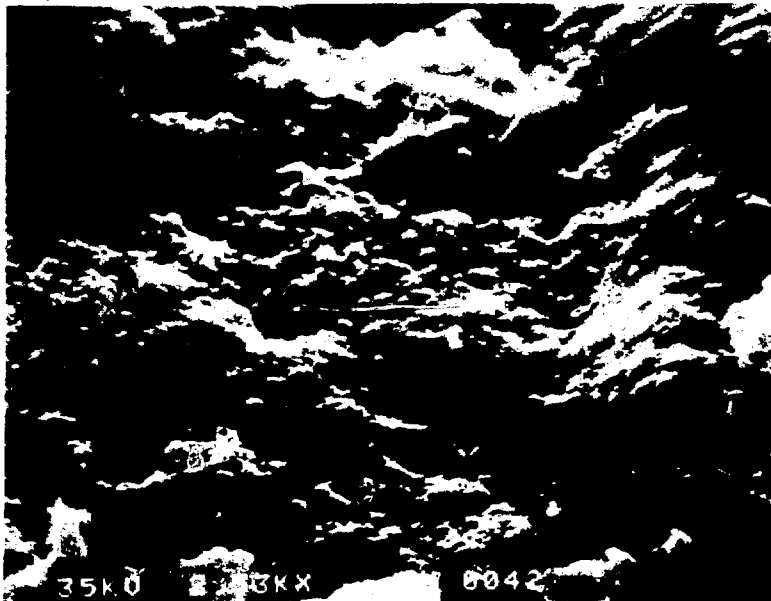Fig. D.4. YM-46, position A, at 256X and 2.55 x 10³X.

Fig. D.5. YM-46, position B, at 254x and 2.53 x 10³X.